EFFECTS OF STRESS ON THE ELECTRICAL RESISTANCE OF YTTERBIUM AND CALIBRATION OF YTTERBIUM STRESS TRANSDUCERS

Michael J. Ginsberg, et al

Stanford Research Institute

Prepared for:

Defense Advanced Research Projects Agency
Defense Nuclear Agency

August 1973

160029

DNA 3577F

EFFECTS OF STRESS ON THE ELECTRICAL RESISTANCE OF YTTERBIUM AND CALIBRATION OF YTTERBIUM STRESS TRANSDUCERS

Stanford Research Institute
333 Ravenswood Avenue
Menlo Park, California 94025

August 1973

Final Report for Period 13 March 1972 – 13 July 1973

CONTRACT DNA001-72-C-0146

Approved for public release;
distribution unlimited.

THIS WORK SPONSORED BY THE DEFENSE
ADVANCED RESEARCH PROJECTS AGENCY UNDER
DARPA ORDER 1695

Prepared for
Director
DEFENSE NUCLEAR AGENCY
Washington, D.C. 20305

STANFORD RESEARCH INSTITUTE
Menlo Park, California 94025 · U.S.A.

UNCLASSIFIED

SECURITY CLASSIFICATION OF THIS PAGE (When Dete Entered)

REPORT DOCUMENTATION PAGE

READ INSTRUCTIONS BEFORE COMPLETING FORM

1. REPORT NUMBER: DNA 3577F

2. GOVT ACCESSION NO.:

3. RECIPIENT'S CATALOG NUMBER: AD-A010 262

4. TITLE (and Subtitle): EFFECTS OF STRESS ON THE ELECTRICAL RESISTANCE OF YTTERBIUM AND CALIBRATION OF YTTERBIUM STRESS TRANSDUCERS

5. TYPE OF REPORT & PERIOD COVERED: FINAL REPORT for Period 13 March to 13 July 1973

6. PERFORMING ORG. REPORT NUMBER: PYU-1797

7. AUTHOR(s): Michael J. Ginsberg, Dennis E. Grady, Paul S. De Carli and John T. Rosenberg

8. CONTRACT OR GRANT NUMBER(s): DNA001-72-C-0146

9. PERFORMING ORGANIZATION NAME AND ADDRESS: Stanford Research Institute, 333 Ravenswood Avenue, Menlo Park, California 94025

10. PROGRAM ELEMENT, PROJECT, TASK AREA & WORK UNIT NUMBERS: DARPA ORDER 1695

11. CONTROLLING OFFICE NAME AND ADDRESS: Defense Advanced Research Projects Agency, Washington, D.C. 20305

12. REPORT DATE: August 1973

13. NO. OF PAGES: 143

14. MONITORING AGENCY NAME & ADDRESS (if diff. from Controlling Office): Defense Nuclear Agency, Washington, D.C. 20305

15. SECURITY CLASS. (of this report): UNCLASSIFIED

15e. DECLASSIFICATION/DOWNGRADING SCHEDULE:

16. DISTRIBUTION STATEMENT (of this report): Approved for public release; distribution unlimited

17. DISTRIBUTION STATEMENT (of the ebstract entered in Block 20, if different from report):

18. SUPPLEMENTARY NOTES:

19. KEY WORDS (Continue on reverse side if necessery and identify by block number)

Ytterbium
Calibration
Piezoresistance
Dynamic stress
Stress gage
Field gage
Stress transducer
Electrical resistance
Release calibration

20. ABSTRACT (Continue on reverse side if necessery and identify by block number)

The effect of dynamic compressive stress on the electrical resistance of 0.005 cm (2 mil) thick ytterbium foil has been studied over the range 0 to 33.40 kbar. This material has been used successfully as the active element in dynamic stress transducers with major application to in situ geological measurements and laboratory measurements in inhomogeneous materials.

DD FORM 1 JAN 73 1473
EDITION OF 1 NOV 65 IS OBSOLETE

UNCLASSIFIED
SECURITY CLASSIFICATION OF THIS PAGE (When Data Entered)

19. KEY WORDS (Continued)

20 ABSTRACT (Continued)

The loading data, obtained from gas gun experiments, was fitted by the function

$$\sigma \text{ (kbar)} = 13.65\left(\frac{\Delta R}{R_o}\right) - 4.358\left(\frac{\Delta R}{R_o}\right)^2 + 0.9227\left(\frac{\Delta R}{R_o}\right)^3 - 0.0684\left(\frac{\Delta R}{R_o}\right)^4$$

where σ is the compressive stress in the direction of wave propagation and $\Delta R/R_o$ is the fractional change in electrical resistance. The standard deviation associated with the above expression is 0.638 kbar. Better prediction at lower stress levels can be obtained by using a different equation:

$$\sigma \text{ (kbar)} = 1.082\left\{1 - \exp\left[-\left[20.80\left(\frac{\Delta R}{R_o}\right)\right]\right]\right\} + 9.168\left(\frac{\Delta R}{R_o}\right)$$

The standard deviation associated with this equation in the range 0-10 kbar is 0.252 kbar. The need for the two equations arises from the shape of the loading curve in the 1 to 2 kbar region--the change in slope which occurs is not adequately described by the fourth order polynomial that fits well over the entire range.

Between 0 and about 10 kbar the unloading paths are a family of straight lines with both slope and intercept being functions of peak stress. The release data from stress levels between about 10 and 33.40 kbar have been fitted by second and third degree polynomials. Stress cycling affects the response, but insufficient data were obtained to quantitatively describe reloading behavior.

The maximum stress at which ytterbium can be used safely is approximately 30 kbar because of the occurrence of a polymorphic phase transition between 30 and 35 kbar that is essentially complete in a few microseconds.

An attempt has been made to assess the effects of the tangential components of a divergent flow field on the response of ytterbium transducers through experiments designed to investigate the tensile strain dependence of electrical resistance. Difficulty in ascertaining how much tangential strain is actually coupled into a gage in a divergent flow field precludes application of the data at this time.

It was ascertained that the piezoresistance coefficient of annealed foil was much greater than the coefficient of the as-rolled foil normally used for gages, but that the greater part of the resistance change during loading is irreversible. In addition, it has been noted that at stresses of 10 kbar and below there is a large difference betweeen the hydrostatic piezoresistance coefficient and the coefficient measured by gas gun experiments. The difference is greatest at about 1.5 kbar.

PREFACE

We greatly appreciate the assistance and contributions of the following people:

Experiment design and construction - J. W. Dempster, A. Urweider, J. H. Hannigan, J. H. Yost, K. A. Hirschberg

Performance of experiments - D. F. Walter, A. J. Bartlett, R. W. Gates, W. Wilkinson, D. L. Clark

Data analysis- B. Y. Lew, R. C. Singleton, C. W. Gossett

We would also like to express our appreciation to A. L. Florence and C. W. Smith for a number of interesting discussions, to C. F. Petersen and D. R. Curran for both administrative support and technical assistance, and to C. B. MacFarland, who monitored the program for the Defense Nuclear Agency. Major D. Burgess of the Defense Nuclear Agency, who succeeded C. B. McFarland as contract monitor, made valuable suggestions concerning the text of this report as did R. Shunk of SAI, Inc., and B. Hartenbaum of RDA, Inc.

CONTENTS

CONTENTS (Cont'd)

CONTENTS (Concl'd)

TABLES

ILLUSTRATIONS

ILLUSTRATIONS (Cont'd)

ILLUSTRATIONS (Concl'd)

1. INTRODUCTION

Prediction of the *in situ* response of rocks and soils to dynamic loading requires accurate knowledge of the constitutive relations among stress, particle velocity, and density during the passage of a stress wave. Good *in situ* measurements would be the best source of data from which constitutive relations could be obtained because these measurements include the effects of cracks, voids, and residual stresses. Such measurements of stress in rocks and soils have been made with transducers having ytterbium as the stress-sensitive element. Keough (1970) first suggested ytterbium for use in this application, primarily because it exhibits a very large positive change in electrical resistance with compressive stress, and the ratio of this signal to any divergent flow-induced strain signal was expected to be small over the stress range of interest. Although high quality resistance-time records have been obtained in the field during a number of nuclear and high explosive detonations (for example, see Smith, 1972; Grady et al.,1973), conversion to stress-time histories has been hampered by a lack of data on the relationship between stress and resistance for ytterbium.

The program described in this report was designed primarily to increase the utility and credibility of ytterbium gages for *in situ* rock and soil stress measurements. However, the calibration data and other results are applicable to ytterbium gages used in other situations. The specific objectives were

(1) To generate loading and release calibration data immediately applicable to the analysis of gage records now being obtained in the field and laboratory with ytterbium stress transducers.

(2) To improve the accuracy and reliability of ytterbium stress transducers through investigation of some of the existing questions about the piezoresistance of ytterbium.

Calibrating dynamic stress gages of the type used in this program requires the following experimental methodology. The material to be calibrated--ytterbium in this instance--is fabricated into some convenient form and sandwiched between two pieces of a material whose stress-particle velocity Hugoniot has been ascertained through the use of some other technique, such as laser interferometry. When we impact this target with a projectile of either the same material or some other material with well-defined shock properties and measure the projectile velocity, we can specify the peak stress reached in the target. Assuming the specimen or gage material comes to stress equilibrium with the target, we have also specified the stress level in the specimen. Measurement of the fractional change in resistance at peak stress gives one point on a loading calibration curve at the stress level calculated from the projectile velocity and the Hugoniots of the target and projectile. The locus of these points on a stress-$\Delta R/R_o$ plot is the loading calibration curve. We normally assume that the gage follows this curve during the loading part of the stress cycle.

This program differed somewhat from other calibration programs in that great emphasis was placed on obtaining unloading calibration data so that complete stress-time histories could be produced from gage records. Experiments designed to obtain both loading and unloading calibration data are no more difficult to perform than experiments that produce only loading data, but the selection of projectile-target systems is restricted by the need for detailed knowledge of the unloading behavior of target and projectile and the proper impedance mismatch.

In addition to and concurrent with the basic calibration phase of the program (which was of first priority), we attempted to gain more understanding of the material parameters that affect gage behavior by examining the gage material and trying to correlate differences in, for example, metallurgical history with piezoresistant response.

Finally, we approaehed the problem of divergent flow effeets on gage response by investigating the effeets of noncompressive strain on the electrical resistance of ytterbium.

This program was not designed to produce a handbook for ytterbium gage users; proper applieation of the data presented in this report will require some effort and experience. The production of a handbook might be a reasonable aetivity to be undertaken in the near future.

2. SUMMARY OF RESULTS

The following is a summary of the results obtained during this program. These results are presented in more detail and discussed in Section 4.6 and 4.7.

2.1 Loading Calibration

The ratio of change in resistance to initial resistance $(\Delta R/R_o)^*$ hereafter referred to as resistance change, of nominal 0.005-cm (2-mil) ytterbium foil was measured over the stress range 0.5 to 33.4 kbar, and the data can be represented in the range from 0 to 10 kbar by the expression

$$\sigma = 1.082 \left\{1 - \exp\left[-20.80 \left(\frac{\Delta R}{R_o}\right)\right]\right\} + 9.168 \left(\frac{\Delta R}{R_o}\right) \qquad (1)$$

The standard deviation around the mean of the curve represented by Equation (1) is ±0.262 kbar. A graphical representation is contained in Figure 33 in Section 4.6. There were 33 data points.

We chose to represent the entire population of loading data (0 to 33.40 kbar) by the function

$$\sigma = 13.65 \left(\frac{\Delta R}{R_o}\right) - 4.358 \left(\frac{\Delta R}{R_o}\right)^2 + 0.9227 \left(\frac{\Delta R}{R_o}\right)^3 - 0.0684 \left(\frac{\Delta R}{R_o}\right)^4 \qquad (2)$$

The standard deviation around the mean of Equation (2) is ±0.638 kbar. There were 53 data points. The need for the two equations arises from the shape of the loading curve in the 1 to 2 kbar region--the change in slope which occurs is not adequately described by the fourth order polynomial that fits well over the entire range. See Section 4.7 and Figure 23 in Section 4.6.

2.2 Unloading Calibration

A number of unloading (release) paths were experimentally determined in the stress range between about 0.75 kbar and 33 kbar. Up to

---

* $\frac{\Delta R}{R_o} = \frac{R_{\text{instantaneous}} - R_{\text{initial}}}{R_{\text{initial}}}$

about 1 kbar, the loading path and the unloading paths coincide. Between 0 kbar and 10 kbar, the unloading paths can be represented by a family of straight lines of the form

$$\sigma_u = A + B(\Delta R/R_o)_u \qquad (3)$$

where both A and B are functions of the peak stress and σ_u and $(\Delta R/R_o)_u$ are the stress and resistance change, respectively, along the unloading path. Between about 10 kbar and 33.4 kbar, the measured unloading paths can be represented by curves of the form

$$\sigma_u = \sum_{n=0}^{i} A_n \left(\frac{\Delta R}{R_o}\right)_u^n \qquad i = 2 \text{ or } 3 \qquad (4)$$

where the A_n are all functions of the peak stress, and σ_u and $(\Delta R/R_o)_u$ are the stress and corresponding resistance change along the unloading path. See Section 4.7.3.

2.3 Reloading

The dynamic piezoresistance function of ytterbium is not strictly constant over successive loading and reloading cycles, but we do not believe the errors in stress measurement attributable to this nonconstancy to be appreciable. See Section 4.7.5.

2.4 Divergent Flow Effects

A series of experiments was performed to determine the effect of tensile strain (in the plane of the foil) on the electrical resistance of ytterbium foil, thereby partially simulating a divergent flow field. The resistance shows an initial decrease, reaches a minimum of $\Delta R/R_o \simeq -0.02$ at about 1.5% strain and then increases linearly with the application of more strain. See Section 4.7.8.

2.5 Characterization of Ytterbium

Representative values of resistivity and hardness were measured, resistivity was found as a function of temperature, and X-ray diffraction

data were obtained on the various types of ytterbium foil used so that some of the basic parameters affecting the piezoresistance of ytterbium could be known. See Sections 4.3.1, 4.3.2, 4.3.3, and 4.3.6.

2.6 Mechanical Properties of Ytterbium

Data were obtained on the mechanical properties of ytterbium foil in tension and of ytterbium ingot material in compression, and the data were related to the observed piezoresistance effects. See Sections 4.3.4 and 4.3.5.

2.7 Comparison with Hydrostatic Piezoresistance Experiments

The difference between the piezoresistance under hydrostatic loading and one-dimensional or two-dimensional strain (in the elastic region) is explained by determining the coefficients in the piezoresistance tensor. The analysis was extended into the plastic region. See Appendix A.

2.8 Determination of Upper Stress Limit for Ytterbium Gage Use

The upper limit for use of ytterbium was determined by shocking foil gages to a constant stress above the pressure required for the phase change under hydrostatic loading and the change was found to occur at as low as about 32 kbar under dynamic loading. See Section 4.7.6.

2.9 Effects of Metallurgical History on Piezoresistance

The electrical response of annealed and unannealed (as-rolled) foil material was compared in dynamic compression and in static tension, and the state of hardening was identified as a major variable. See Sections 4.7.4 and 4.7.5.

2.10 Time Effects

Static experiments were performed and the results compared with dynamic experiments; resistance changes were measured at constant loads over longer times. No time effects are expected for times in the millisecond range, but effects were observed during static loading rates. See Section 4.7.7.

3. CONCLUSIONS AND RECOMMENDATIONS

3.1 Conclusions

3.1.1 Calibration Data--In the range from 0 to 10 kbar, the loading calibration curve for as-rolled ytterbium foil is described adequately by a single function, Equation (1). The unloading paths from peak stress up to about 10 kbar can be said to form a family of straight lines where the slope and intercept are functions of peak stress. The loading calibration path shows curvature above about 10 kbar up to the highest stress considered, and the release paths become nonlinear as well. After attempting to fit a number of curves to the entire population of loading data, we decided that it would be better to present the data using one analytical expression for the range 0-10 kbar and another for the entire set of data going from zero to about 33 kbar, Equation (2).

3.1.2 Upper Limit of Utility--The transition from face-centered cubic (FCC) to body-centered cubic (BCC) ytterbium, with its attendant drastic change in electrical resistance, begins as low as about 32 kbar under dynamic loading conditions (rise time under 500 nsec) and is substantially complete in less than 2 μsec. We have, therefore, concluded that 30 kbar is the upper limit for use of ytterbium as a dynamic stress transducer if some margin of safety is desired by the experimenter.

3.1.3 Divergent Flow Effects--At stress levels around 1 kbar and below and for long times, it is possible that changes in resistance arising from the effects of divergence in the flow field could be of sufficient magnitude to significiantly affect the shape of the recorded signal. However, no definite conclusions can be drawn from our results because (1) we do not know how much tangential strain is coupled into the gage element in the field and (2) the experiments that were performed to ascertain the magnitude of strain effects have shown that the response seems to be

sensitive to the experimental configuration, suggesting that a gage in a field package might behave differently because of, for example, Poisson contraction effects.

3.1.4 Reproducibility and Accuracy--A variation in the metallurgical history of ytterbium foil (annealed vs cold-worked) has a profound effect on the magnitude of the resistance change with stress at lower stresses (up to about 5 kbar) and we have surmised that the effect persists at higher pressures. We have not shown any such effect for variations in chemical purity.

We believe that the state of cold work of the foil is the major variable affecting the reproducibility of the calibration data and the accuracy of measurements made with ytterbium gages.

3.1.5 Time Effects--No time effects of importance were observed in the time regime of interest to us in dynamic measurements. However, the static response of ytterbium is time-dependent during release over long periods of time (minutes to hours) and should be used with caution for measurements in static experiments.

3.2 Recommendations

Ytterbium shows very high sensitivity, is well-behaved and sufficiently reproducible (although not linear) in its calibration, shows relatively small sensitivity to noncompressive stress fields over most of its usable stress range, is fabricable, and reasonably economical. We believe, therefore, that cold-rolled ytterbium foil is suitable for use as the active element in stress transducers designed to measure dynamic geological properties in situ and has laboratory applications as well, such as making stress history measurements in inhomogeneous materials. This section contains our specific recommendations and suggestions for using ytterbium gages and analyzing experimental data.

3.2.1 Ytterbium Gages--Suggestions concerning the fabrication and use of ytterbium foil gages are:

(1) Be sure that the foil used is cold-rolled (not annealed or rolled with intermediate anneals) from a cast ingot--not from distilled lump material.

(2) Do not use ytterbium gages at expected stress levels above 30 kbar without a back-up system (such as a manganin or carbon gage or a particle velocity gage) in case the phase transformation begins during loading and makes the recorded data unreliable.

(3) Do not expose the foil to excessive heat (above about 100°C) for any length of time. This suggestion is made to avoid any annealing and the attendant changes in sensitivity.

(4) Given the state of our knowledge about sensitivity to divergent flow, we suggest that attempts be made to minimize tangential flow and bending rather than correcting for it.

3.2.2 Calibration Data--We have not yet ascertained the best way to use the loading and release data presented in this report, or if there actually is a single best way for all situations. Further experience in the systematic application of the data would be necessary before detailed recommendations for ytterbium users could be made in some type of handbook form. However, some general suggestions about the use of the calibration data are:

(1) If the peak stress level associated with the event is 10 kbar or below, use Equation (1) for the loading and the unloading curves described by Equation (3). There are two ways to do this--graphically and analytically.

For the graphical method, plot Equation (1) (shown in Figure 33) and find the peak stress (σ_p) reached in the experiment. Then find the zero-stress residual resistance ($\Delta R_H/R_o$) in Figure 40 and draw a straight line between σ_p and ($\Delta R_H/R_o$). This is the unloading path from that peak stress. Repeat the process for subsequent loading and release cycles. This will cause some error, but we do not have sufficient data to assess its magnitude.

The equations describing the 0 to 10-kbar behavior will lend themselves to a simple computer code treatment. Essentially, the computer finds $\sigma(t)$ in the wave front using Equation (1) until it comes to a maximum. It knows that

$$\sigma_u = A + B\left(\frac{\Delta R}{R}\right)_{o\ u} \tag{3}$$

and it knows $A(\sigma_p)$ and $B(\sigma_p)$ from the data, so it solves Equation (3) and analyzes the entire stress-time record.

(2) If the peak stress is above 10 kbar, the situation is not as straightforward. Use Equation (2) for the loading if the fit and detailed behavior of the wave around one kbar and below are not of extreme importance. If the peak stress is above 10 kbar and low-stress behavior is important, we suggest some combination of Equation (1) and some other function, possibly Equation (2). We have not yet found a best solution to this problem for all cases.

The unloading data from stresses above 10 kbar should be used carefully because the curves that represent the individual data sets sometimes do not intersect the loading curve at the peak stress of the experiment in which they were measured. This often happens with fitted data, and we suggest graphical or analytical interpolation between the curves representing the data.

4. TECHNICAL DISCUSSION

4.1 Piezoresistivity and Piezoresistance

The resistivity ρ_{ik}, of a solid is an intensive property and is representable by a second-rank tensor relating electric field intensity E_i and electric current density j_k, i.e.,

$$E_i = \rho_{ik} j_k \tag{5}$$

The resistivity is a function of the instantaneous state of strain existing in the solid and of the strain history. A change in resistivity caused by a change in the state of strain is called the elastoresistivity* effect. If we wish to consider the change in resistance to be caused by the application of stress, we call the effect piezoresistivity. It has been suggested that interpretation of these effects in terms of fundamental parameters of the material is more conveniently formulated with respect to the elastoresistivity effect, and measurement problems are more easily discussed from the viewpoint of piezoresistivity (Keyes, 1960).

The fractional change in resistivity induced by the application of a generalized stress σ_{mn} is given by

$$\frac{d\rho_{ik}}{\rho} = \pi_{ikmm} \sigma_{mn} \tag{6}$$

where the π_{ikmn} are the piezoresistivity coefficients, which form a fourth rank tensor. In the simplified matrix notation† this can be written

---

* Valid only in the elastic region of the solid.

† It will also be shown that we are interested only in principal directions in Appendix A.

$$\frac{d\rho_i}{\rho_o} = \pi_{ij}\sigma_j \tag{7}$$

The resistance of a material depends not only on the resistivity, but also on the dimensions. A differential change in resistance is given by (from differentiating $R = \rho\ell/A$)

$$\frac{dR_i}{R} = \frac{d\rho_i}{\rho} + \frac{d\ell_i}{\ell} - \frac{dA_i}{A} \tag{8}$$

or

$$\frac{dR_i}{R} = \pi_{ij}\sigma_j + \frac{d\ell_i}{\ell} - \frac{dA_i}{A} \tag{9}$$

where i corresponds to the x, y, or z direction, ℓ is the length of the conductor, A the cross-sectional area normal to the current flow direction, and R is the resistance. In ytterbium the change in resistivity is by far the dominant effect, but this varies from material to material.

When choosing a material for the active element in a stress transducer the important properties are:

(1) Sensitivity--The resistance change with stress should be large enough to produce a usable signal, and the dependence of the resistance on stress should increase (or decrease) monotonically.

(2) Reproducibility--The uncertainty in the stress measurements traceable to variations in the gage material should be within acceptable limits.

(3) Temperature sensitivity--The ratio of resistance change induced by temperature (either from shock or joule heating) to that arising from mechanical stress should be as small as possible.

(4) Sensitivity to strains other than those caused by the principal compressive stress--When a transducer element experiences a divergent flow field, there are strains induced other than the

principal compressive stress. It is important that the sensitivity of the gage material to stresses other than the principal compressive stress be as small as possible relative to the compressive stress sensitivity. Signals arising from bending or tensile stresses can distort the gage output if they become large enough.

(5) Unloading behavior--It would be advantageous if the loading and unloading behavior of a transducer element were the same; however, unloading behavior can also be calibrated experimentally, as we have done here.

(6) Fabrication and economics--Ease of fabrication, including ease of handling, chemical inertness, etc., and reasonable price are of greater or less importance depending on the quantity of measurements that are envisioned.

4.2 Ytterbium

Ytterbium is a rare earth element located between thulium and lutetium in the Lanthanide series. Its atomic weight is 173.04, and its atomic number is 70. At 25°C and one atmosphere pressure, its equilibrium crystal structure is FCC. The electrical resistance of ytterbium increases markedly between atmospheric pressure and a maximum located somewhere between 30 and 40 kbar (depending on the state of strain) where the resistance decreases to about 80 percent of the original value at one atmosphere. The maximum resistance change under hydrostatic pressure has been reported to be as much as 23 times the value of the resistance at one atmosphere (Stromberg and Stephens, 1964) and as little as 6 times (Stager and Drickamer, 1963). This phase transition is especially interesting because the high pressure modification is BCC, which is usually more open than the low pressure FCC structure, but the phase change does involve an overall volume decrease (Stephens, 1964).

The phase change has been discussed by Hall and Merrill (1963), Hall et al. (1963), Souers and Joura (1963), and Stager and Drickamer (1963). All agreed that the FCC → BCC transformation was accompanied by a decrease in the size of the individual ytterbium atoms, and the necessary shift in electronic structure was the cause of the decrease in resistance and return to metallic conduction behavior. However, the kinetics of the conductivity change do not fit with an atom shrinkage model. This is discussed in more detail in Section 4.7.6.

Other polymorphic changes that have been noted are a FCC → BCC transformation at one atmosphere and approximately 798°C (Daane, 1961), and a shear transformation from a FCC to hexagonal close-packed (HCP) structure occurring at one atmosphere and approximately 0°C (Kayser and Soderquist, 1969; Kayser, 1970; Tanuma et al., 1970; Bucher et al., 1970). Results showing other temperature-induced effects have been presented by Hurd and Alderson (1973). The large difference between the extremes of the peak resistance values measured by various investigators might have arisen from impurity effects at high pressures, from the effect of nonhydrostatic components of stress, or from differences in sample preparation techniques. As the investigators who have studied this problem have improved their techniques, they have obtained fractional resistance changes at the transition stress which are in the range of 6 to 8.

It is not surprising that a substance that displays such complex behavior has attracted considerable attention from both experimentalists and theoreticians. The large dependence of electrical resistance on stress has also aroused a practical interest in the properties of ytterbium because of its attractiveness for use as a quantitative dynamic stress sensor, especially in the low stress (1-20 kbar) region. Development and calibration programs have been recently carried out at SRI (Keough 1970; Williams, 1970; Ginsberg, 1971), and ytterbium gages have been used successfully in laboratory experiments (Petersen and Erlich, 1972; Erlich et al., 1971) as well as in the field.

4.3 Preparation and Characterization of Specimens

Ytterbium metal is obtained by mixing its oxide with a reducing agent such as calcium, silicon, aluminum, or magnesium (or a combination of these metals) and heating the mixture under vacuum. The oxide reacts with the reducing agent and the resulting ytterbium vapor is condensed on a cold collector placed above the crucible. The metal obtained from this process is often purified further by redistillation under vacuum, and the final product is called distilled lump. This lump can be rolled directly into foil, or it can be remelted, cast into ingot, and then rolled into foil.

The specimens used in our dynamic calibration experiments were four-terminal grids (see Figure 1) fabricated from as-rolled (from ingot) ytterbium foil of nominal 0.005-cm (2-mil) thickness. Most of the experiments were done on foil purchased from Research Chemicals, Inc., Phoenix, Arizona. For comparison purposes, some work was done with foil obtained from American Rare Earth and Foil Co., Tempe, Arizona. Both suppli claimed 99.9% purity. A spectrographic analyses of five samples for the Research Chemicals (RC) material is shown in Table 1. The purity of the material from American Rare Earth and Foil (AREF) was also quoted to be 99.9%. An analysis is included in Table 1.

Each grid was made from a 2-cm square cut from the as-received foil. The thickness of all squares was measured, they were cleaned carefully with a small glass fiber brush, and the grid photoetched on an epoxy-fiberglass or strippable mylar substrate using a mixture of ethanol and hydrochloric acid. The cover of fiberglass cloth was added and then also impregnated with epoxy, making the package shown in Figure 2.

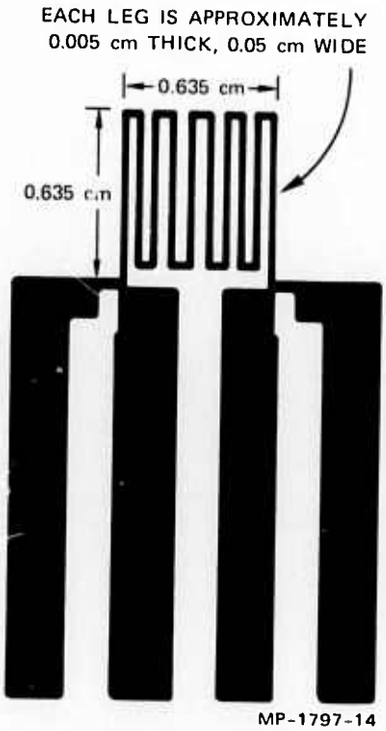

FIGURE 1 GAGE CONFIGURATION USED IN ALL DYNAMIC CALIBRATION EXPERIMENTS

Table 1

SPECTROGRAPHIC ANALYSIS OF YTTERBIUM FOIL

Element	Sample No. RC-1	RC-2	RC-3	RC-4	RC-5	AREF-1
Ytterbium	Major	Major	Major	Major	Major	Major
Thulium	<0.005	<0.005	<0.005	<0.005	<0.005	ND
Erbium	0.006	0.02	0.005	<0.005	0.005	ND
Lutetium	<0.005	<0.005	<0.005	<0.005	<0.005	ND
Dysprosium	<0.005	<0.005	<0.005	<0.005	<0.005	NA
Yttrium	<0.005	<0.005	<0.005	<0.005	<0.005	NA
Silicon	0.01	0.01	0.01	0.01	<0.01	ND
Iron	0.04	0.04	0.02	0.03	0.02	ND
Tantalum	ND	ND	ND	ND	ND	<0.5*
Magnesium	0.01	0.01	0.01	0.01	0.01	<0.001
Calcium	<0.01	<0.01	<0.01	<0.01	<0.01	<0.001
Aluminum	<0.01	0.02	<0.01	0.01	0.02	<0.001
Nickel	NA	NA	NA	NA	NA	ND
Copper	NA	NA	NA	NA	NA	ND
Manganese	NA	NA	NA	NA	NA	<0.001

ND = not detected

NA = not analyzed for

< = less than

* No standards for Ta content less than this were available.

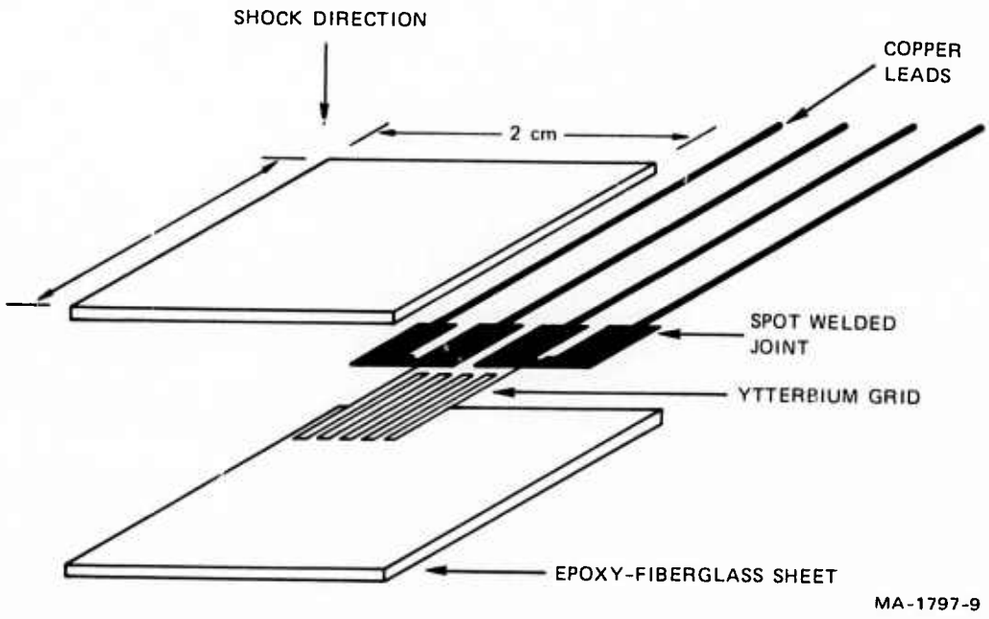

FIGURE 2 YTTERBIUM-FIBERGLASS-EPOXY PACKAGE (EXPLODED VIEW)

4.3.1 Resistivity Measurements--We determined the resistivity of a number of samples of both the RC and AREF foils by carefully measuring the line lengths and widths of individual grids (the thickness had been measured previously) and then measuring the resistance with a Cimron Model 6853 digital multimeter. The results are contained in Table 2.

Table 2

RESISTIVITY OF 0.005-cm (2-mil) YTTERBIUM FOIL

Foil Type	Resistivity (ρ) $\mu\Omega$-cm
RC (Lot 109-C, as rolled)	27 ± 3
AREF (as-rolled)	39 ± 5
AREF (annealed)	19 ± 5

The value of resistivity usually quoted for ytterbium is around 30 $\mu\Omega$-cm. Higher values have been reported (Keough, 1970; Williams, 1970), but the value of ρ we obtained for the annealed AREF foil is lower than any we have seen reported. The major uncertainty is in the thickness measurement. Although we know that the electrical properties of ytterbium are strongly dependent on its metallurgical history, its resistance should also be very sensitive to its purity, so we cannot unequivocally account for the differences among the three readings, except that the low value for the annealed foil would seem to be qualitatively correct.

4.3.2 Measurements of Temperature Coefficient or Resistance--We measured the temperature coefficient of resistance of four-terminal ytterbium gages packaged in thin fiberglass by immersing them in a silicone oil bath and measuring the resistance change of the gage as a function of temperature. The temperature of the oil bath was monitored with mercury thermometers; the bath was insulated and stirred to minimize temperature gradients within the bath. The resistance of the gages was measured with a Cimron Model 6853 digital multimeter having a specified accuracy of 0.02% in the range of interest. Our own cross-checks against a recently calibrated Kelvin double bridge confirmed the accuracy. The power dissipated in the gage by the ohm meter current was only $\sim$0.01 watt, and the temperature of the gage did not rise (evidenced by an absence of resistance drift) during the course of a measurement.

The RC foil had a temperature coefficient of approximately 1.35×10^{-3} $\Omega/\Omega^{o}C$, between 30 and $100^{o}C$, and the AREF material had a lower coefficient, approximately 0.51×10^{-3} $\Omega/\Omega^{o}C$. The annealed material, also AREF, had a higher coefficient than either of the other two as-rolled foil samples, this being 2.65×10^{-3} $\Omega/\Omega^{o}C$. Keough (1970) and Ginsberg (1971) also found that higher resistivity material tends to have a lower temperature coefficient of resistance, but we are not able to present an explanation for this observation based on our experimental data.

4.3.3 Hardness--The hardness of representative pieces of foil was measured with a Kentron microhardness* testing machine, using a diamond pyramid indenter and a 10-gram load. Six indentations were made in each 2 x 2 cm square. We were hoping that these tests would be a good foil quality control test because hardness is a good measure of the amount of cold work a metal has experienced. We found, however, that the measured hardness of the annealed material did not differ from the measured hardness of the as-rolled material, which is very unlikely. Our average measured DPN hardness for the two lots of as-rolled foil was 23 ± 2.

Although performing hardness measurements on thin foils is difficult, we at least expected that the test could distinguish between annealed and unannealed foil. Our inability to do so was ascribed to the presence of a surface oxide film on the foils. Mechanical removal of the film hardens the surface, thereby making hardness measurements meaningless, and we were not able to find a good chemical means of removal. It would be very useful if some means to do these tests accurately could be devised because it represents a possible way to separate potentially bad gage material from acceptable material.

4.3.4 Yield Strength in Tension--The mechanical response of a gage to a divergent flow field is dependent on its mechanical properties in tension normal to the direction of the principal stress. We decided, therefore, that it would be useful to ascertain the yield stress of our ytterbium foil gage stock in simple tension. This would also help us interpret our tensile strain piezoresistance experiments, which are described later.

Four small tensile specimens were prepared from the RC as-rolled 0.005-cm (2-mil) ytterbium foil and tested on an Instron mechanical testing machine at a strain rate of 0.0254-cm/min. Three of the specimens were made so that the long dimension was the direction of the rolling texture in the foil; the other was made with the rolling texture normal

* Riehle Division of Ametek, Inc., East Moline, Illinois.

to the direction of applied strain. Our best estimate of the yield strength of the foil used as gage stock, which is believed to be representative of our field gage stock, was 0.50 ± 0.06 kbar. The corresponding yield strain, assuming a modulus of 187 kbar, is 0.0027. This figure was obtained by estimating the first deviation from linearity in the measured stress-strain* data. No difference was seen in yield stress between the specimens pulled with the rolling texture parallel and normal to the direction of applied strain, but this could very well be attributed to rather large experimental uncertainty.

4.3.5 Static Compressive Mechanical Properties--Since the change in slope in the stress-resistance curve was considered a yield-point effect (Ginsberg, 1971), it was thought useful to make some static measurements and obtain an approximate lower bound value of the static compressive yield point of ytterbium. To do this, a number of small cylinders with varying diameter to height (D/H) ratios (Dieter, 1961) were machined out of 99.9% pure ytterbium ingot that was on hand† and stress-strain tests were performed on these cylinders, using an Instron testing machine in the compressive mode of operation. Although the experiments are straightforward, the interpretation of the results is not simple. Frictional effects cause the pressure distribution to vary from the edge to the center of the cylinder, and the effects of porosity, which were undoubtedly present, tend to lower the measured yield point. However, these experiments, the results of which are contained in Table 3, have given us a good qualitative estimate of the yield point in compression so that we can more easily discuss the piezoresistance of ytterbium where yield point effects could be important. The extrapolated (D/H = 0) value of the compressive yield point is about 0.27 kbar, which we consider a lower bound because of the porosity and the fact the ingot is not work-hardened.

---

* Engineering stress and strain.

† This ingot was used by Keough (1970) as a source of material for vapor-deposited gages.

Table 3

COMPRESSIVE YIELD STRENGTH OF YTTERBIUM INGOT

Specimen No.	Height cm	Diameter cm	D/H	σ_o (measured) kbar
1	0.635	0.947	1.50	0.37 ± 0.07
2	0.635	0.792	1.25	0.36 ± 0.07
3	0.635	0.635	1.00	0.30 ± 0.07
4	0.635	0.321	0.50	0.30 ± 0.07

4.3.6 X-Ray Crystallography--Samples of ytterbium foil were examined by standard X-ray diffraction techniques, using nickel-filtered copper radiation and a General Electric XRD-3 diffractometer. The most intense peaks of each diffraction pattern could be indexed as reflection from FCC ytterbium having a lattice constant of 5.486 Å. Most of the patterns contained additional reflections, which could be indexed as the strongest reflections of HCP ytterbium having lattice constants c = 6.328 Å and a = 3.884 Å. The relative intensities of HCP and FCC reflections provided a quantitative measure of the proportion of HCP phase in the ytterbium samples that were judged to consist of randomly oriented fine grains, on the basis of the relative intensities of FCC diffraction peaks. These randomly oriented samples contained about 10% HCP and the proportion of HCP remained constant for samples subjected to plastic deformation and to temperature cycling over the range of -196°C to 150°C. A sample of shock-loaded ytterbium foil was also examined, and the proportion of HCP was essentially the same as in the original material.

In the flat sample diffractometer geometry that was used, the diffraction pattern originates from those crystallographic planes that are oriented parallel to the sample plane, i.e., parallel to the surface of the foil. Preferred orientation of the fine individual grains that make up the sample may be inferred by comparison of observed relative

diffraction peak intensities with the relative intensities calculated for an assemblage of randomly oriented grains. We noted large differences in the extent of preferred orientation among samples from different lots of foil. The criterion for preferred orientation was the intensity ratio of (220) reflection to (111) reflection for the sample. For randomly oriented grains the calculated intensity ratio I(220)/I(111) is 0.4. One group of foil samples, having I(220)/I(111) in the range of 0.3 to 0.6, was classed as isotropic, within the limits of the measurement technique. Another group of foil samples, having I(220)/I(111) in the range of 1.2 to 3.0 was classed as having moderate preferred orientation. A third group of samples, for which I(220)/I(111) was in the range of 6.0 to 8.0, was classed as showing very strong preferred orientation. The type of preferred orientation noted, an alignment of (110) planes parallel to the plane of the foil, is common to all heavily rolled FCC metals.

HCP reflections were observed in the diffraction patterns of the ytterbium samples that showed strong preferred orientation, but the preferred orientation interfered with quantitative determination of the proportion of HCP. Qualitatively, we estimate that the HCP content does not differ significantly from the 10% observed in the isotropic ytterbium samples. All of the samples of commercially obtained foil and bulk ytterbium that we have examined appear to contain about 10% of the HCP phase. The only samples that contained no detectable HCP phase were films obtained by vacuum vapor deposition on kapton substrates. These films were from the same batch as the samples studied by Spataro (1972).

4.4 Dynamic Calibration Experiments

In the overall program the highest priority was given to obtaining dynamic loading and release calibration data that would be immediately applicable to the analysis of field data. Less emphasis was placed on

the other parts of the program, although they were important to our understanding of the behavior of ytterbium and the field gage. We chose this method because we felt that a good data base was needed before other effects of unknown magnitude could be sought.

All of the specimens used in the dynamic calibration shots were encapsulated in epoxy-impregnated fiberglass packages--smaller versions of the field transducer described by Grady et al. (1973) and Smith et al. (1972) and shown in Figure 3. This was done because Keough (1970) suggested that piezoresistant stress transducer response can be affected by the material surrounding it and, in fact, by the target material itself. We did not wish to test this hypothesis in detail because of the effort involved, but chose rather to encapsulate the specimens in the same immediate environment they would see if they were in the field, i.e., epoxy-fiberglass. This procedure reduces some of the uncertainty in transferring laboratory data to the field, but there was a price to be paid in terms of response time and disturbances to the main wave arising from the presence of the gage package. This problem will be treated in more detail later when individual shots are discussed. In the next sections we will describe our experimental facilities and the four basic shot designs we used to obtain the dynamic calibration data.

4.4.1 Experimental Facilities--The dynamic calibration experiments were performed on our 10.16-cm and 6.35-cm bore light-gas guns. Helium was used as the driving gas. The velocity was measured with pins which triggered and then stopped a pair of digital time counters, and another independent set of pins which triggered and produced time marks on a Cordin oscilloscope. Alignment of the target was accomplished by a device which lines up the target mount at the end of the barrel with the gun barrel. The targets were made flush with their respective mounting rings, and were installed on the prealigned target mount. All recording was done with oscilloscopes, and a Pulsar Model 301 three-channel constant current power supply was used to power the gages.

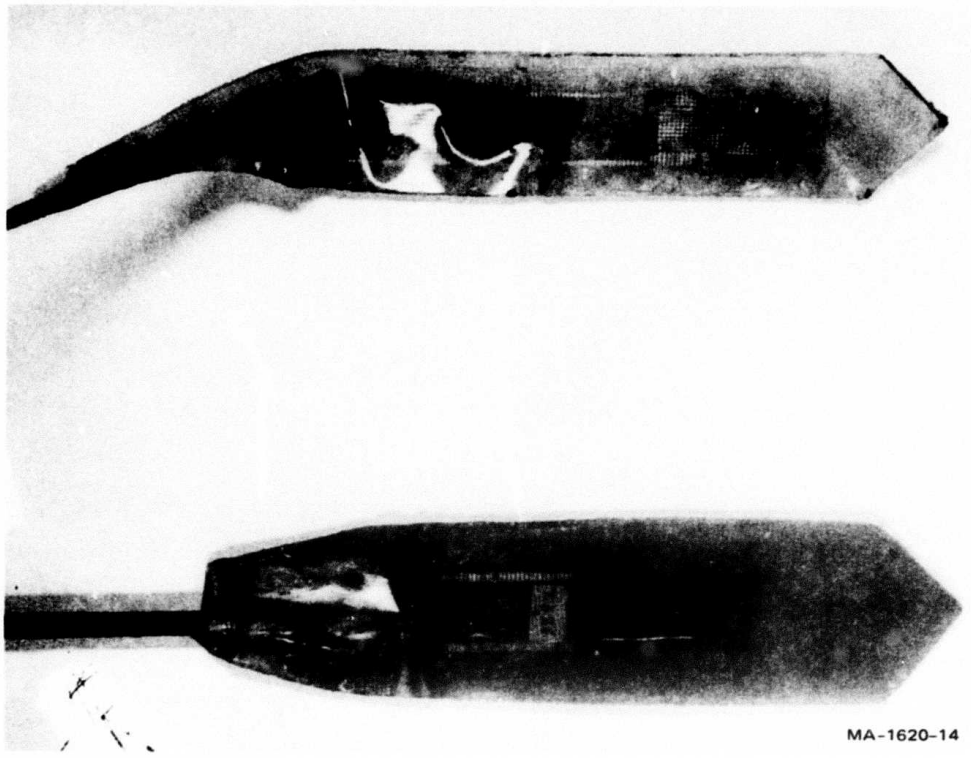

FIGURE 3 YTTERBIUM STRESS GAGE—RESISTANCE GRID ENCAPSULATED IN AN EPOXY-FIBERGLASS MATRIX; (UPPER) IN SITU PACKAGE, (LOWER) PACKAGE FOR GROUTING IN DRILL HOLES

A circuit for monitoring the pressure-induced resistance change in the transducer is shown in Figure 4. R_G is the gage resistance and R_S is a resistance in series with the recording transmission cable. The cable is terminated at the oscilloscope with R_T, a resistance equal to the characteristic impedance of the cable. I, the constant current, is provided by the gage power supply. To provide proper termination at both ends of the cable, the usual procedure has been to select R_S such that the sum of R_S and R_G is close to the characteristic impedance of the cable (Keough, 1967). The assumption of constant current in the gage is not satisfied, however, since a shunting current (I_2 in the figure) occurs. This creates an error in the gage factor and a correction including the effect of the shunt current must be performed. When

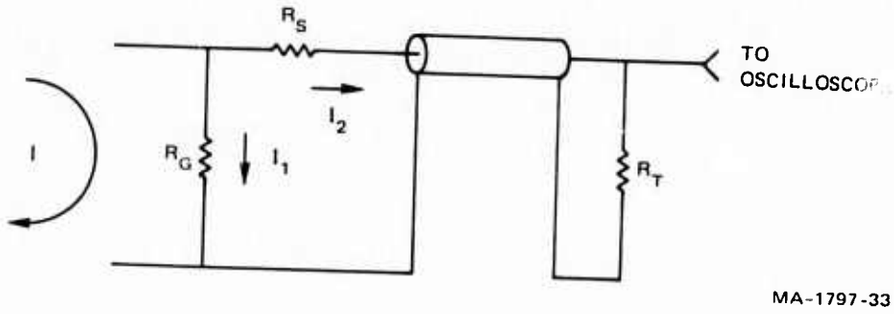

FIGURE 4 CIRCUIT FOR MONITORING TRANSIENT RESISTANCE CHANGES IN YTTERBIUM FOILS

ytterbium is used as the transducer material the correction term is considerable and the complication can be lessened by adjusting R_S such that the constant current assumption is satisfied. Single-ended cable termination is adequate. In the present work values of R_S equal to 500 and 1000 Ω were used at higher stress levels. This precaution reduced the shunting current to less than 1/2% of the total current in individual experiments. The voltage-time records were digitized directly from the oscillograms with a Whittaker Telecordex counter. The output was fed into a keypunch and the cards were used to plot the data and tabulate the fractional voltage change as a function of time. Conversion of $\Delta V/V_o$ to $\Delta R/R_o$ was done using Wilkinson's analysis (in Keough, 1968) of the recording circuit which is discussed in more detail in Appendix B.

4.4.2 High-Stress Step-Release Experiments--The step-release technique (Keough, 1970) produces one peak stress calibration point and a series of points on the unloading path originating at the peak stress obtained during the experiment. When a thin, high-impedance flying plate impacts a thicker target of lower shock impedance, a location in the target near the impact surface will first load up to some peak stress and then experience a series of transmitted release waves originating at the back of the projectile head. If both the projectile material and the target behave elastically (linear or nonlinear) in the stress

range of interest,* a series of stress states on one unloading path can be determined from a stress-particle velocity diagram of the two materials. Figure 6 shows a schematic of typical experiment design, and Figure 7 is a schematic x-t diagram which depicts the expected wave shape. Figure 8 is an impedance match diagram showing the stress states reached in a step-release experiment.

The targets were constructed from two pieces of 10.15-cm diameter GE Type 151 fused quartz. The dynamic properties of this material have been studied in detail by Barker and Hollenbach (1970). The front pieces (impact surfaces) were 0.2 cm thick and the backs approximately 1.9 cm thick. The gage leads were brought out through holes drilled in the back piece. In order to improve the probability of lead survival, dental amalgam was packed into the holes after the copper leads were brought out. This lead arrangement was very successful, and recording times of up to 10 μsec were achieved at stress levels of up to 20 kbar and more. The gage packages were glued to the back piece with Homolite epoxy. More epoxy was then poured around the packages and the front plate was pressed on, giving a total gage plane glue line and package thickness of between 0.020 and 0.025 cm. Figure 9 is a plot of a digitized oscillogram taken during Shot S19, the records from which are shown in Figure 10. The steps are evident, which allowed us to obtain good release data, but it can be seen that there were some transient disturbances to the flow caused by the presence of the low-impedance gage packages and glue line. There was also some apparent dispersion, which was caused by a small amount of shock tilt in conjunction with the presence of the thick glue line and gage package.

---

* Or, if (as shown in Figure 5) the release paths from all stress states up to and including the highest peak stress in the experimental series lie on the Hugoniot and are coincident, as in Plexiglas up to about 6 kbar.

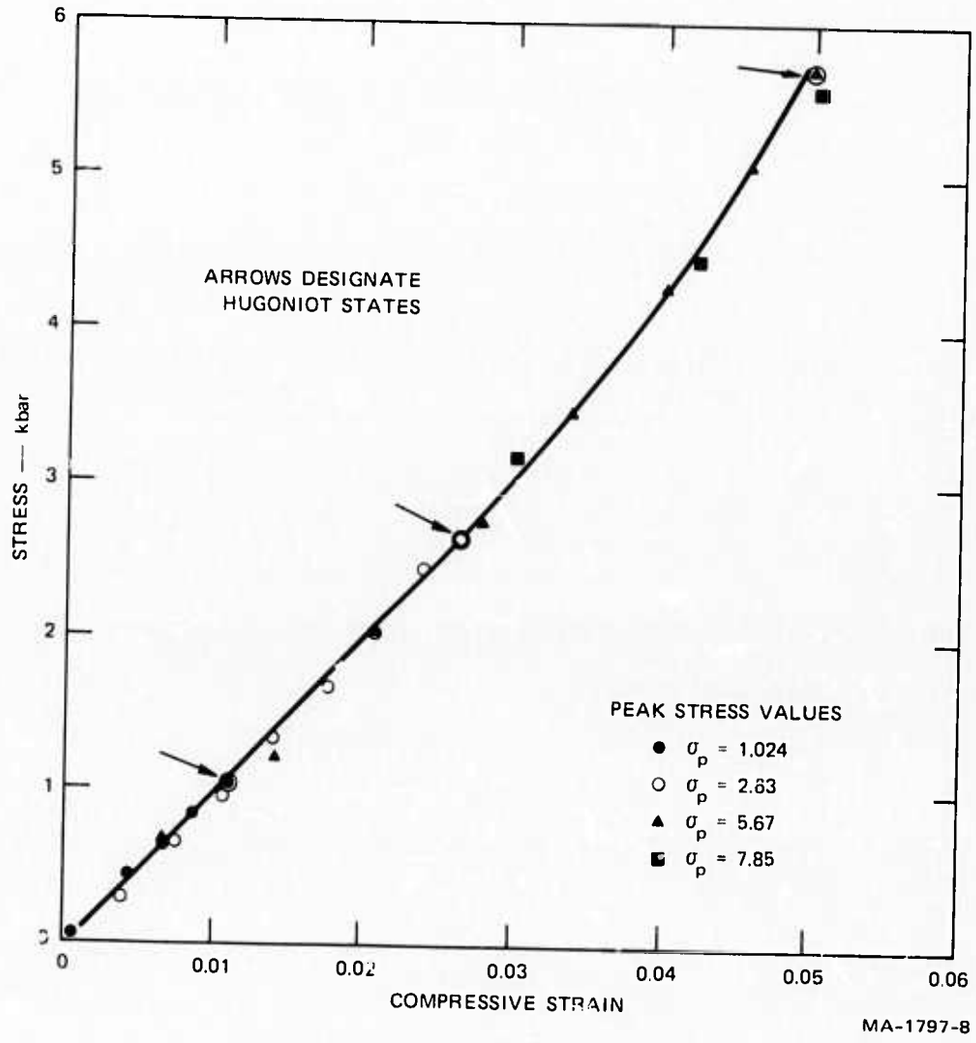

FIGURE 5 UNLOADING STRESS-STRAIN DATA FOR PMMA (BARKER AND HOLLENBACH, 1970)

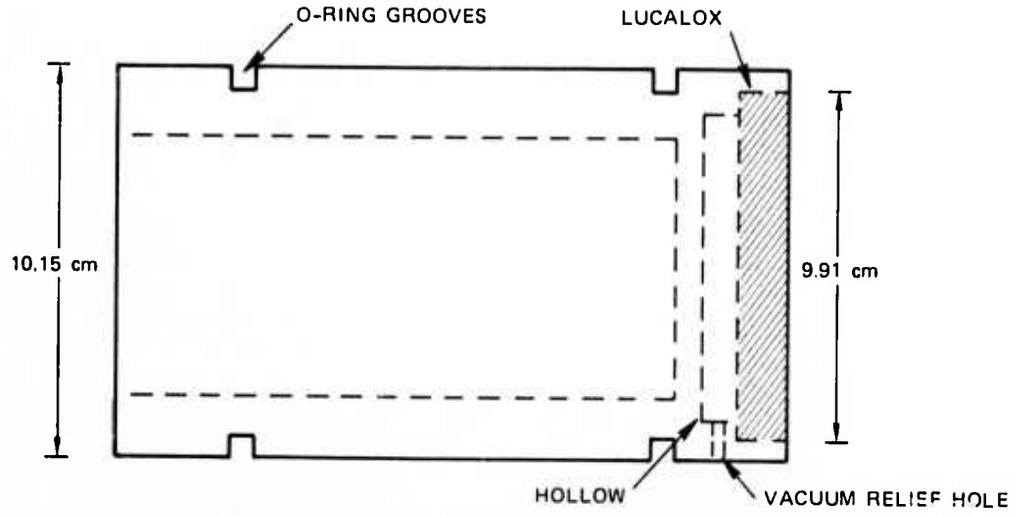

PROJECTILE: LUCALOX (HOT-PRESSED ALUMINUM OXIDE) HEAD, 0.5 cm THICK
6061-T6 ALUMINUM BODY

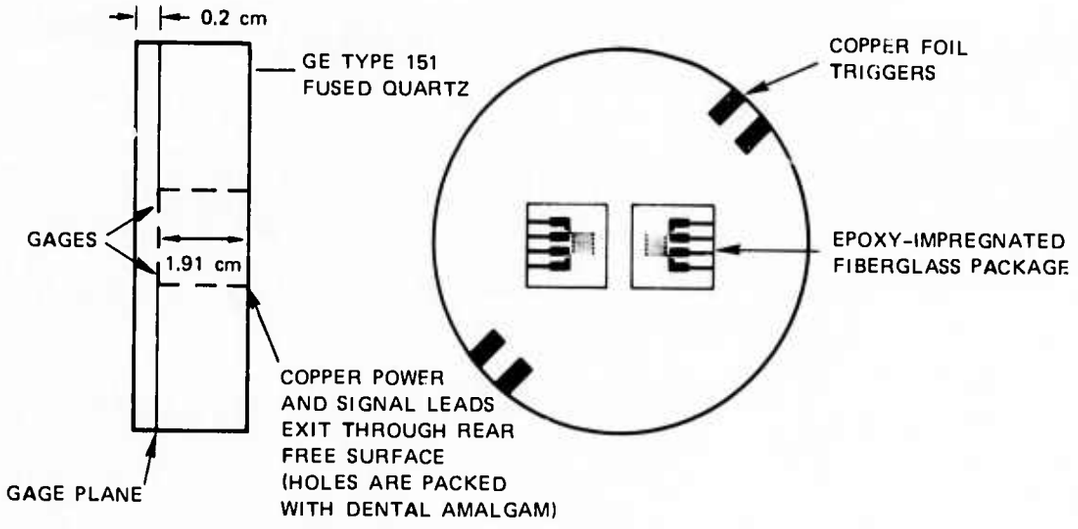

TARGET: GE TYPE 151 FUSED QUARTZ. DIAMETER 10.15 cm

Fiberglass-epoxy gage package is approximately 2 cm square and 0.025 cm thick. Gage grids are 0.635 cm square with ten elements, each 0.005 cm thick and 0.05 cm wide.

MA-1797-6

FIGURE 6 SCHEMATIC DIAGRAM OF LUCALOX-QUARTZ STEP-RELEASE EXPERIMENTS

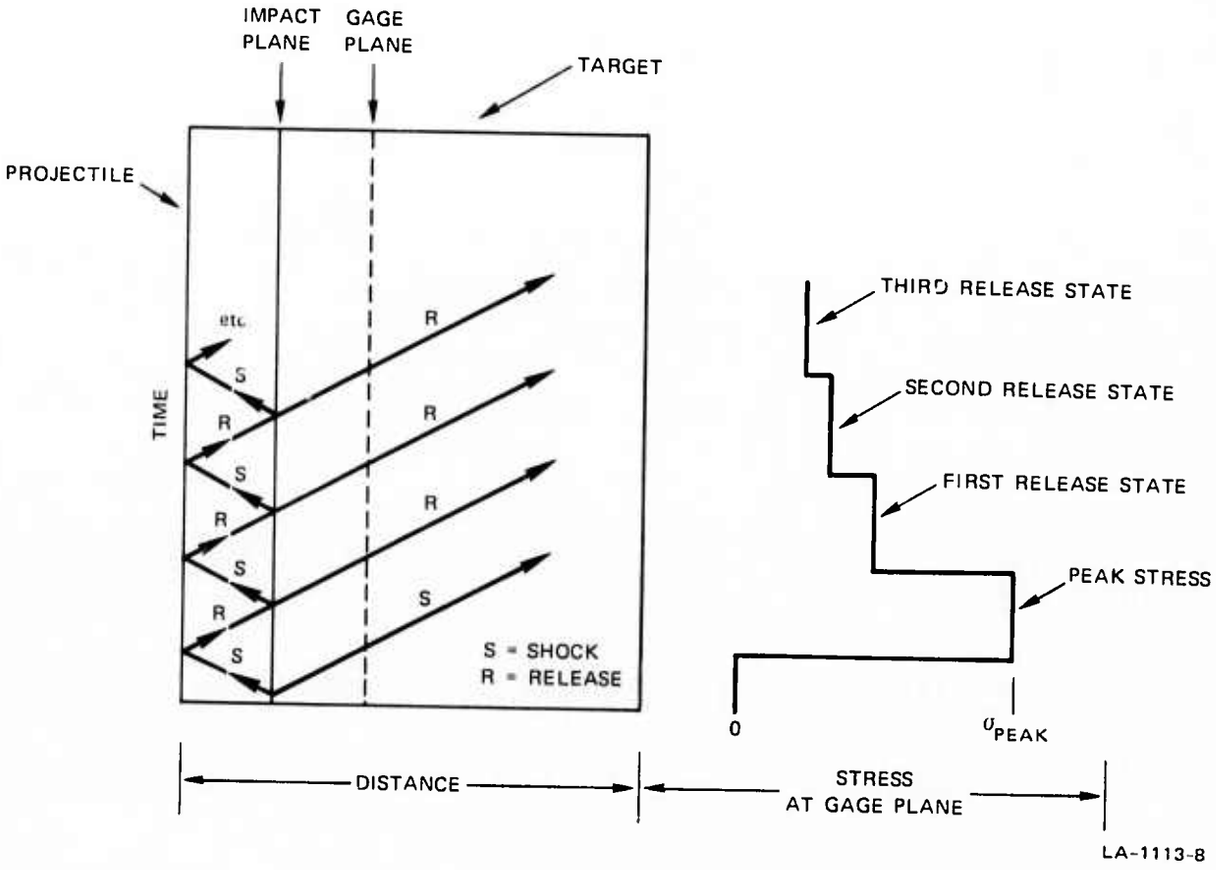

FIGURE 7 SCHEMATIC DIAGRAM OF WAVE BEHAVIOR IN STEP-RELEASE EXPERIMENT AND EXPECTED GAGE RECORD

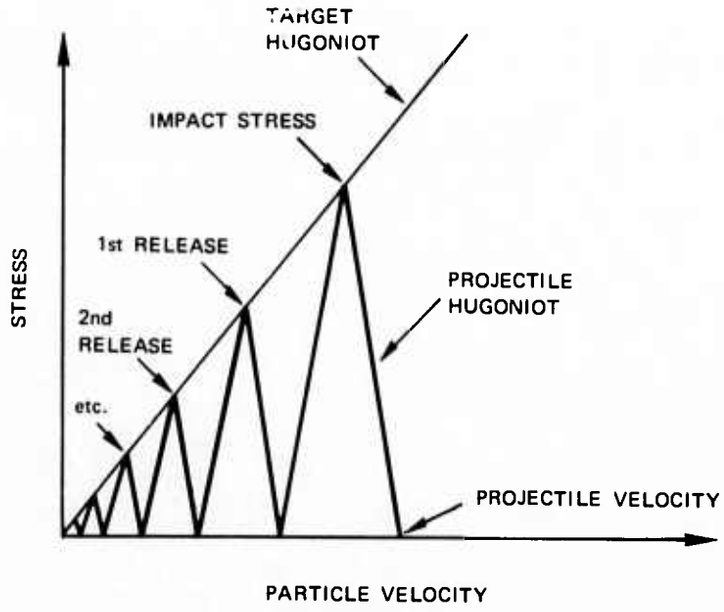

FIGURE 8 RELEASE STRESS STATES, IMPACT OF HIGH SHOCK IMPEDANCE MATERIAL ON LOWER IMPEDANCE TARGET

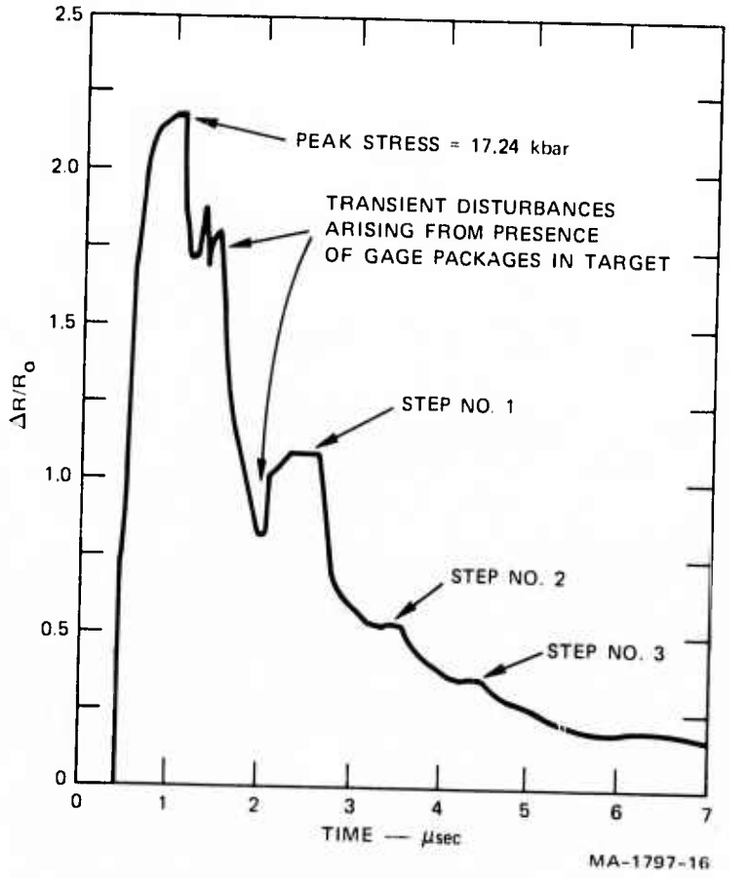

FIGURE 9 PLOT OF DATA FROM SHOT S19

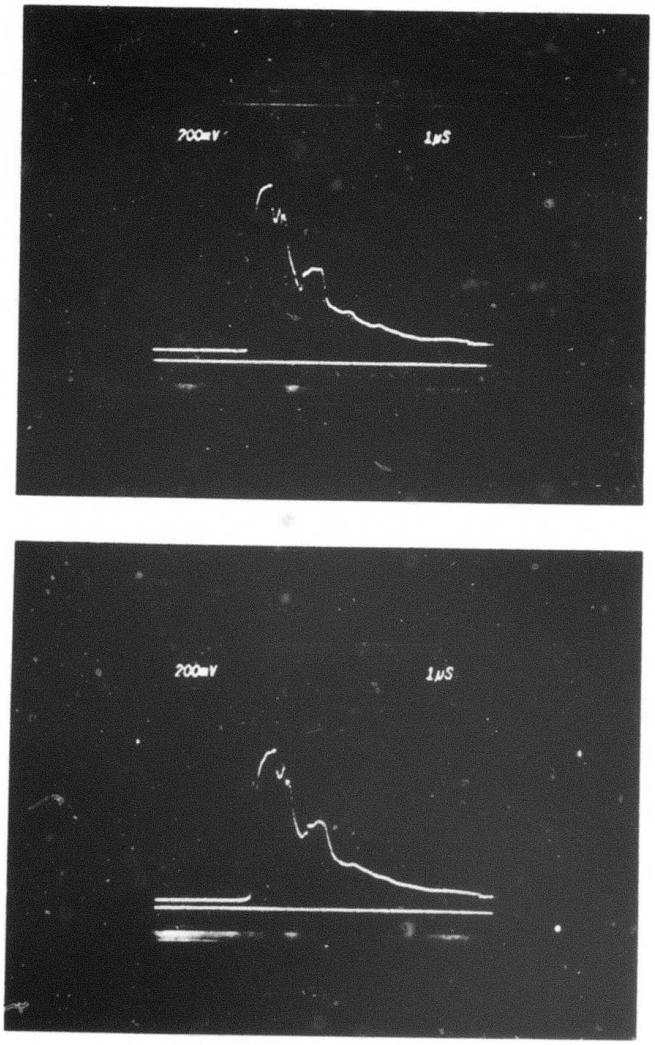

MP-1797-13

FIGURE 10 OSCILLOSCOPE RECORDS FROM SHOT S19

The power supply and slow-sweeping oscilloscopes were triggered with radial pins placed 2 to 5 mm from the impact surface, the arrival of the projectile closing a circuit between a pin and ground. Faster sweeping oscilloscopes were triggered with copper foil switches placed on the impact surface.

Two types of projectiles were used, depending on the velocity required to reach the proper stress level. Both were fabricated from 6061-T6 aluminum alloy and had 10.15 cm diameters, but the projectile used for the lower stress (8-15 kbar) experiments weighed approximately 15 kg and was 75 cm long, while the projectile used above this stress range weighed approximately 2 kg and was 18 cm long. The projectile heads were 0.5-cm thick Lucalox* plates approximately 9.9 cm in diameter. These plates were ground flat and parallel to within 0.0013 cm and were glued to the projectile with epoxy cement. There was a 0.635-cm hollow behind each head so that the release could originate at the rear free surface of the projectile head.

These shots were designed for a 4.5-μsec one-dimensional strain state in the projectile head over the gage package area. Actual time of one-dimensional flow in the target was greater than this, so that data obtained at times greater than 4.5 μsec were accepted as valid.

4.4.3 Low-Stress Step-Release Experiments--Figure 11 is a schematic diagram of the target and projectile used for a series of step-release shots in the 0.75-to-6-kbar range. The targets were made from two pieces of 7.62-cm diameter Type II UVA Plexiglas.† The dynamic mechanical properties of this material have also been studied by Barker and Hollenbach (1970). The front pieces (impact surfaces) were 0.2 cm thick, and the backs were 0.312 cm thick. The gage leads were brought out the sides of the targets. Recording times of 10 μsec and more were routinely obtained with this configuration. The gage packages were glued into a slot milled into the rear section, and then the target was assembled with Homolite epoxy.

* General Electric Co. brand of hot-pressed, high density aluminum oxide.

† Rohm and Haas, Inc.

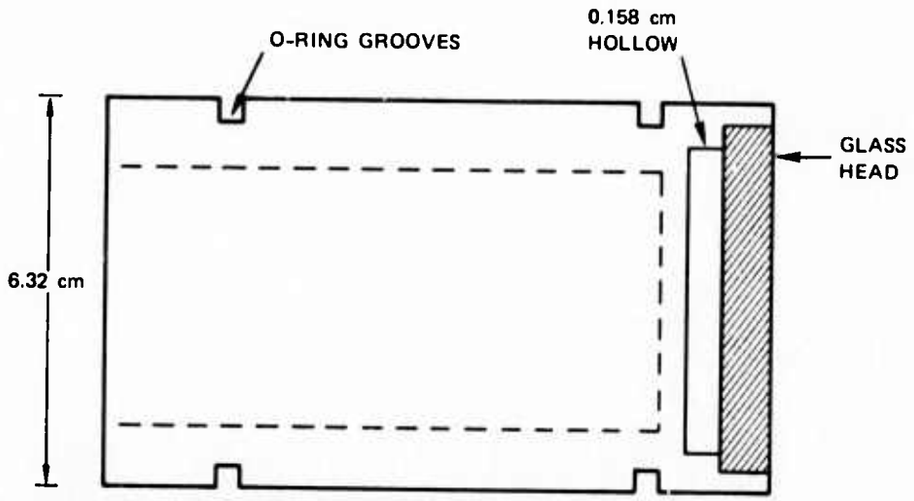

PROJECTILE: MIRROR OR SODA-LIME GLASS HEADS, EITHER 0.318 cm, 0.475 cm, OR 0.635 cm THICK
6061-T6 ALUMINUM BODY

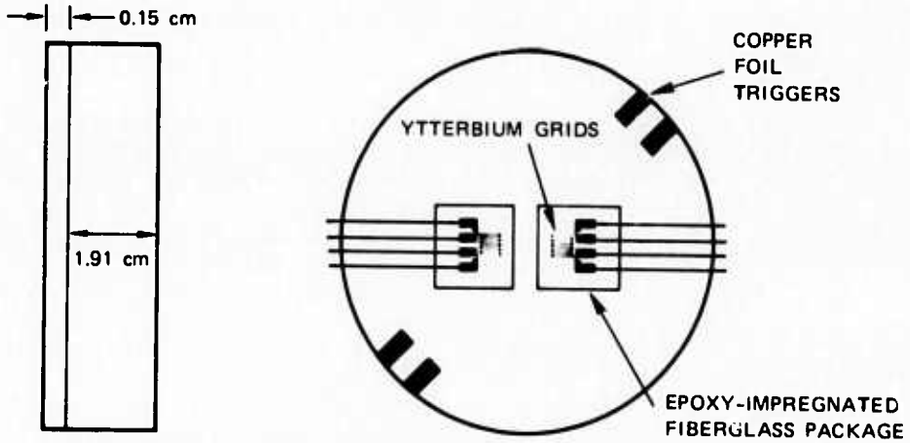

TARGET: TYPE II UVA PLEXIGLAS. DIAMETER: 7.62 cm

Fiberglass-epoxy gage package is approximately 2 cm square and 0.025 cm thick. Gage grids are 0.635 cm square with ten elements, each 0.005 cm thick and 0.05 cm wide.

MA-1797-7

FIGURE 11 SCHEMATIC DIAGRAM OF GLASS-PLEXIGLAS STEP-RELEASE EXPERIMENTS

The total thickness of the gage packages and glue was about 0.025 cm. The oscilloscopes and power supply were triggered in the same way as the other step-release shots.

Figure 12 is a plot of the data obtained during Shot S14, and Figure 13 shows the actual records. Because the impedance of the epoxy and the epoxy-impregnated fiberglass is closer to that of Plexiglas than it is to fused quartz, the transient disturbances are of much smaller magnitude and do not interfere in any important way with the wave shape. The amount of dispersion is very small, and the data from this series are generally of very good quality with easily discernible steps.

Two types of projectiles were again used, the choice depending on the velocity required in the experiment. For low stress shots (2 kbar and below) we used 30.5-cm long, 6.32-cm diameter hollow-bodied projectiles weighing approximately 2.2 kg. To achieve stress levels between 2 and about 6 kbar, we used a 15.25-cm long, 6.32-cm diameter hollow-bodied projectile which weighs approximately 0.6 kg. The projectile heads were glass disks either 0.318, 0.476, or 0.635 cm thick with 5.75-cm diameters. The disks were glued into a recess in the front of the projectiles with epoxy cement. A 0.158-cm vacuum-relieved hollow area was left behind each disk. The density and sound velocity of each disk were measured separately so the peak stress and the steps could be accurately calculated.

The maximum stress at which this shot configuration could be used was approximately 6 kbar. There are no rate effects below this stress level, and the release paths for Plexiglas obtained by Barker and Hollenbach (1970) no longer coincide with the Hugoniot of the material nor do they coincide with each other above this limit. These conditions of no rate effects and coincidence of Hugoniot and release paths were required for calculation of the release states in the calibration experiments. The glass was assumed to be linearly elastic in this low stress region

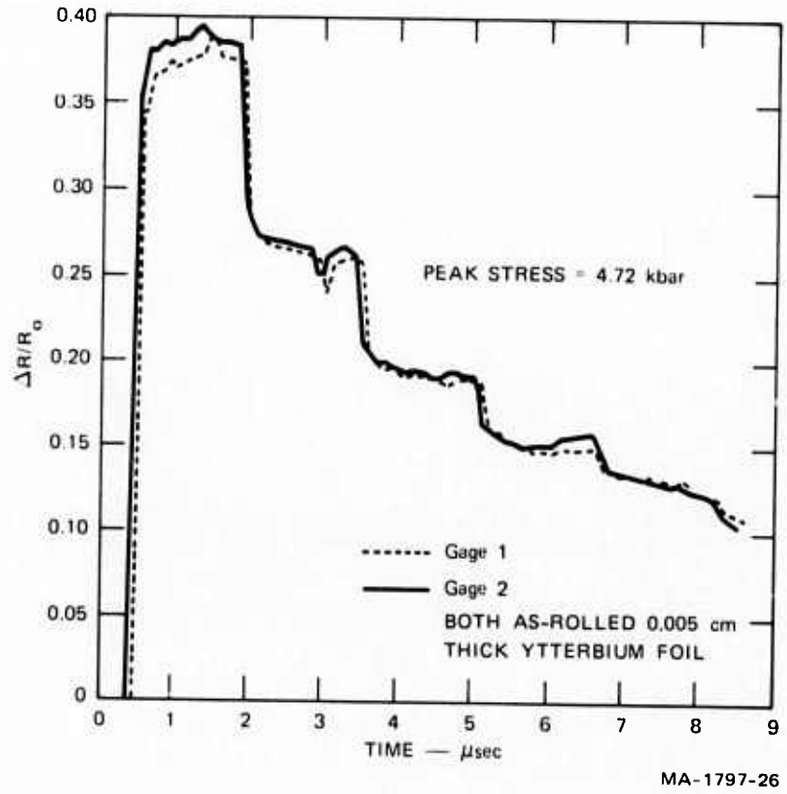

FIGURE 12 PLOT OF DATA FROM SHOT S14

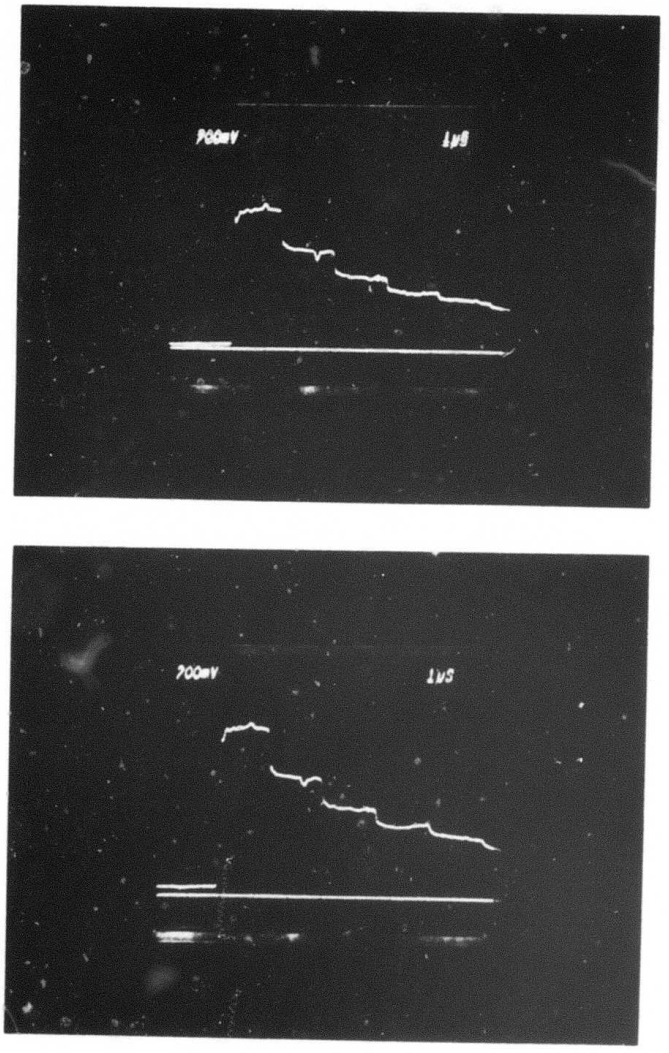

MP-1797-12

FIGURE 13 OSCILLOSCOPE RECORDS FROM SHOT S14

(Seaman et al. 1969; Rosenberg and Ginsberg, 1972) and the two types used had shock impedances of 14.7 ± 0.1 and 14.5 ± 0.1 g · mm/cm^3 · μsec.

We expected that the minimum one-dimensional strain recording time, calculated by finding the time of arrival of edge rarefactions at the gage area using the glass projectile head shock velocity rather than the plexiglas target velocity, was about 4 μsec. Actual usable recording time was considerably greater than this.

4.4.4 Double-Shock Experiments--Figure 14 is a schematic diagram of the target and projectile used for a series of low stress experiments in which we obtained two loading points and data on the zero-stress residual resistance in each experiment. Figure 15 is a schematic diagram of the wave interactions, and Figure 16 shows how the second wave stress level is obtained.

The targets were again made from two pieces of 7.62-cm diameter Type II UVA Plexiglas. The front piece was 0.15 cm thick and the back 0.317 cm thick. Copper electrical leads were brought out the sides of the targets. Recording times of up to 10 μsec were obtained at the lowest stress levels. The targets were assembled in the same way as the low stress step-release shots described earlier, and power supply and oscilloscope triggering was also accomplished by the same methods.

The projectiles were 6061-T6 aluminum, 30.5 cm long and 6.32 cm in diameter, and weighed about 2.2 kg. The projectile heads were 1.06-cm thick disks of Plexiglas glued to the projectile with epoxy cement. There was no hollow space behind the head, so stress release originated at the rear free surface of the target.

Figure 17 is a plot of the data obtained during Shot S7 and Figure 18 contains the actual records. The small spikes occurring between 5 and 6 μsec and between 7 and 8 μsec arise from flow disturbances caused by the gage package, but the trace returns to the equilibrium level very quickly. We consider the value of $\Delta R/R_o$ at the first peak and the residual resistance at zero stress ($\Delta R_H/R_o$) to be more reliable data than the

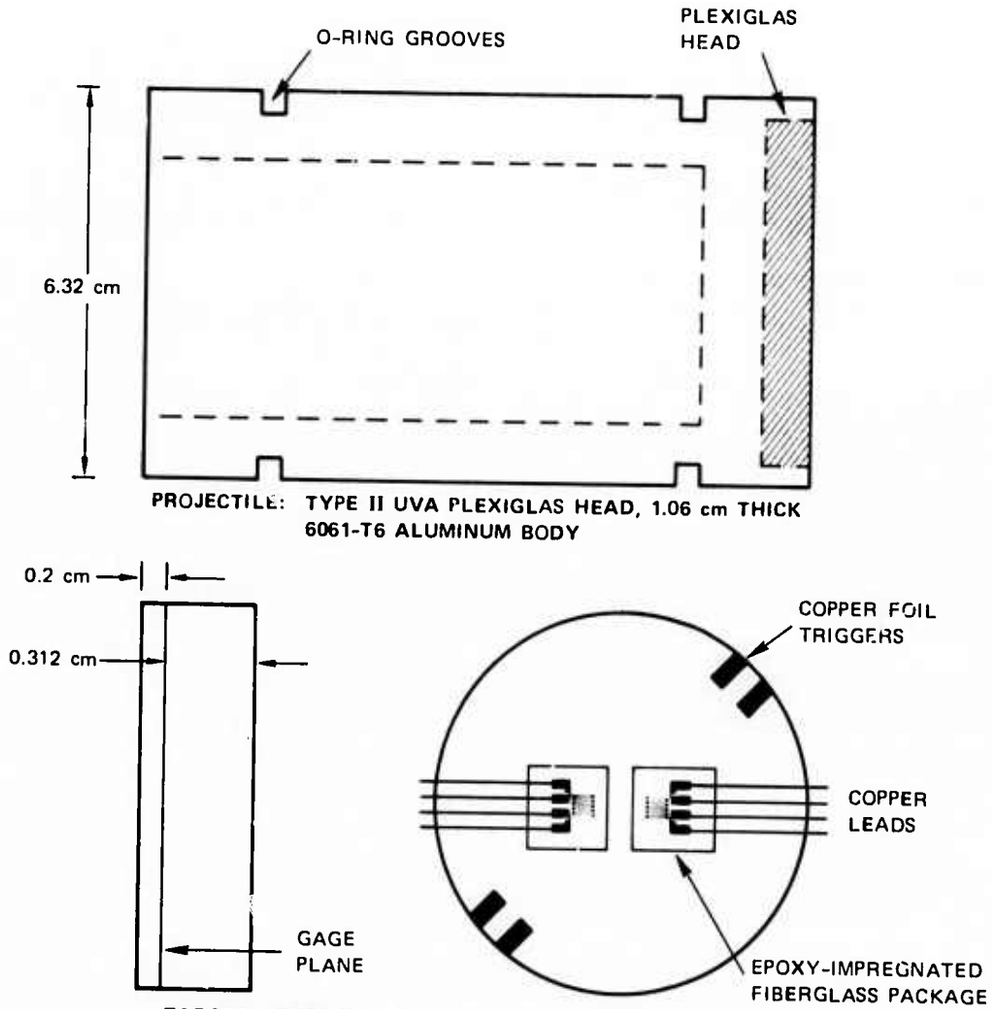

FIGURE 14 SCHEMATIC DIAGRAM OF PLEXIGLAS-PLEXIGLAS DOUBLE SHOCK EXPERIMENTS

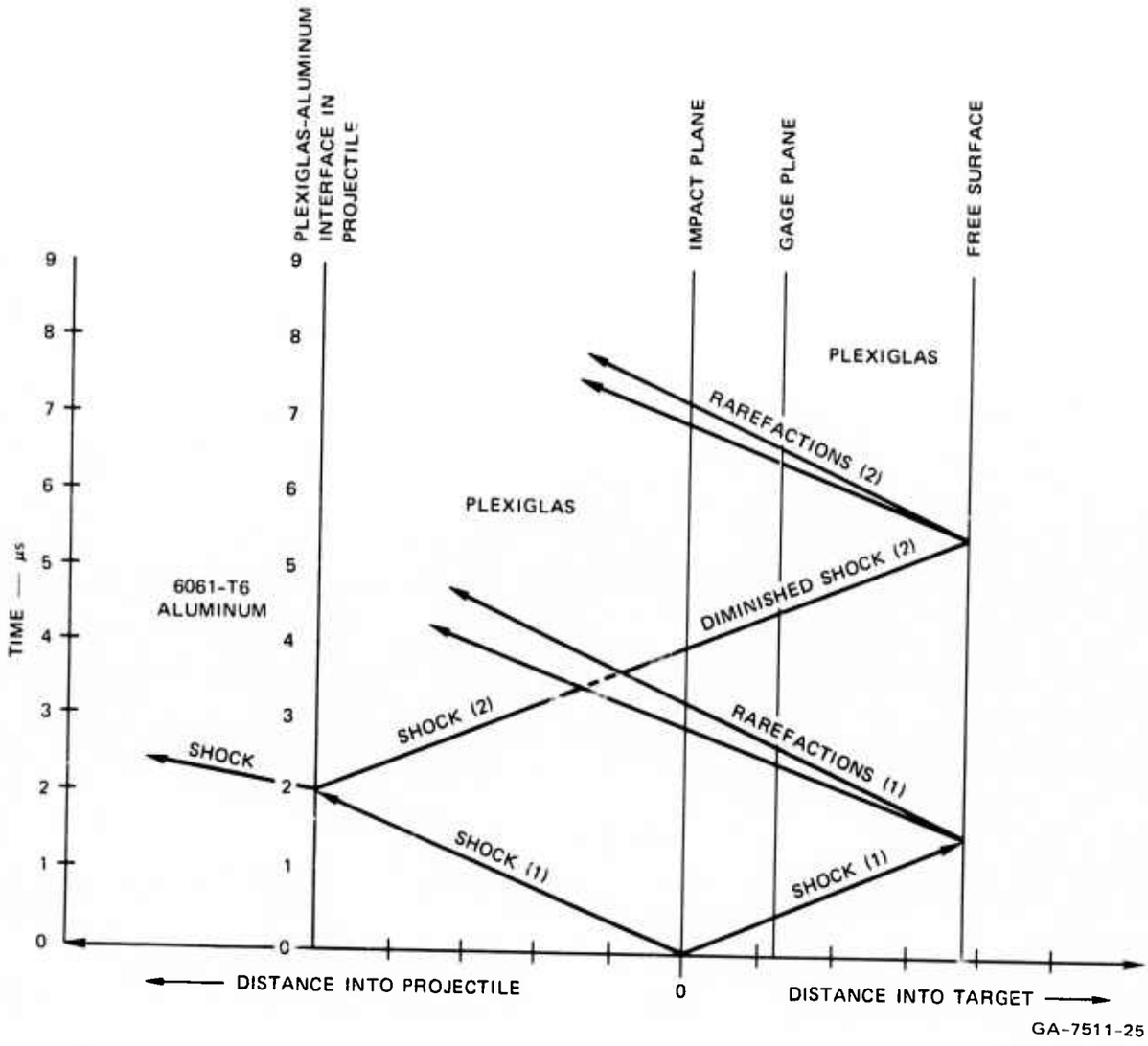

FIGURE 15 SCHEMATIC DIAGRAM OF WAVE INTERACTIONS IN DOUBLE SHOCK EXPERIMENTS

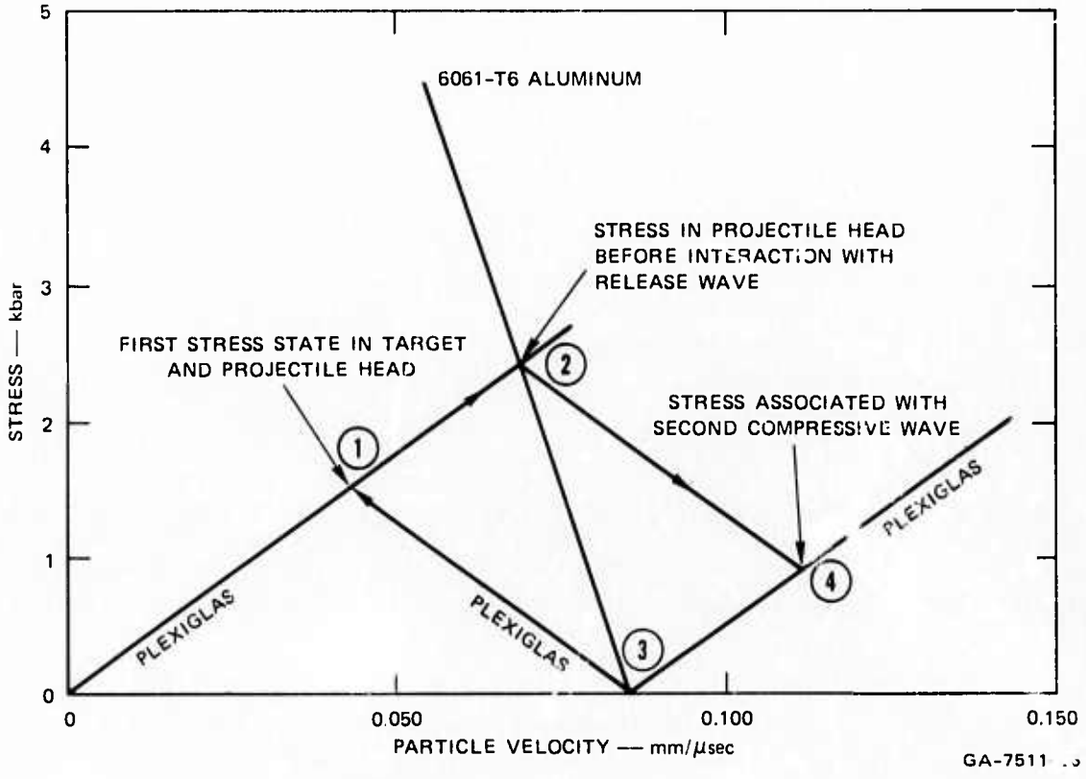

FIGURE 16 SCHEMATIC DIAGRAM OF IMPEDANCE MATCHING TECHNIQUE FOR DETERMINATION OF STRESS ASSOCIATED WITH SECOND COMPRESSIVE PULSE

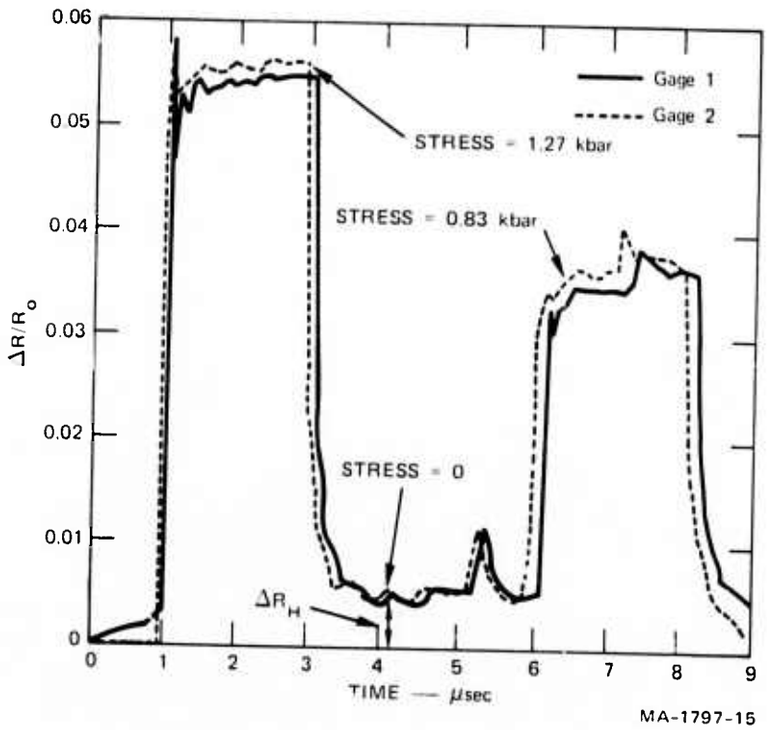

FIGURE 17 PLOT OF DATA FROM SHOT S7

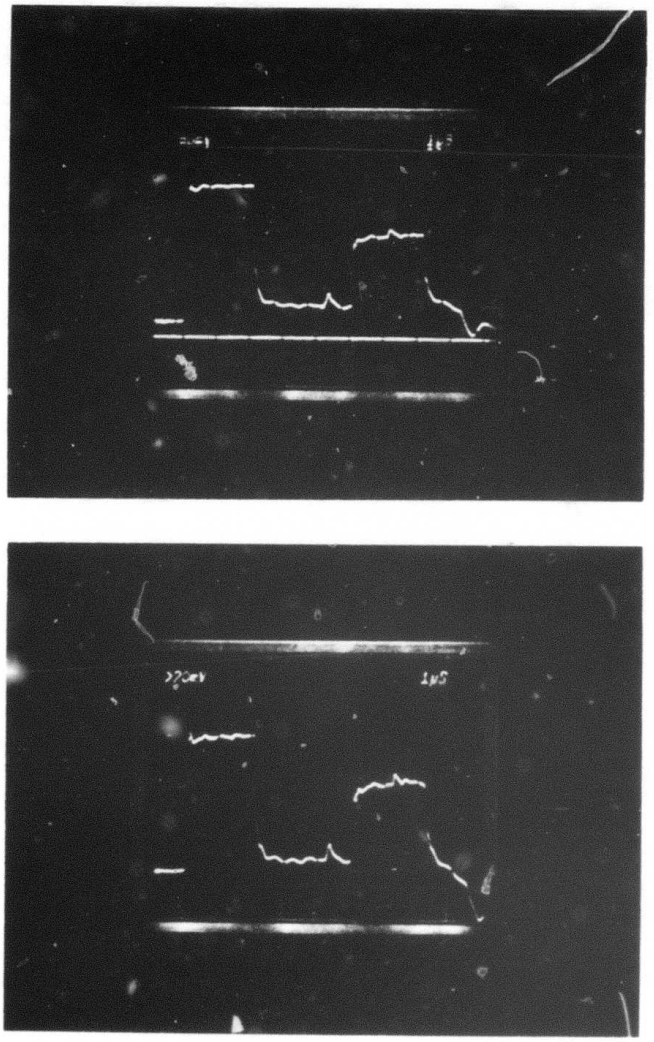

MP-1797-11

FIGURE 18 OSCILLOSCOPE RECORDS FROM SHOT S7

resistance change associated with the second loading. We base this on our uncertainty about the reloading behavior of both Plexiglas and ytterbium, especially around the yield point of ytterbium. The magnitude of this uncertainty will be discussed in Section 4.7.5. We expected approximately 8 μsec of one-dimensional flow time in the gages and we believe the data are good out to at least this time.

Two other double-shock experiments (S29 and S30) of a different type were tried to see if there was a significant amount of path dependence during loading. Figure 19 is a schematic diagram of the target and projectile arrangement used to produce waveforms of the type shown in Figure 20.

The targets contained a total of four gage packages, two in Type II UVA Plexiglas and two in soda-lime glass (impedance = 14.7 ± 0.1 g.mm/cm^3. μsec). Each target consisted of two 15-cm diameter 0.158-cm thick Plexiglas disks and two 15-cm diameter, 0.317-cm thick soda-lime glass disks. Two gage packages were placed between the Plexiglas disks and two between the glass disks, and all four disks were then cemented together with epoxy-resin. The leads were brought out the sides of the target.

The projectiles were fabricated from 6061-T6 aluminum cylinders 10.15 cm in diameter and 18 cm long, and weighed approximately 2 kg. The heads were 9.9-cm diameter, 1.27 cm thick Plexiglas disks, which were glued directly into a machined space in the front of the projectile and butted directly up against the aluminum so that all stress relief originated at the rear free surface of the targets. Triggering of the power supply and oscilloscopes was accomplished in the same way as in the low stress step-release shots. We expected one-dimensional strain states in the target area occupied by the gage packages of about 8 μsec.

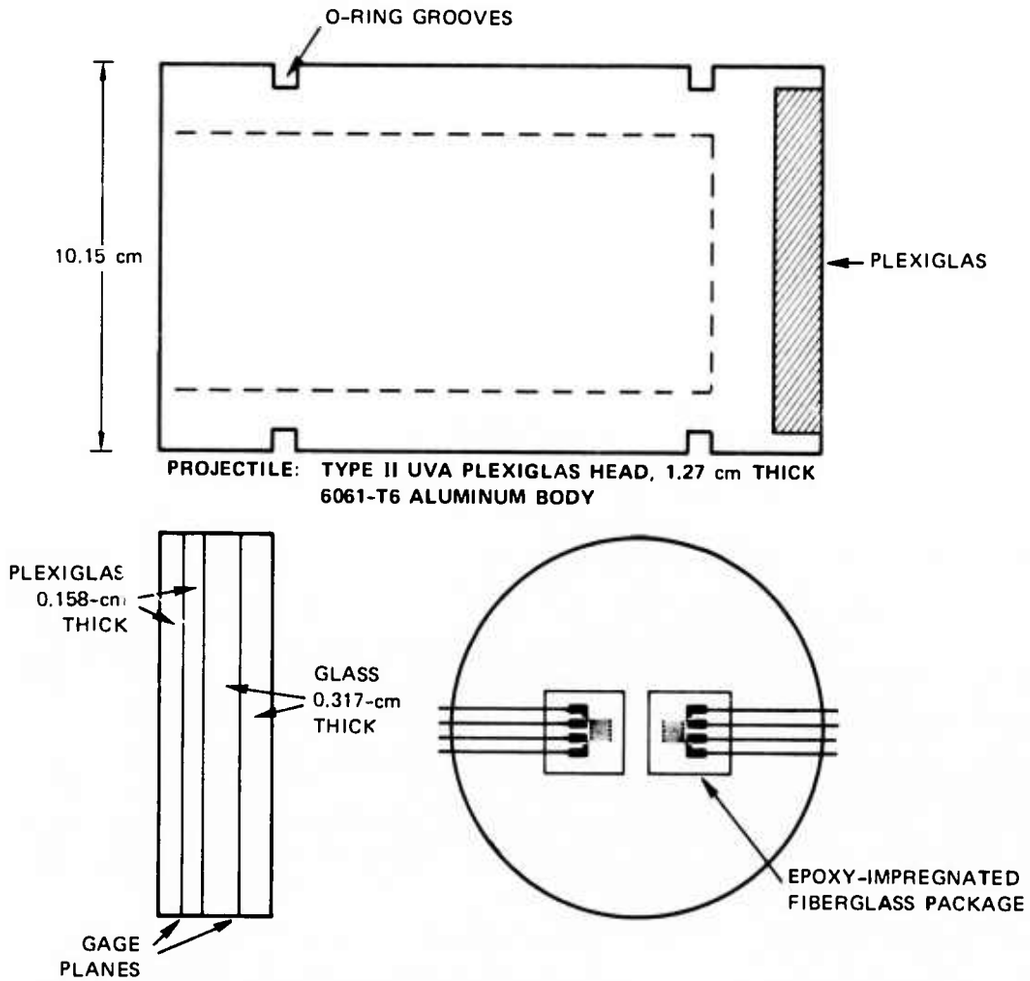

FIGURE 19 SCHEMATIC DIAGRAM OF STEP-LOADING EXPERIMENTS

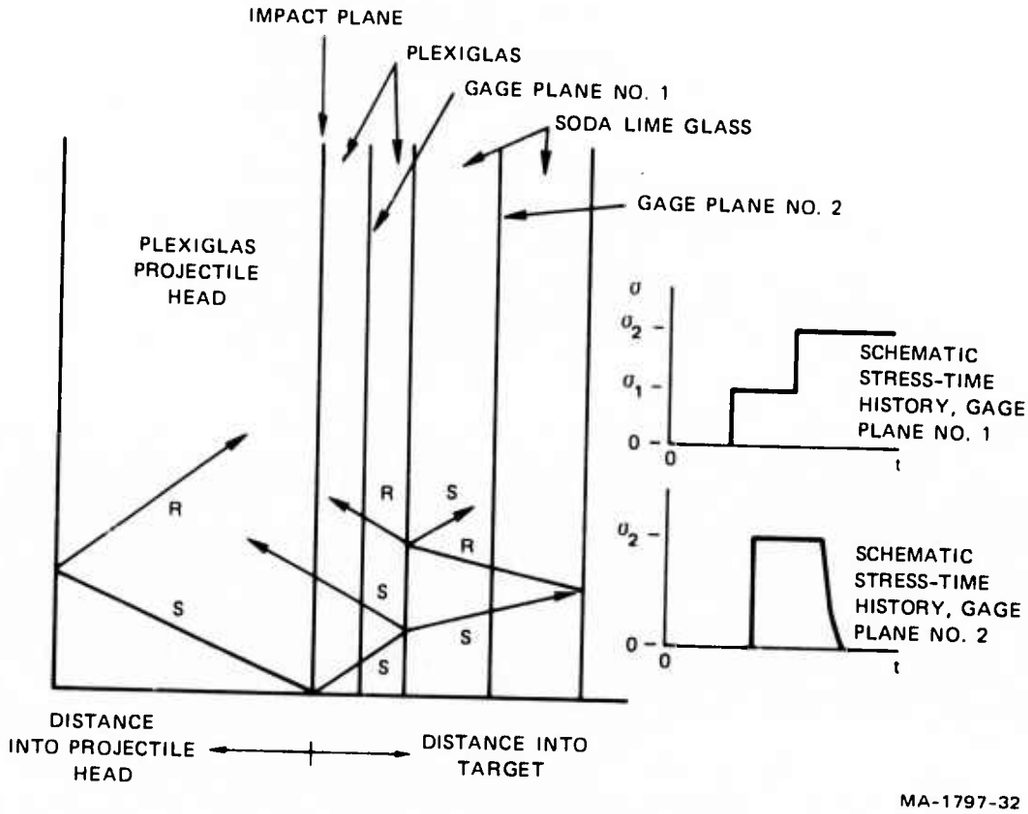

FIGURE 20 SCHEMATIC DIAGRAM OF SURFACE INTERACTIONS FOR EXPECTED STRESS-TIME HISTORIES FOR SHOTS S29 AND S30

4.4.5 Phase Transition Experiment--A number of investigators (Hall and Merrill, 1963; Hall et al. 1963) have reported that the pressure-induced FCC → BCC phase transition seen in ytterbium is quite slow under hydrostatic pressure conditions, sometimes requiring many hours for completion. This raised the possibility that ytterbium might be usable as a stress transducer above the phase transition point if the transition did not take place during dynamic loading in the microsecond or millisecond time scale. If the metastable FCC phase could be retained, we could, theoretically, calibrate above the equilibrium transition point and continue to use ytterbium as a transducer material at stresses as high as we could go without causing the transformation. In addition, an experiment where the peak stress reached was above the ~ 39-kbar hydrostatic transition point was necessary to fix the upper limit of usefulness of ytterbium if the transition did take place. Keough (1970) did one experiment in which he double-shocked an ytterbium film to a final stress of approximately 44 kbar (the first wave stress was about 33 kbar) and he reported seeing a decrease in resistance when the second wave reached the ytterbium and said that the decrease continued to be gradual, not immediate. We have examined Keough's original oscilloscope records and found (1) the resistance decrease attributed to the phase change occurs within 200 nsec after the arrival of the second compressive pulse and (2) a decrease to about 50 per cent of the peak resistance change required less than 1 μsec. Our only hesitation in accepting these data as a measure of the kinetics of the FCC → BCC transition was that the gage showed some anomalous behavior during the decrease, and the shape of the trace could have conceivably been attributed to gage failure after the arrival of the second compressive pulse. In addition, Keough assumed that the resistance change he saw at the shock-induced phase transition point corresponded to the hydrostatic phase change stress, i.e., ~ 39 kbar, whereas if he had fit his data to a curve

without that point and extrapolated, he would have predicted a shock-induced phase change stress of closer to 35 kbar, and the upper end of his curve would have had a different shape.

One experiment was done in an attempt to answer some of the questions discussed above. A soda-lime glass target was constructed (impedance - 14.7 ± 0.1 gm · mm/cm^2 · μsec) which contained two 0.005-cm thick ytterbium foil grids and a 0.0025-cm thick manganin* foil stress gage. It was impacted with a glass-headed projectile designed to produce a 1-μsec flat-topped wave of approximately 40-kbar stress intensity. The release originated at the back of the projectile head, and triggering was done with the usual combination of radial pins and foil switches. The manganin gage was included as a standard for comparison because it should produce the correct wave-form in a simple material like glass, and also should give the magnitude of the stress within the confidence limits associated with manganin gages. The results of this experiment are discussed in Sections 4.6.2 and 4.7.6.

4.5 Static Experiments

Two other types of experiments were performed to ascertain the effects of stress (or strain) on the electrical resistance of ytterbium. These were static (but not hydrostatic) compression tests and tensile strain tests. The compression tests were done to explore the possible significance of rate effects in the relationship of stress to electrical resistance. If there was no significant difference between static and microsecond tests, then the millisecond response should be no different. The tensile strain experiments were done to ascertain the effect of strain caused by divergent flow on field gage response.

---

* Driver-Harris, Inc.

4.5.1 Static Compression Tests--Static electrical resistance vs compressive stress tests were done on bare 0.0025-cm (1-mil) foil so that results could be compared with previous data (Ginsberg, 1971) and on fiberglass-encapsulated 0.005-cm foil to compare the results with the data from this program. The bare specimens, which were grids identical to those used in the shock experiments, were glued down to a 5-cm diameter Plexiglas disk, 0.6 cm thick and covered with a disk of the same size. The encapsulated specimens were tested in the same manner, but in one experiment steel disks were substituted for the Plexiglas. Pressure was applied by a hydraulic ram system, and resistance measurements were made with either a double Kelvin bridge or Cimron Model 6853 digital multimeter.

4.5.2 Tensile Strain Tests--Stress waves originating from the detonation of high explosives or nuclear devices in or above the ground have a diverging component which probably causes some distortion of the signal obtained with piezoresistant stress gages. This distortion would arise from deformation of the active element in directions contained in the plane of the gage element. Discussions of this phenomenon are contained in Keough (1970) and Keough et al. (1971), but these discussions assume that the flow field is cylindrically divergent (rather than spherically divergent), that all flow in the gage is plastic, and that the resistivity of the gage remains constant. Each of these assumptions can have a major effect on any analysis of the real situation. See further discussion in Section 4.7 and Appendix A.

Our tensile strain experiments were designed to be exploratory in nature; that is, it was not completely obvious which of many possible experiments would be the most relevant to the field gage interpretation problem. The configuration finally chosen was the dog-bone tensile specimen with attached ytterbium grid and strain gage, as shown in Figure 21.

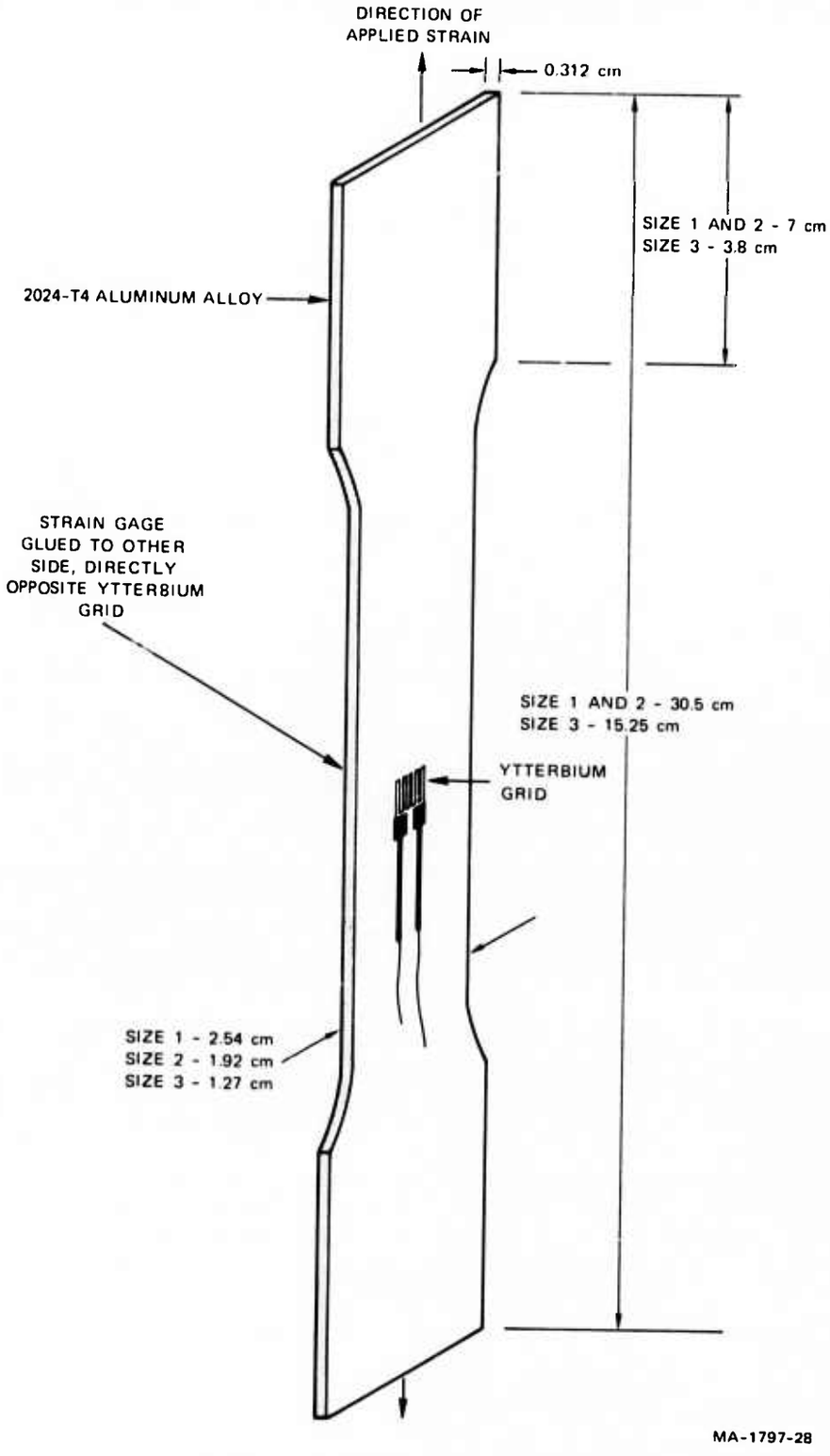

FIGURE 21 DOGBONE TENSILE SPECIMENS

The dog bones were mechanically cleaned and then treated with M-Prep Conditioner* and M-Prep Neutralizer 5* and both the strain gages (Model No. EP-08-250BG-120*) and ytterbium grid were bonded to the center of the gage section with GA-5 or GA-2 strain gage cement.* Electrical connections were made through copper strips which were spot-welded to the ytterbium gage leads. Electrical lead wire was then soldered to the copper. Strain was applied to the smaller dog bones with a screw-driven tensile tester, and to the larger ones with an hydraulically driven apparatus.

The 120-Ω strain gages were monitored by a Wheatstone bridge circuit driving the X-axis of a high-impedance X-Y recorder. One leg of the bridge was the active gage and the opposite leg was an identical gage mounted on a similar aluminum test strip to provide gage temperature compensation.

The 1.5 Ω ytterbium gages could not be measured with a standard Wheatstone bridge because of their low resistance, so a bridge circuit with a high gain amplifier was used to provide an adequate signal to drive the Y-axis of the X-Y recorder. This arrangement made it possible to plot the change in resistance of the ytterbium gages as a function of the specimen strain, which was the information we wished to obtain from these experiments.

4.5.3 Direct Divergent Flow Simulation--Simulation of spherical divergent flow was attempted by cementing ytterbium grids to the inflatable sphere† shown in Figure 22 and the change in electrical resistance monitored as a function of local strain (measured optically) as the sphere was inflated. Although changes were seen in resistance as the sphere size was changed, we were unable to show conclusively that the strain measured on the sphere surface adjacent to the ytterbium grid was equal to or had

---

* Micro-Measurements, Inc., Romulus, Michigan.

† Sun Products Corp., Barberton, Ohio 44203, No. 10135.

FIGURE 22 DIVERGENT FLOW SIMULATOR (YTTERBIUM GRID IS ATTACHED TO HAND SECTION AT LOWER RIGHT)

some simple relationship with the strain in the grid, and we were unable to measure the actual grid strain with sufficient accuracy. This experiment was abandoned, but the same type of experiment using a stiffer sphere material might give useful results.

4.6 Results

This section presents the results of each of the types of experiments performed to study the electrical resistance of ytterbium as a function of stress, strain, or temperature. These results are discussed in detail in the Interpretation and Discussion Section (Section 4.7) that follows.

4.6.1 Dynamic Calibration Experiments--The results of our dynamic calibration shots are shown in Tables 4 and 5 and Figures 23 through 41. Table 4 contains all of the data points obtained during the course of this program and some that were obtained between the completion of our previous effort (Ginsberg, 1971) and the beginning of the present program from shots that were performed to solve specific calibration problems. The latter are designated as the IRD series shots. All data that were rejected are identified, and the reasons for rejection are discussed later in the report. The loading data are the set of all points reached by single shock loading to a steady-state end state, and consist of the set of $\Delta R/R_o$ and σ values contained on the first line of the data identified with each shot. The unloading data are, for each shot, the set of points (starting with the peak stress) contained in the columns labeled Gage 1, $\Delta R/R_o$ and Gage 2 $\Delta R/R_o$. Brief information of particular interest about each shot is included in the comments where appropriate. Table 5 contains the function $\sigma_i = f_i(\Delta R/R_o)$ we have chosen to represent each of the unloading paths* and the standard deviation in stress associated with each fitted equation.

---

*Our criteria for the choice of the function are discussed in Section 4.7; the choice is not always the best fit in terms of minimizing the sum of the squares of residuals about the mean.

Table 4

SUMMARY OF DYNAMIC CALIBRATION EXPERIMENTAL DATA

Shot Number	Type	Stress kbar	Gage 1 $\Delta R/R_o$	Gage 2 $\Delta R/R_o$	Comments
S1	Lucalox	13.82	1.492	1.485	Excessive shock tilt present.
	Quartz	7.74	0.817	0.831	
	Step release	4.24	0.373	0.347	
		0	0.136	0.125	
S2	Lucalox	29.97	4.332	4.912	
	Quartz	17.48	2.060	2.262	
	Step release	9.90	0.799	0.967	
		5.47	0.594	0.702	
		0	0.153	0.173	
S3	Plexiglas-	1.02	0.0384	0.0383	
	Plexiglas	0.62*	0.0231*	0.0242*	* Reload data
	Double shock	0	0	0	
S4	Glass-	1.11	0.0505	0.0442	
	Plexiglas	0.70	0.0336	0.0309	
	Step release	0.44	0.0198	0.0176	
		0.28	0.0119	0.0109	
S5	Plexiglas-	1.75	0.0902	0.0932	*Reload data. Note that reload
	Plexiglas	1.11	0.0427*	------	value of 1.11 kbar is less than
	Double shock	0	0.0187	0.0178	single shock value obtained in S4.
S6	Glass-	1.95	0.106	0.101	
	Plexiglas	1.20	0.0771	0.0729	
	Step release	0.75	0.0527	0.0501	
		0.48	0.0341	0.0341	
S7	Plexiglas-	1.27	0.0562	0.0575	
	Plexiglas	0.83	0.0316*	0.0321*	* Reload data
	Double shock	0	0.0052	0.0053	
S8	Glass-	1.46	0.0808	0.0629	
	Plexiglas	0.91	0.0576	0.0445	
	Step release	0.57	0.0387	0.0288	
		0.37	0.0291	0.0172	

Table 4 (continued)

Shot Number	Type	Stress kbar	Gage 1 $\Delta R/R_o$	Gage 2 $\Delta R/R_o$	Comments
S9	Plexiglas-	0.52	0.0180	0.0170	
	Plexiglas	0.32	0.0132*	0.0131*	* Reload data
	Double shock	0	0	0	
S10	Glass-	0.736	0.0336	0.0235	
	Plexiglas	0.466	0.0219	0.0164	
	Step release	0.298	0.0140	0.0106	
		0.192	0.0075	0.0058	
S11	Lucalox-	24.03	3.560	3.922	Bare (nonencapsulated) gages.
	Quartz	13.85	1.721	1.872	Compare with S12.
	Step release	7.76	0.769	0.793	
		4.25	0.325	-----	
		0	0.175	0.163	
S12	Lucalox-	23.84	3.447	3.493	
	Quartz	13.74	1.623	1.632	
	Step release	7.70	0.742	0.750	
		4.21	0.306	0.347	
		0	0.163	0.173	
S13	Glass-	3.99	0.303	0.391	Gage 2 data rejected.
	Plexiglas	2.37	0.214	0.289	
	Step release	1.43	0.151	0.206	
		0.88	0.121	0.176	
S14	Glass-	4.72	0.399	0.388	
	Plexiglas	2.77	0.275	0.270	
	Step release	1.66	0.200	0.200	
		1.02	0.158	0.158	
		0.63	0.134	0.134	
S15	Glass-	5.70	0.504	0.573	
	Plexiglas	3.29	0.328	0.369	
	Step release	1.97	0.234	0.258	
		1.20	0.180	0.198	
		0.74	0.155	0.164	
S17	Lucalox	33.40	-----	5.156	Gage 1 began to transform
	Quartz	19.62	-----	2.712	to BCC phase in shock front.
	Step release	11.16	-----	1.223	Data were rejected.
		6.19	-----	0.724	
		0	-----	0.200	

Table 4 (continued)

Shot Number	Type	Stress kbar	Gage 1 $\Delta R/R_o$	Gage 2 $\Delta R/R_o$	Comments
S18	Lucalox	15.50	1.955	1.766	
	Quartz	8.73	0.997	0.896	
	Step release	4.80	0.446	0.420	
		2.60	0.312	0.333	
		0	0.134	0.134	
S19	Lucalox	17.24	2.044	2.285	
	Quartz	9.78	1.012	1.118	
	Step release	5.41	0.484	0.543	
		2.94	0.324	0.364	
		0	0.144	0.174	
S21	Lucalox	11.10	1.183	1.176	
	Quartz	6.16	0.672	0.672	
	Step release	3.36	0.353	0.353	
		1.81	0.154	0.188	
		0	0.120	0.154	
S22	Lucalox	8.22	0.686	0.857	
	Quartz	4.52	0.425	0.530	
	Step release	2.45	0.226	0.301	
		0	0.091	0.138	
S24	Glass-	2.23	0.153	0.139	S24 and S25 were shot to look for possible effects of flyer thickness.
	Plexiglas	1.36	0.112	0.104	
	Double shock	0.84	0.0822	0.0758	
		0.53	0.0649	0.0586	
S25	Glass-	2.09	0.131	0.128	
	Plexiglas	1.27	0.0975	0.0963	
	Double shock	0.78	0.0733	0.0726	
		0.49	0.0572	0.0577	
S26	Glass on	5.36	1.132	0.462	S26, 27, and 28 were shot to ascertain difference in behavior between annealed and unannealed (as-rolled) foil. We normally use as-rolled foil. Gage 1 is the annealed gage. AREF foil.
	Plexiglas	3.11	0.861	0.296	
	Step release	1.86	0.746	0.214	
		1.14	0.683	0.173	

Table 4 (concluded)

Shot Number	Type	Stress kbar	Gage 1 $\Delta R/R_o$	Gage 2 $\Delta R/R_o$	Comments
S27	Glass on Plexiglas Step release	3.21	0.795	0.222	Gage 1 is the annealed gage. AREF foil.
		1.92	0.670	0.154	
		1.17	0.593	0.111	
		0.72	0.552	0.0848	
S28	Glass on Plexiglas Step release	1.40	0.0880	0.0638	Gage 1 is the annealed gage. AREF foil.
		0.86	0.0580	0.0402	
		0.54	0.0421	0.0259	
		0.34	0.0311	0.0153	
IRD-1	Glass-Plexiglas Step release	2.79	0.185	0.201	
		1.68	0.137	0.148	
		1.04	0.102	0.109	
IRD-2	Glass-Plexiglas No steps	19.4	2.61	2.61	
IRD-3	Plex-plex	0.50	0.016		
IRD-6	Plex-plex	5.36	0.395		
		0	0.087		
IRD-9	Plex-plex	5.31	0.472	0.420	Gage 1 is made from 2 mil foil.
		0	0.093	0.077	Gage 2 is made from 1 mil foil.
IRD-10	Plex-plex	5.5	0.458	0.374	Gage 1 is made from 1 mil foil.
		0	0.103	0.077	Gage 2 is made from 0.5 mil foil.

The following two shots contained four gages;

Shot Number	Type	Stress kbar	Gage 1 $\Delta R/R_o$	Gage 2 $\Delta R/R_o$	Gage 3 $\Delta R/R_o$	Gage 4 $\Delta R/R_o$
S29	Step-load	7.5	0.658	0.692		
		11.9	1.092*	1.143*	1.262	(1.512)
S30	Step-load	12.9	1.502	1.563		
		21.5	2.873*	2.892*	(2.752)	2.956

* Second step data

( ) Rejected data

Table 5

NONLINEAR UNLOADING PATHS

Shot Number	σ_{peak} kbar	Least-Squares Fit	Std Dev
S17	33.40	$\sigma = -2.997 + 15.40\,(\Delta R/R_o) - 3.696\,(\Delta R/R_o)^2 + 0.4036\,(\Delta R/R_o)^3$	0.235
S2 S11	23.84 24.03 →	$\sigma = -1.916 + 14.59\,(\Delta R/R_o) - 3.542\,(\Delta R/R_o)^2 + 0.4093\,(\Delta R/R_o)^3$	0.796
S12	29.97	$\sigma = -2.274 + 14.70\,(\Delta R/R_o) - 3.276\,(\Delta R/R_o)^2 + 0.3407\,(\Delta R/R_o)^3$	0.865
S19	17.24	$\sigma = -1.512 + 13.15\,(\Delta R/R_o) - 2.103\,(\Delta R/R_o)^2$	0.785
S18	15.50	$\sigma = -1.433 + 13.61\,(\Delta R/R_o) - 2.458\,(\Delta R/R_o)^2$	0.649
S1	13.82	$\sigma = -1.169 + 13.23\,(\Delta R/R_o) - 2.179\,(\Delta R/R_o)^2$	0.760
S21	11.10	$\sigma = -0.8039 + 11.52\,(\Delta R/R_o) - 1.218\,(\Delta R/R_o)^2$	0.590

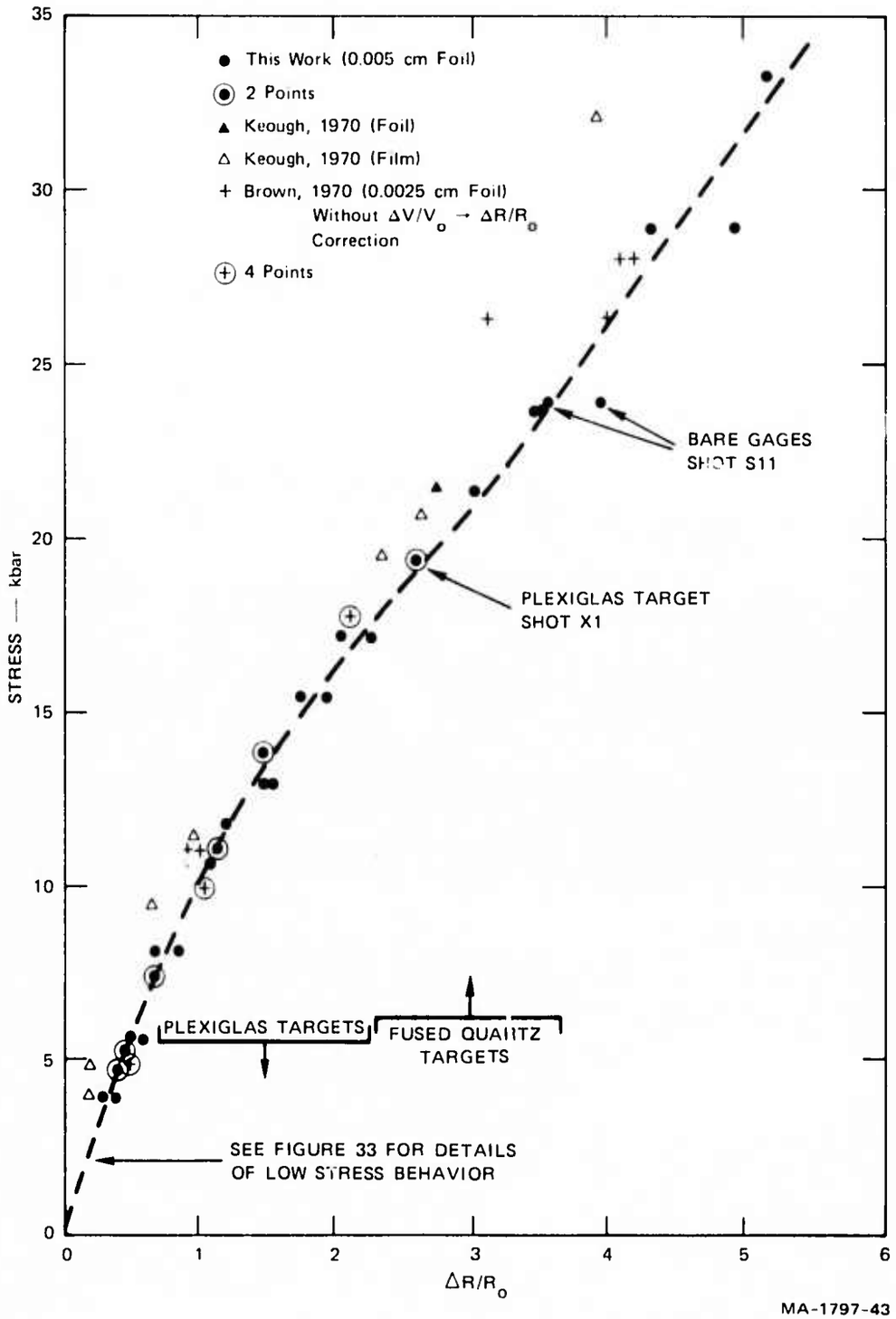

FIGURE 23 DYNAMIC LOADING DATA

Dashed line is fit to data from this work.

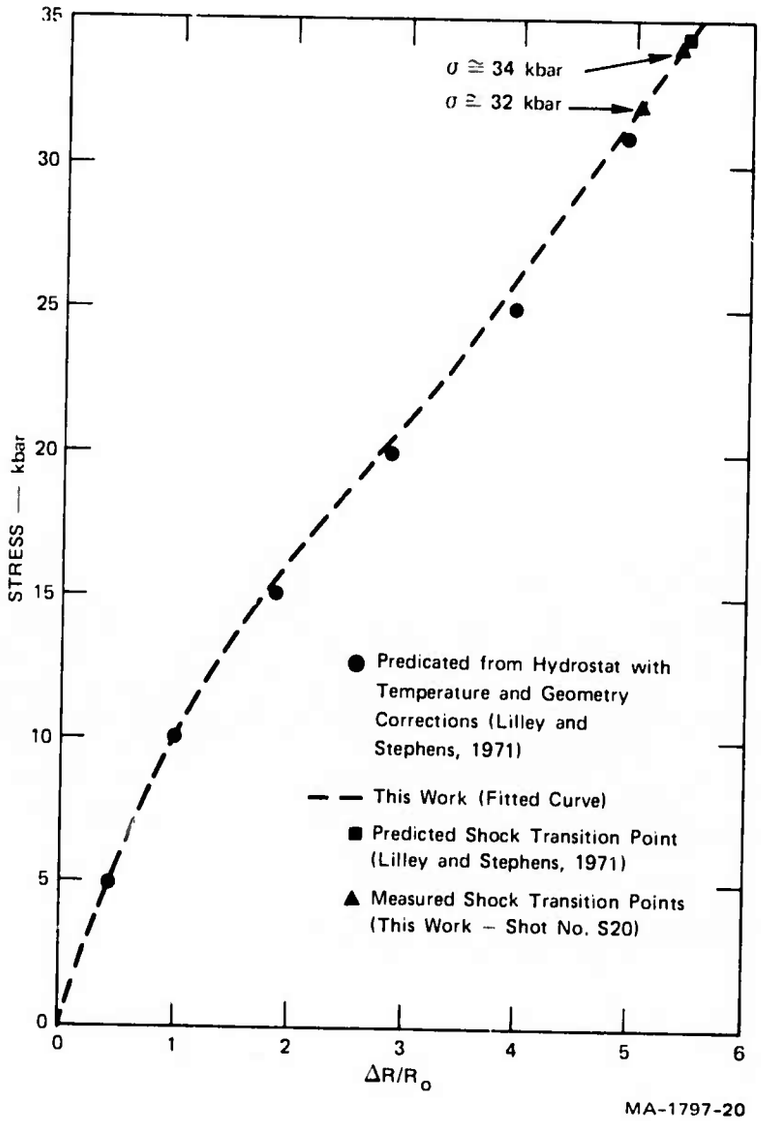

FIGURE 24 COMPARISON OF PREDICTED DYNAMIC BEHAVIOR WITH EXPERIMENTAL DATA

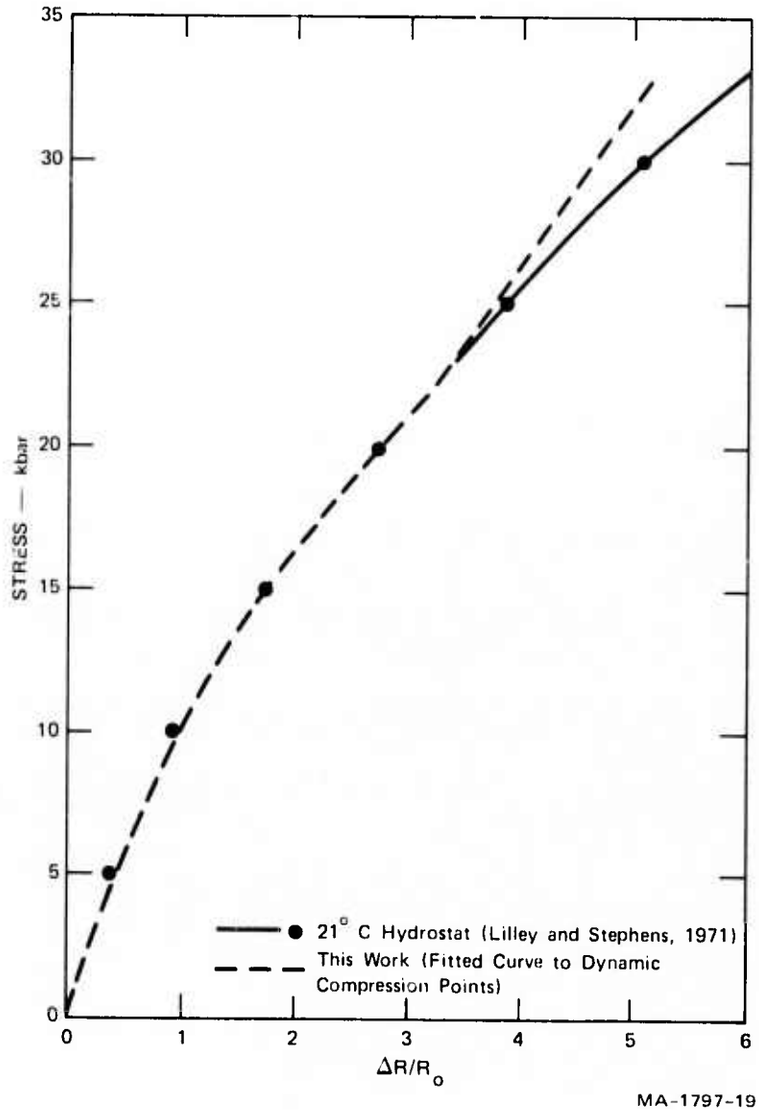

FIGURE 25 COMPARISON OF HYDROSTATIC PIEZORESISTANCE VALUES WITH DYNAMIC EXPERIMENTAL CURVE

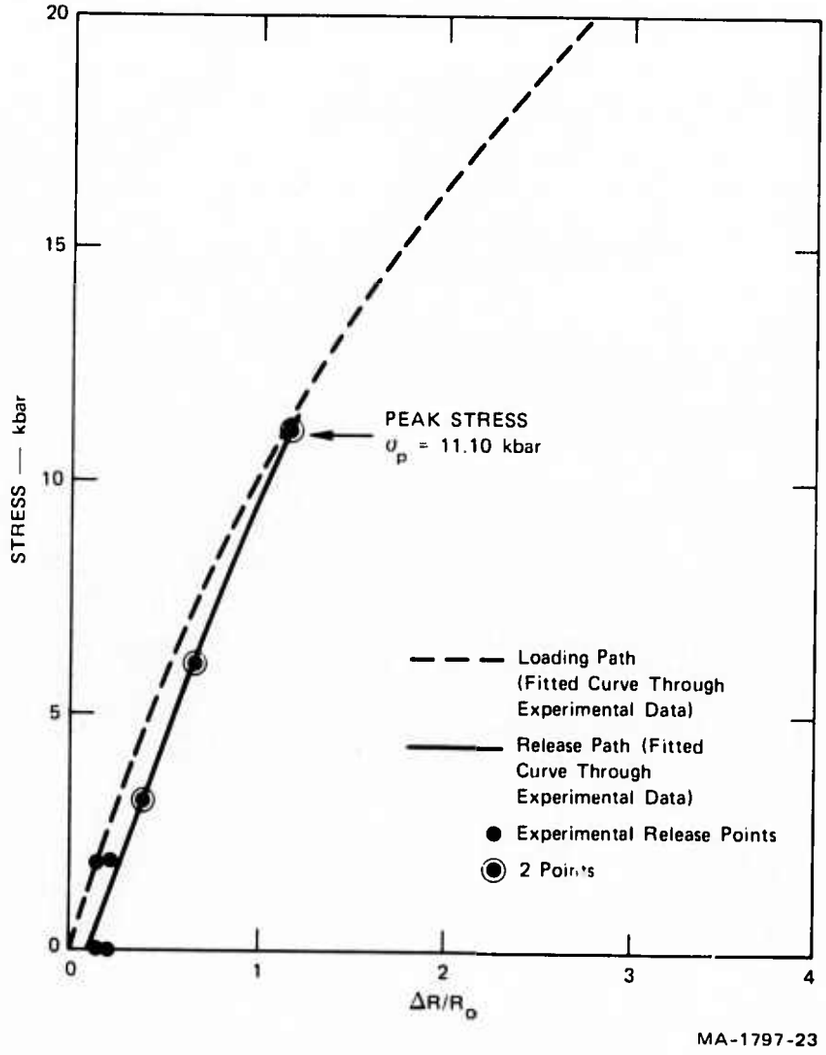

FIGURE 26 LOADING AND RELEASE PATHS, SHOT S21

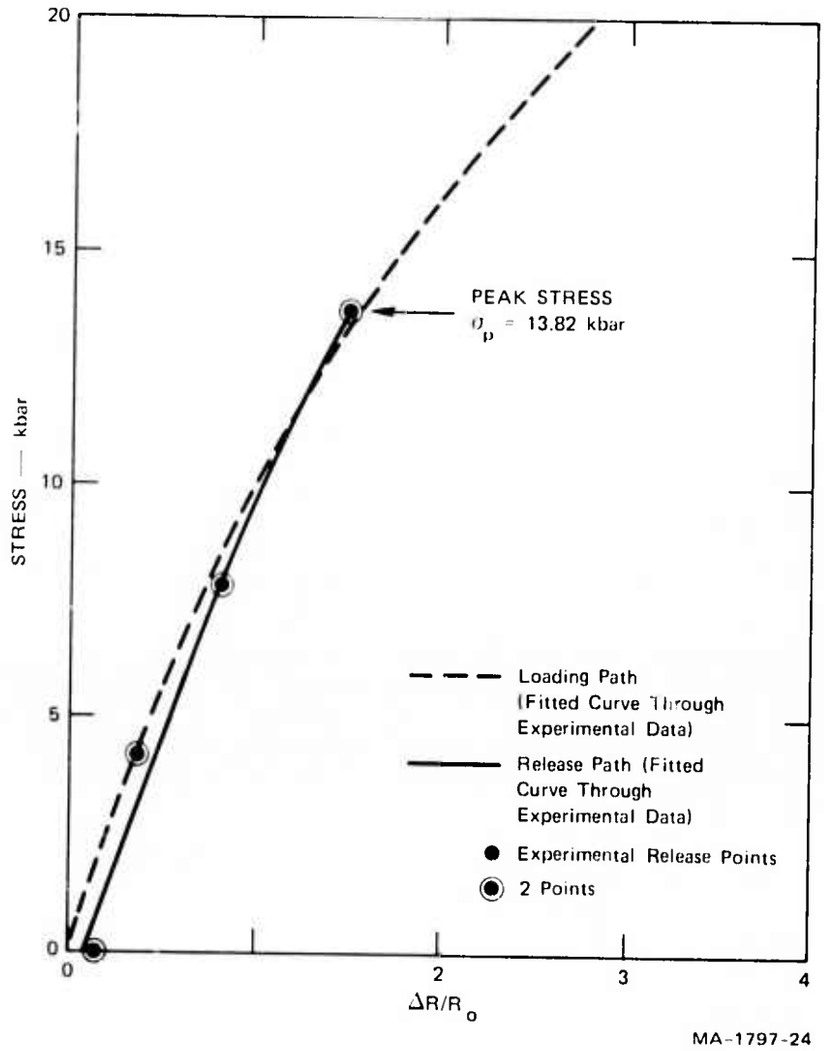

FIGURE 27 LOADING AND RELEASE PATHS, SHOT S1

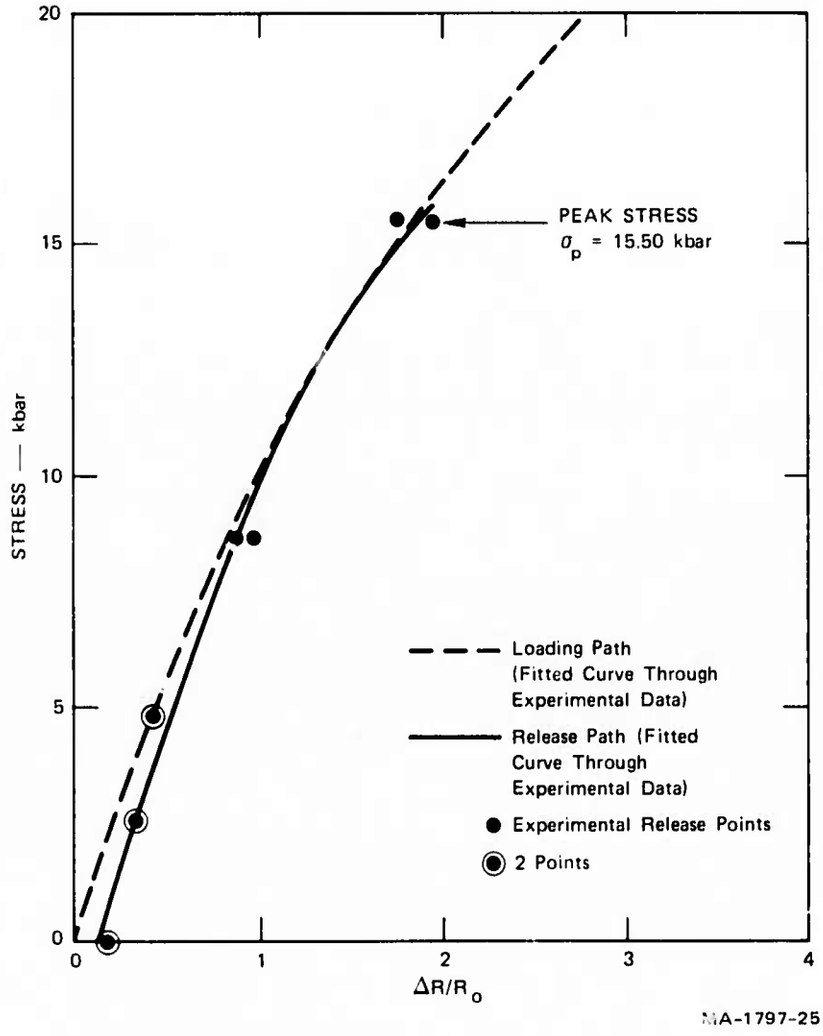

FIGURE 28 LOADING AND RELEASE PATHS, SHOT S18

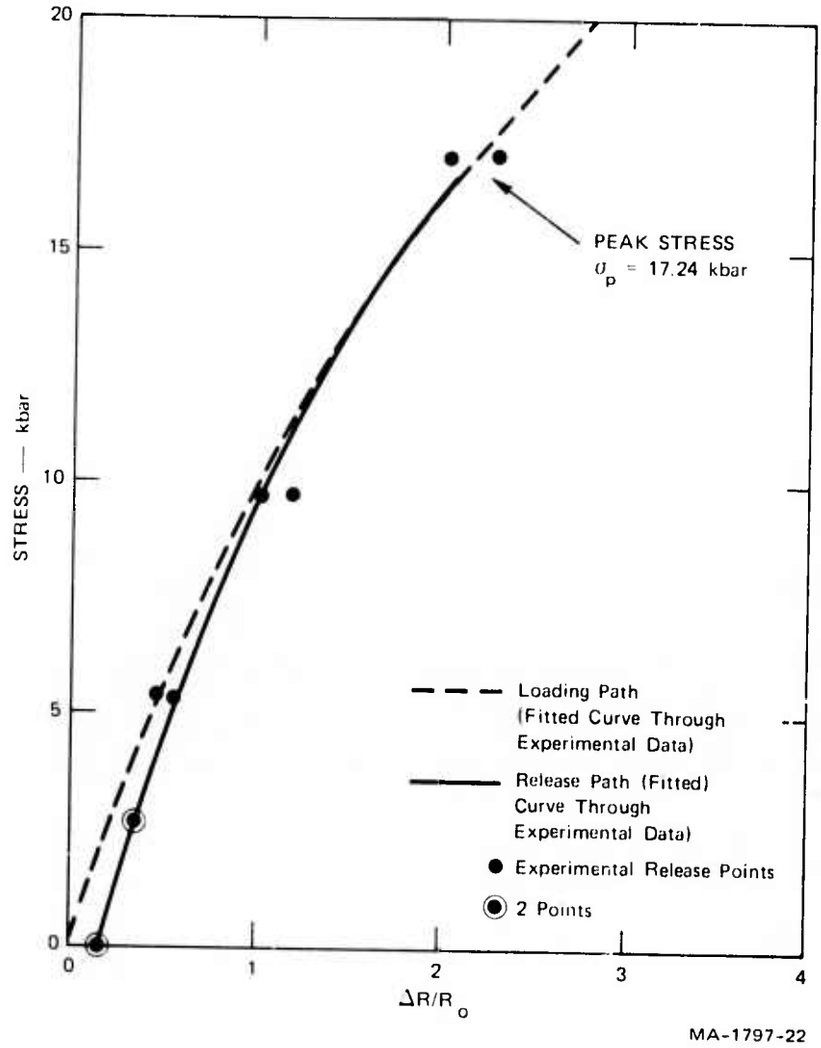

FIGURE 29 LOADING AND RELEASE PATHS, SHOT S19

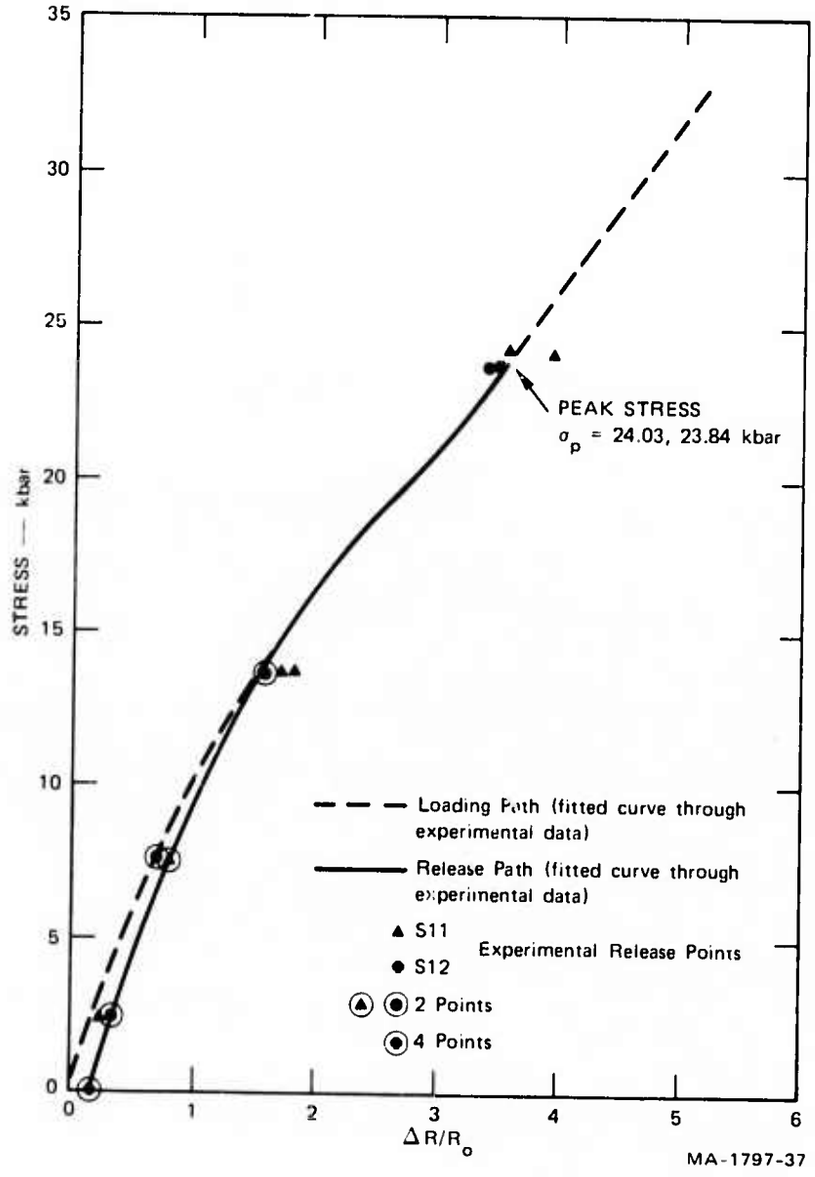

FIGURE 30 LOADING AND RELEASE PATHS, SHOTS S11 AND S12

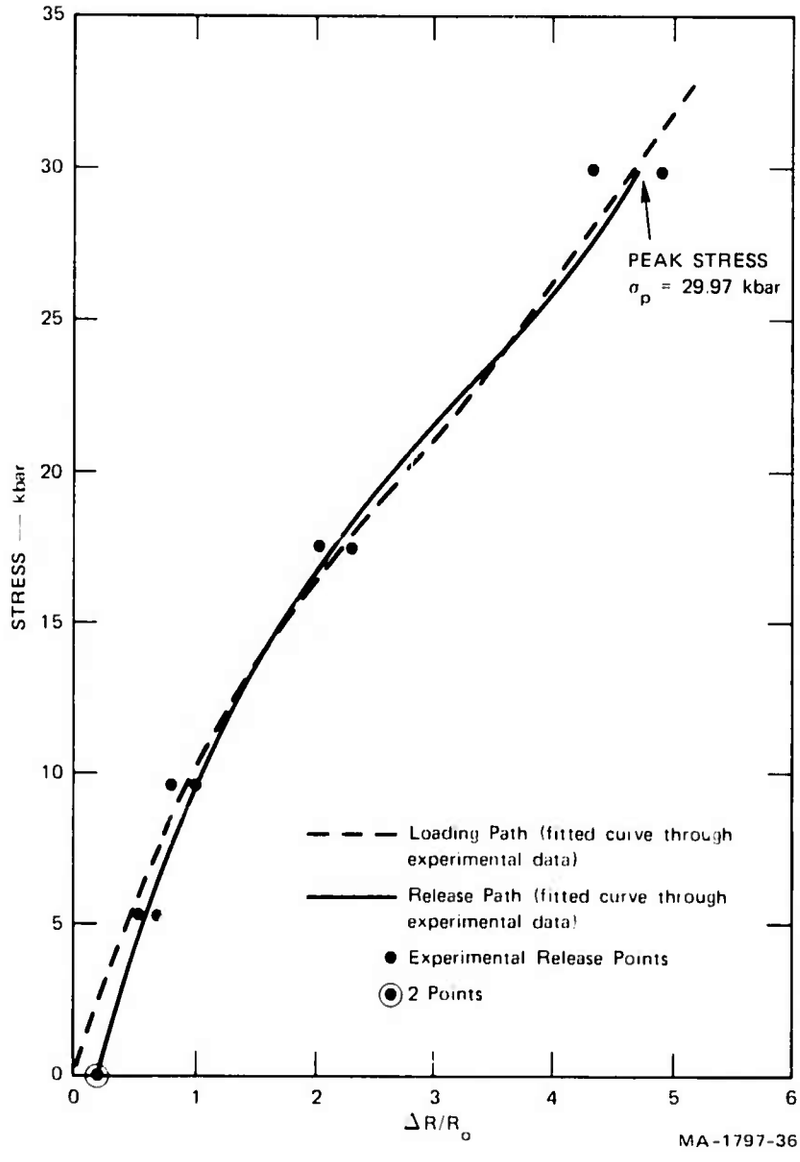

FIGURE 31 LOADING AND RELEASE PATHS, SHOT S2

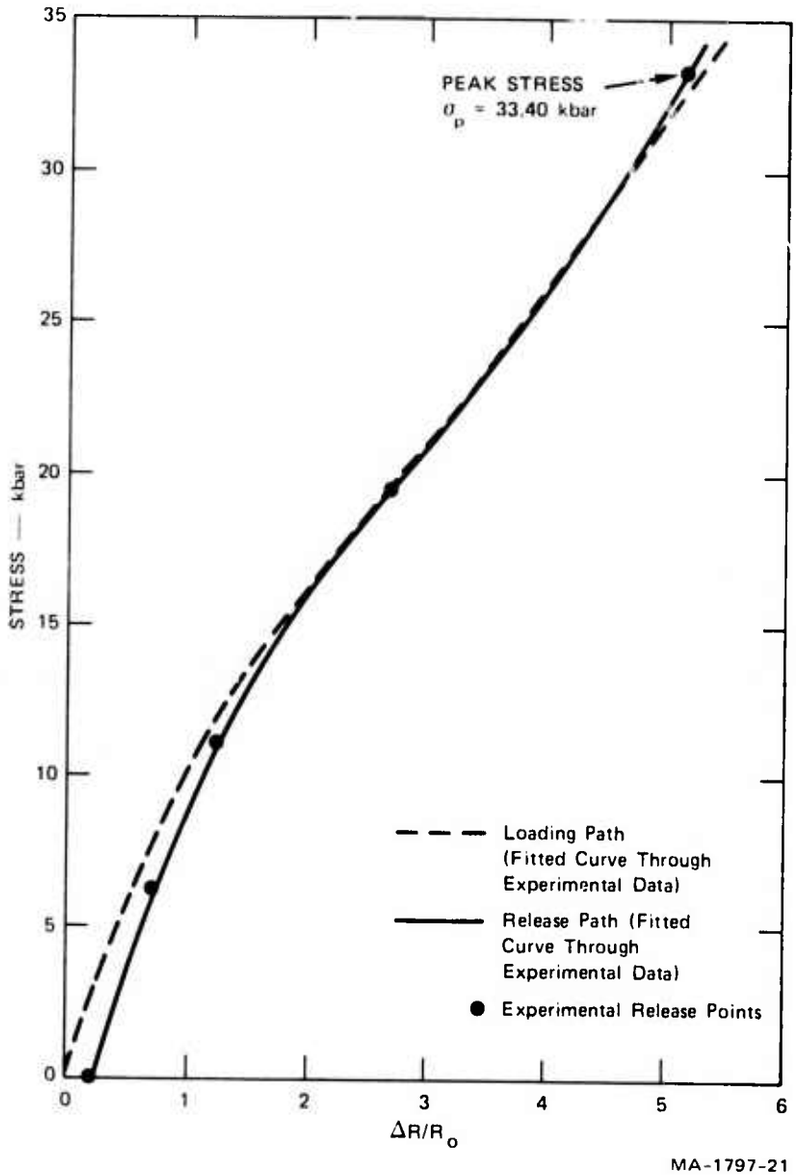

FIGURE 32 LOADING AND RELEASE PATHS, SHOT S17

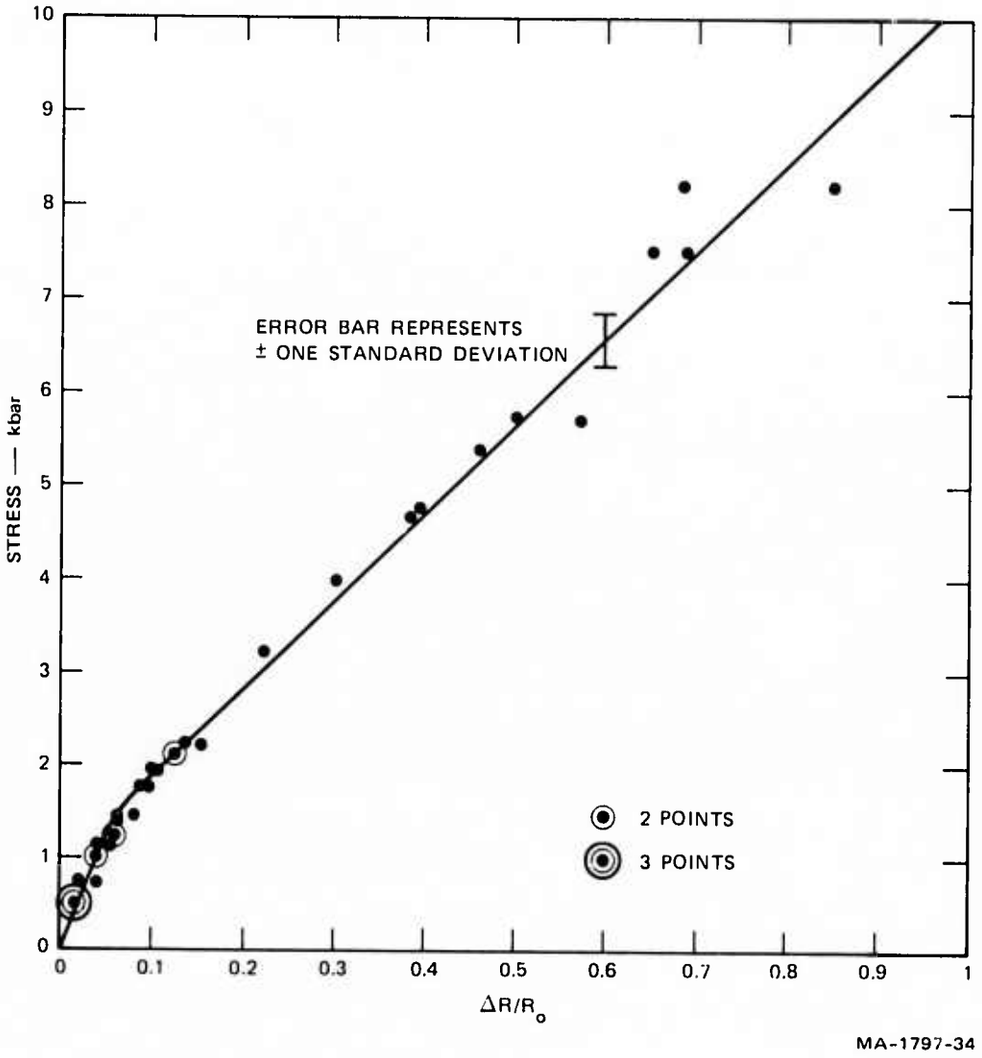

FIGURE 33 LOADING DATA, 0.005-cm (2-mil) FOIL

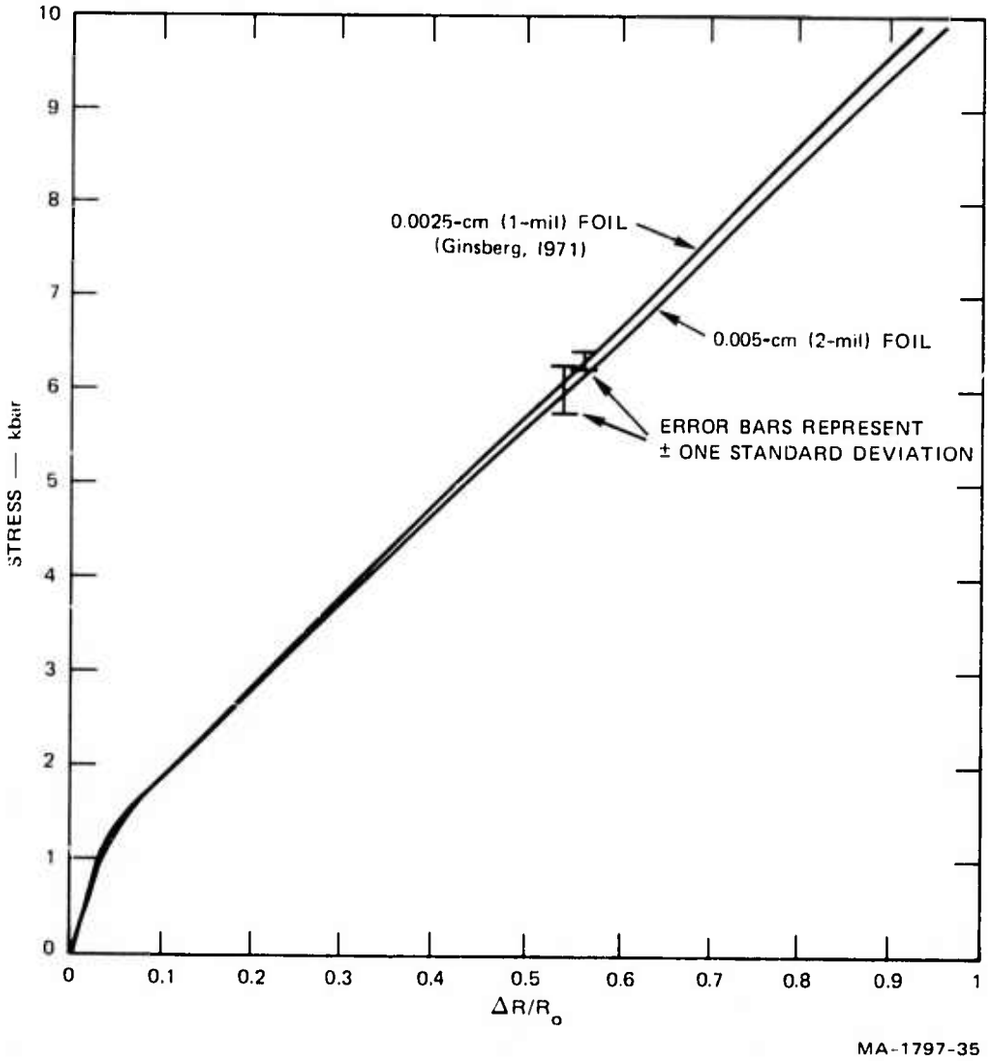

FIGURE 34 STRESS VERSUS FRACTIONAL RESISTANCE CHANGE FOR TWO FOIL THICKNESSES (NO RELOAD POINTS INCLUDED IN FIT)

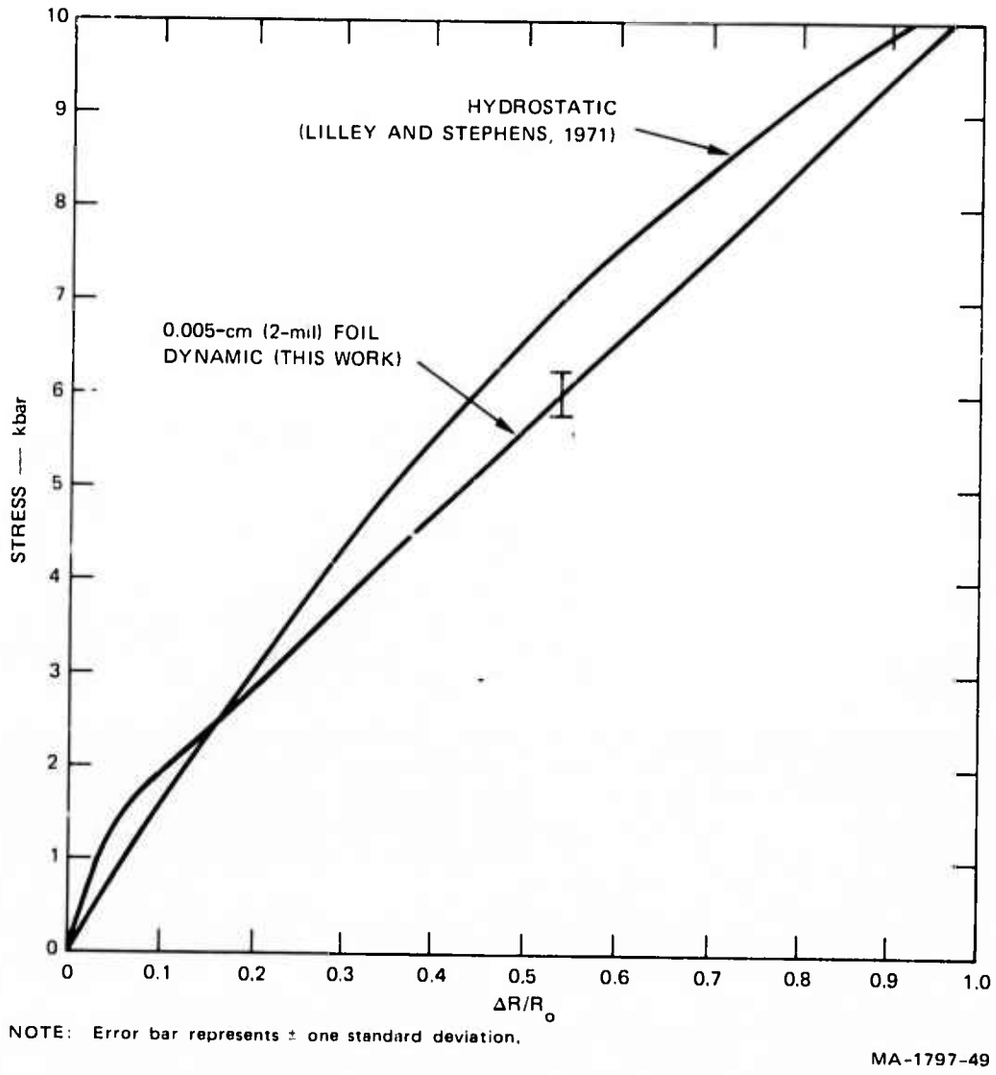

FIGURE 35 COMPARISON OF HYDROSTATIC AND DYNAMIC BEHAVIOR BELOW 10 kbar

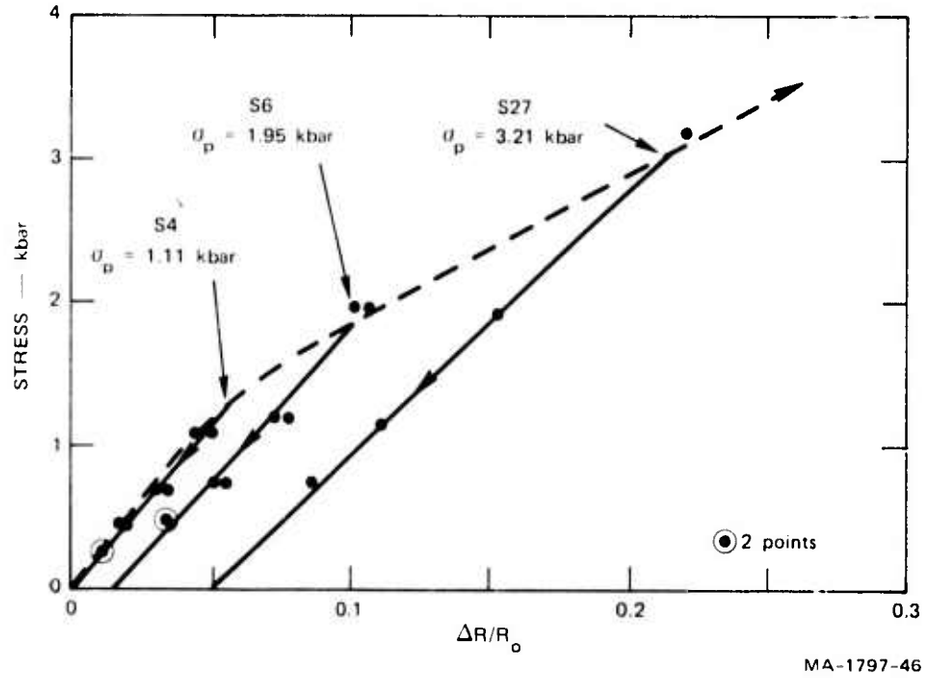

FIGURE 36 LOADING CURVE AND SOME REPRESENTATIVE EXPERIMENTAL UNLOADING CURVES, $\sigma_p < 4$ kbar

Other release paths have been measured in this stress range, but have been omitted for clarity.

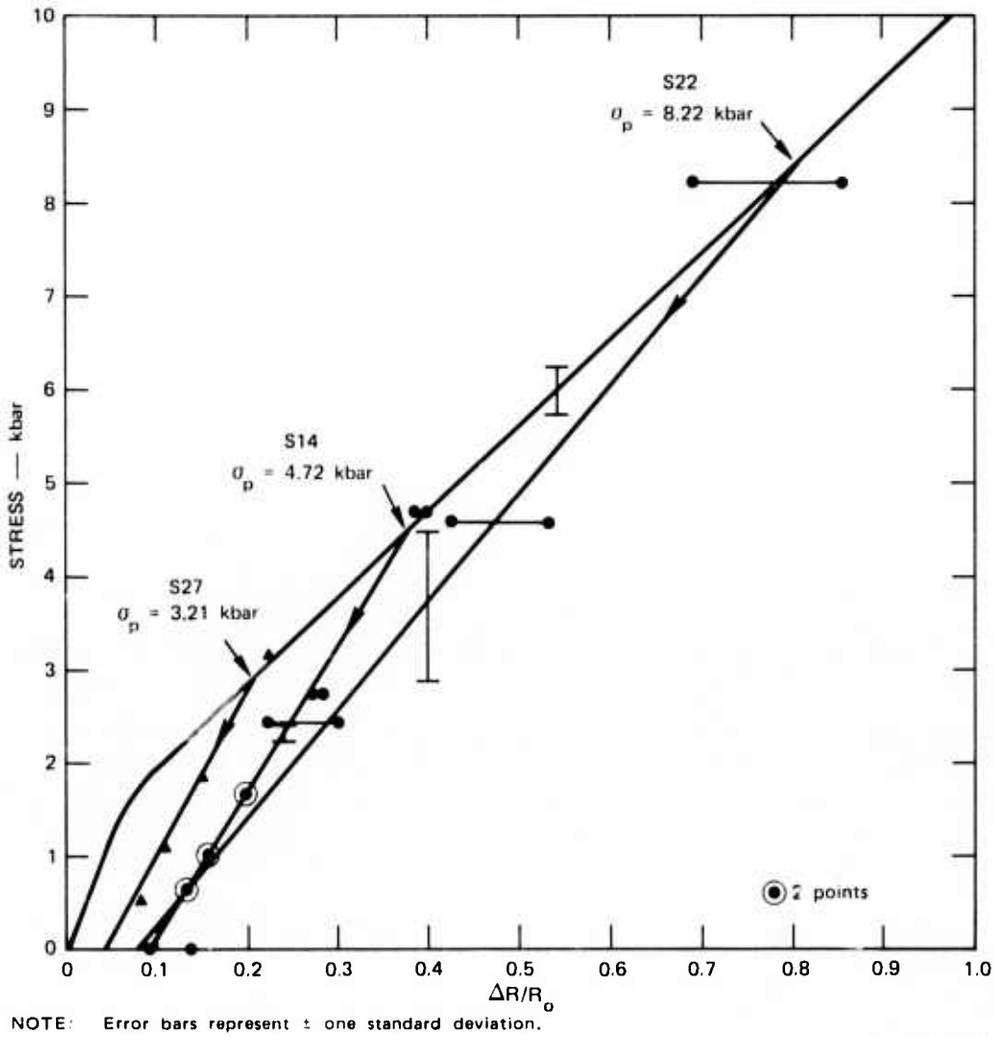

NOTE: Error bars represent ± one standard deviation.

MA-1797-45

FIGURE 37 LOADING PATH AND SOME REPRESENTATIVE MEASURED RELEASE PATHS ($10 \geq \sigma_p > 3$ kbar) 0.005-cm (2-mil) FOIL

Other release paths have been measured in this stress range, but have been omitted for clarity.

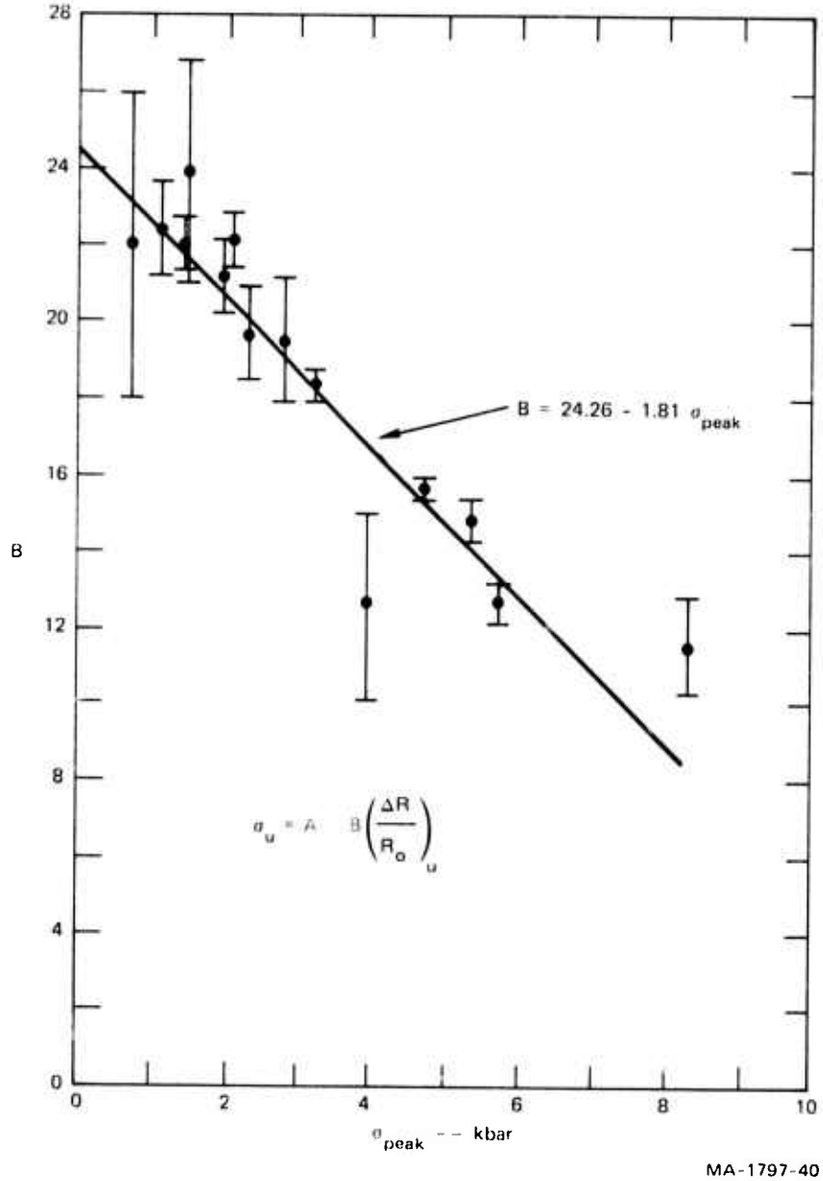

FIGURE 38 SLOPE OF LEAST-SQUARES FIT TO LINEAR UNLOADING DATA AS A FUNCTION OF PEAK STRESS

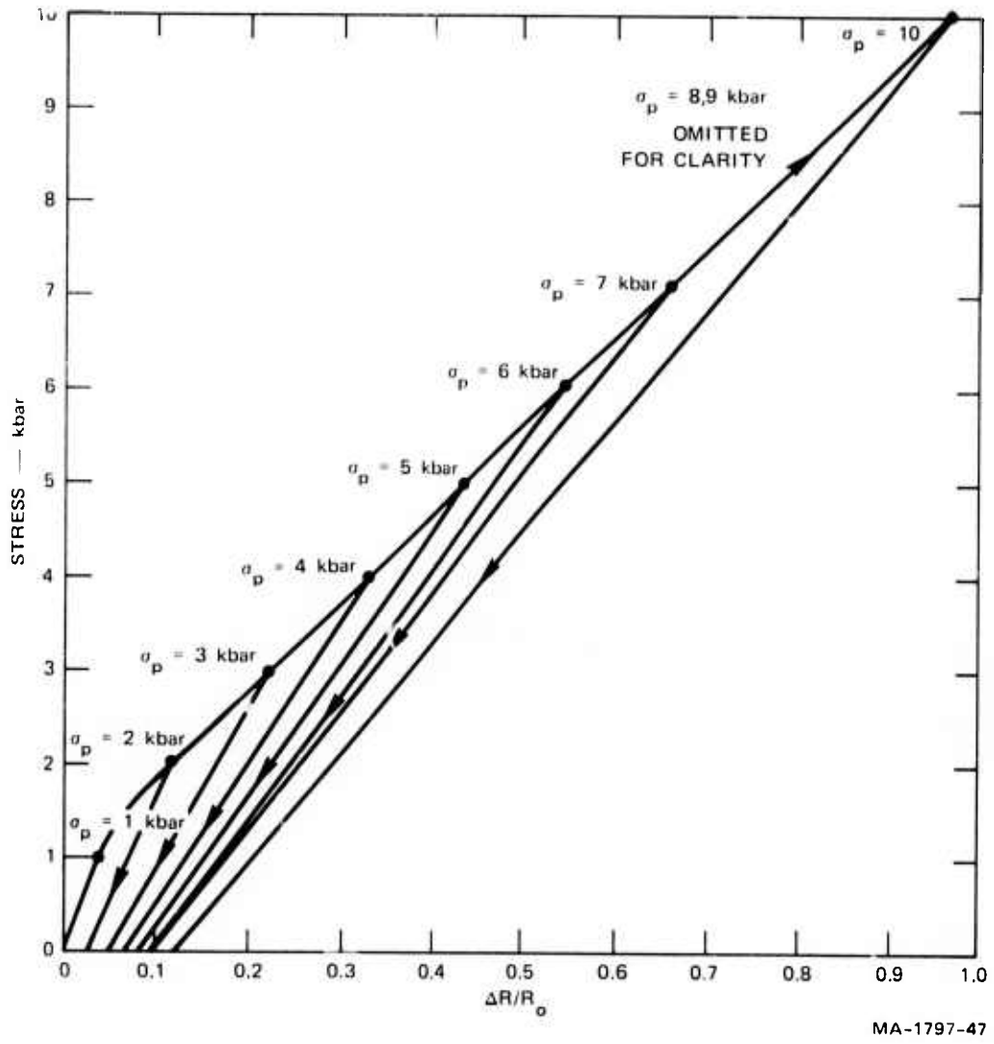

FIGURE 39 FAMILY OF UNLOADING PATHS FOR PEAK STRESS OF 10 kbar OR LESS

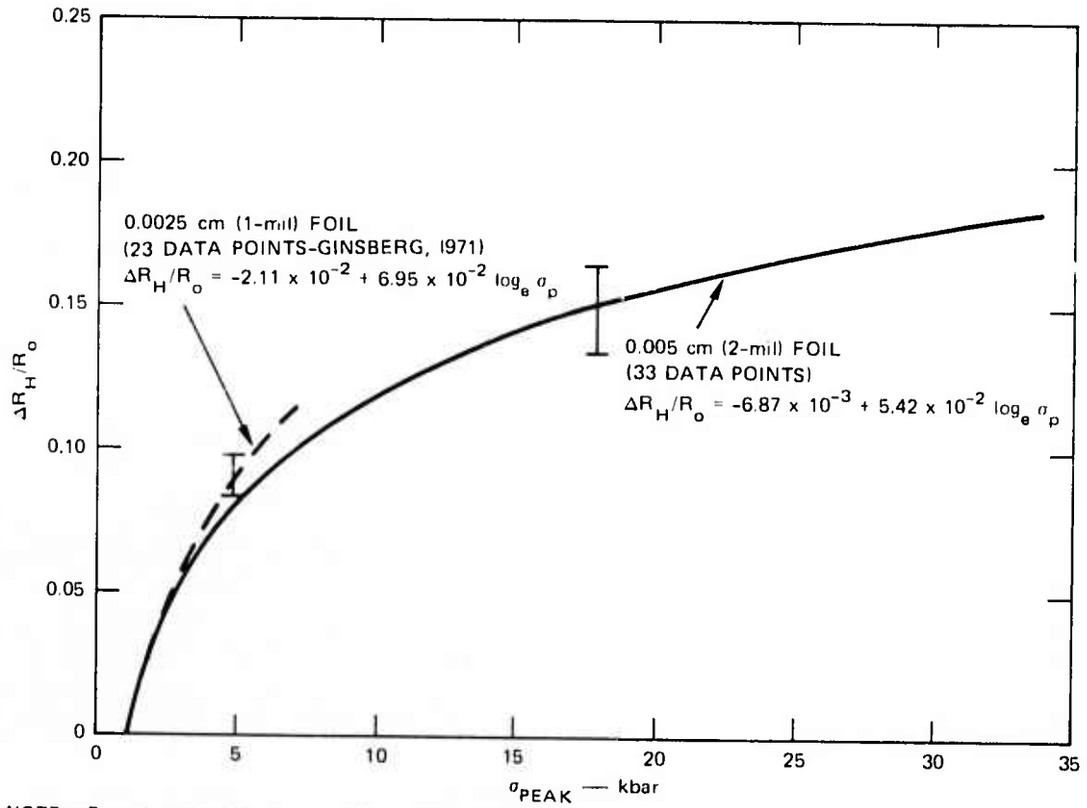

NOTE: Error bars represent ± one standard deviation.

MA-1797-41

FIGURE 40 ZERO-STRESS RESIDUAL RESISTANCE ($\Delta R_H/R_o$) VERSUS PEAK STRESS

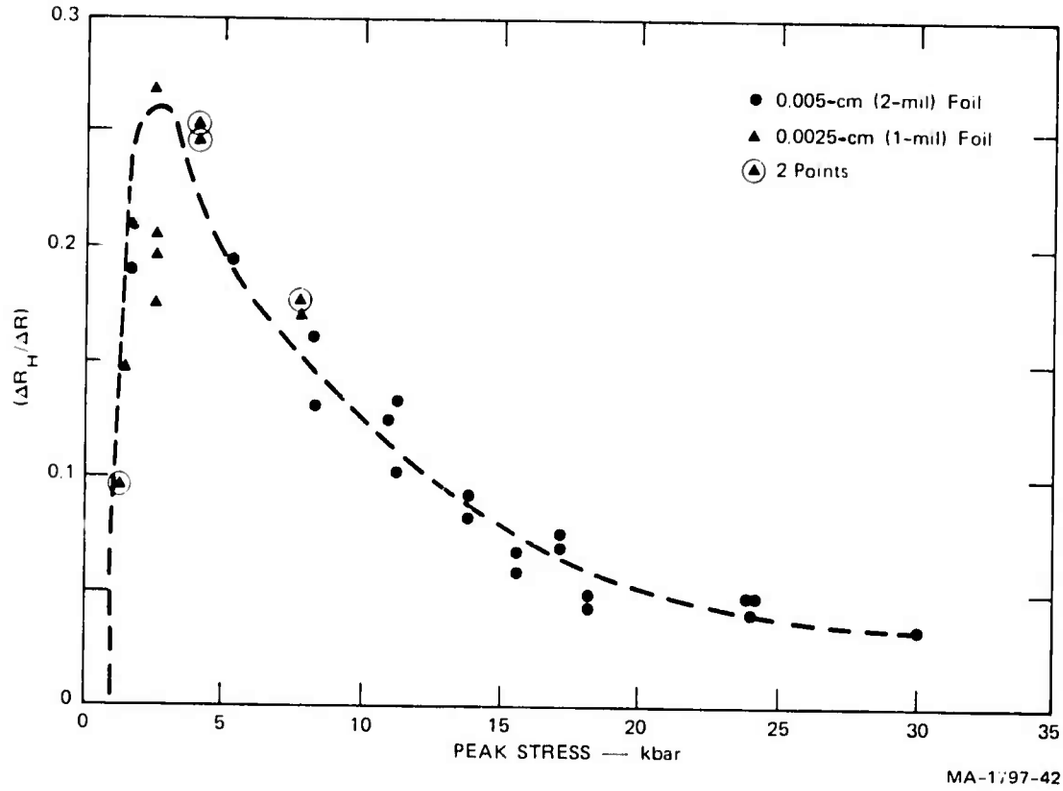

FIGURE 41 ZERO-STRESS RESIDUAL RESISTANCE AS A FRACTION OF TOTAL RESISTANCE CHANGE $(\Delta R_H/R_o)/(\Delta R/R_o)$ VERSUS PEAK STRESS

Figure 23 contains the curve chosen to represent the full set of data up to about 33 kbar and contains our data points as well as those of some other investigators (Keough, 1970; Brown, 1970). Figure 24 compares our dynamic data with the dynamic piezoresistance function Lilley and Stephens (1971) calculated from their hydrostatic data by making corrections for temperature and geometry effects and Figure 25 shows our data and Lilley and Stephens' hydrostatic data, as does Figure 35, but at lower stresses. Figures 26 through 32 are the unloading data from peak stress levels above 10 kbar along with the fitted curves. Figure 33 contains the loading data for peak stress values up to 10 kbar, and Figure 34 has a comparison between these data and the data we obtained previously on 0.0025 cm (1-mil) foil (Ginsberg, 1971). Figures 36, 37, 38, and 39 show unloading data for $\sigma_p < 10$ kbar. Figure 40 contains the values of the zero-stress residual resistance ($\Delta R_H/R_o$) as a function of peak stress, and Figure 41 presents these values in a different manner, showing the zero-stress residual resistance divided by the total resistance change at peak stress. Figures 42, 43, and 44 contain the results of our comparison experiments between annealed and cold-worked foil.

4.6.2 Phase Transition Experiment--Figure 45 shows the records obtained during Shot S20 which was fired to explore the kinetics of the high pressure phase transition seen during static experiments and to ascertain the stress level at which it starts. Figures 45a and 45b are the ytterbium gage records, while 45c is the record from the manganin gage in the same plane as the two ytterbium gages. Figure 46 is a combined plot of the data and shows some of the more interesting features of the experimental records.

4.6.3 Tensile Strain Experiments--Figures 47 through 49 contain the results of the experiments we performed to obtain data applicable to the solution of the divergent flow problems encountered in field gage use.

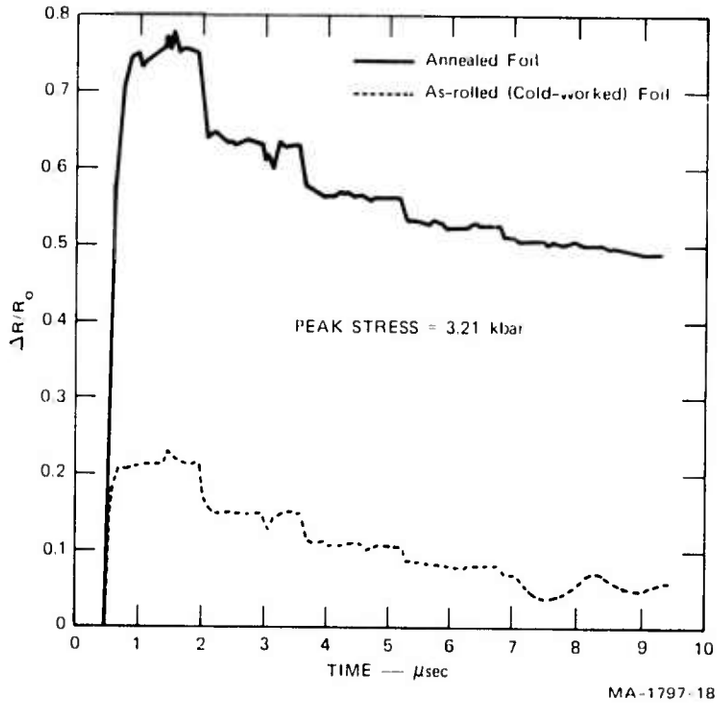

FIGURE 42 PLOT OF DATA FROM SHOT S27

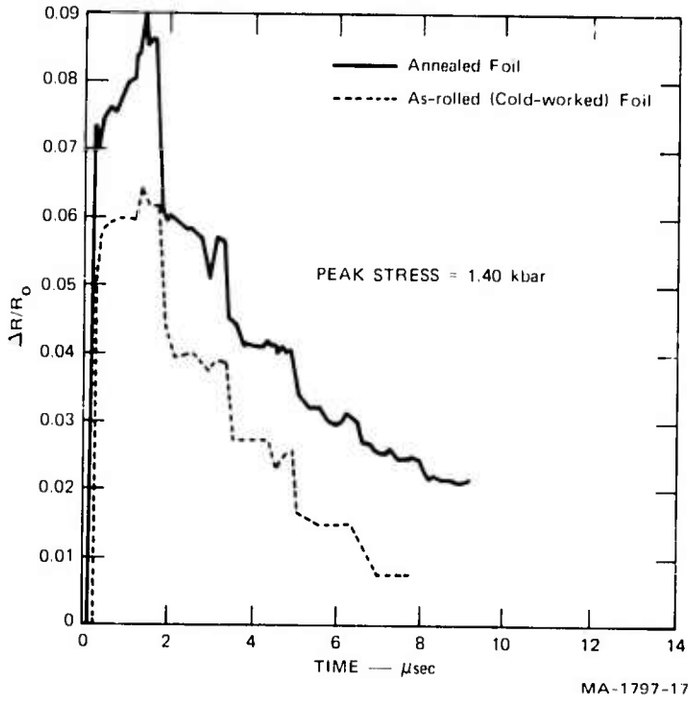

FIGURE 43 PLOT OF DATA FROM SHOT S28

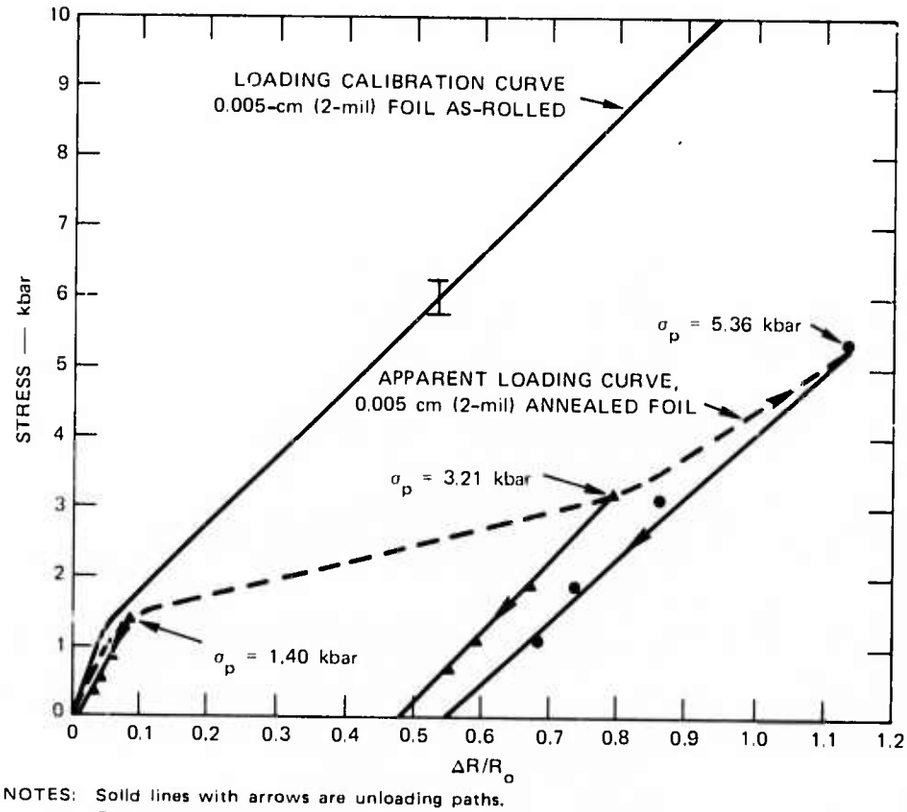

NOTES: Solid lines with arrows are unloading paths.
Error bar represents ± one standard deviation.

MA-1797-48

FIGURE 44 COMPARISON OF RESPONSE OF ANNEALED AND AS-ROLLED (COLD-WORKED) YTTERBIUM FOIL

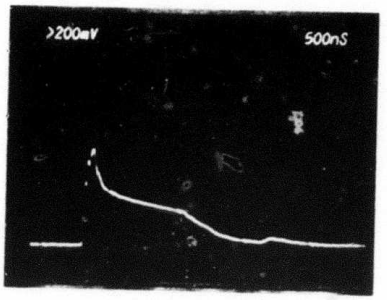

(a) YTTERBIUM GAGE NO. 1.
Vertical sensitivity = 0.35 V/cm
Horizontal sweep = 0.5 μs/cm

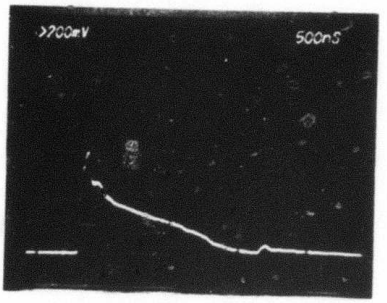

(b) YTTERBIUM GAGE NO. 2.
Vertical sensitivity = 0.35 V/cm
Horizontal sweep = 0.5 μs/cm

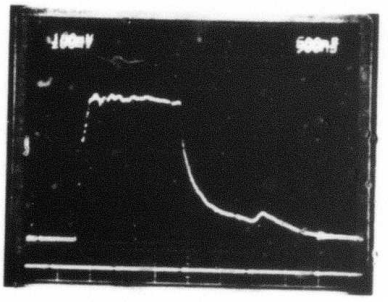

(c) MANGANIN GAGE.
Vertical sensitivity = 0.1 V/cm
Horizontal sweep = 0.5 μs/cm

MP-1797-38

FIGURE 45 OSCILLOGRAMS FORM SHOT S20

Peak stress ~ 40 kbar. All gages in same plane in target.

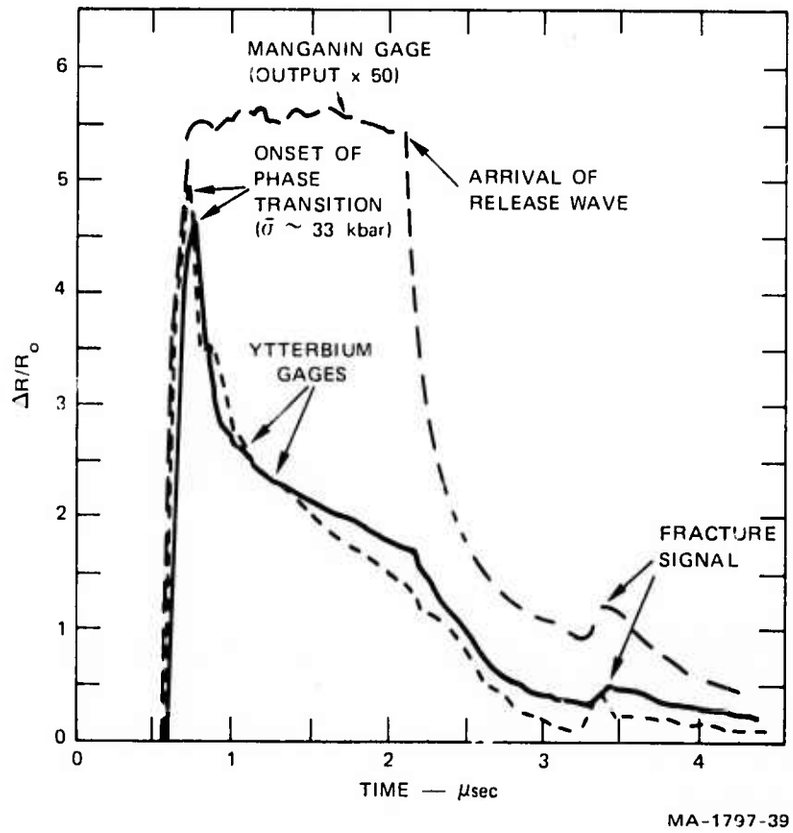

FIGURE 46 PLOT OF DATA FROM SHOT S20 SHOWING PHASE TRANSITION IN YTTERBIUM

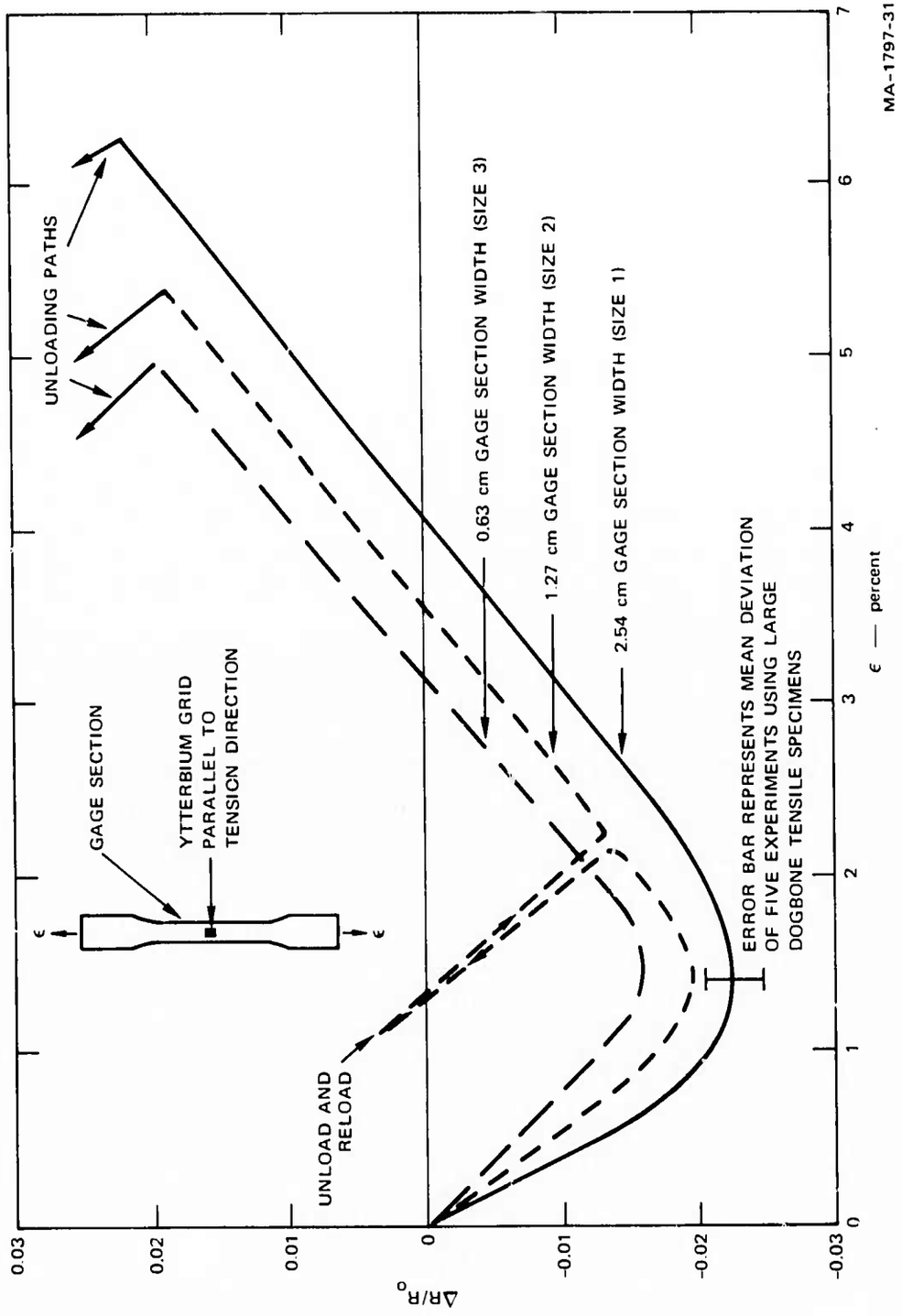

FIGURE 47 FRACTIONAL CHANGE IN RESISTANCE VERSUS TENSILE STRAIN

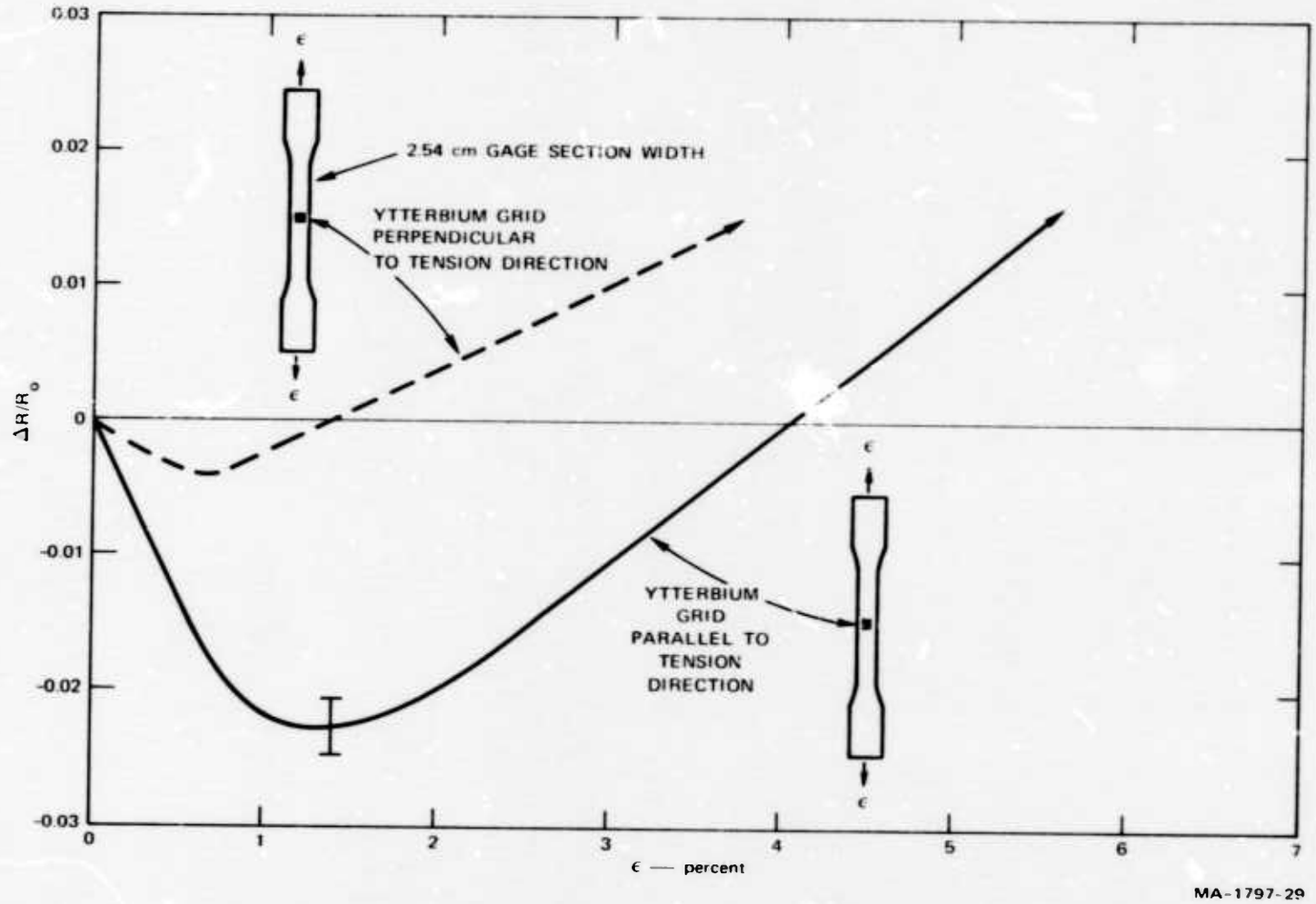

FIGURE 48 FRACTIONAL CHANGE IN RESISTANCE VERSUS TENSILE STRAIN, PERPENDICULAR AND PARALLEL GRID ORIENTATION

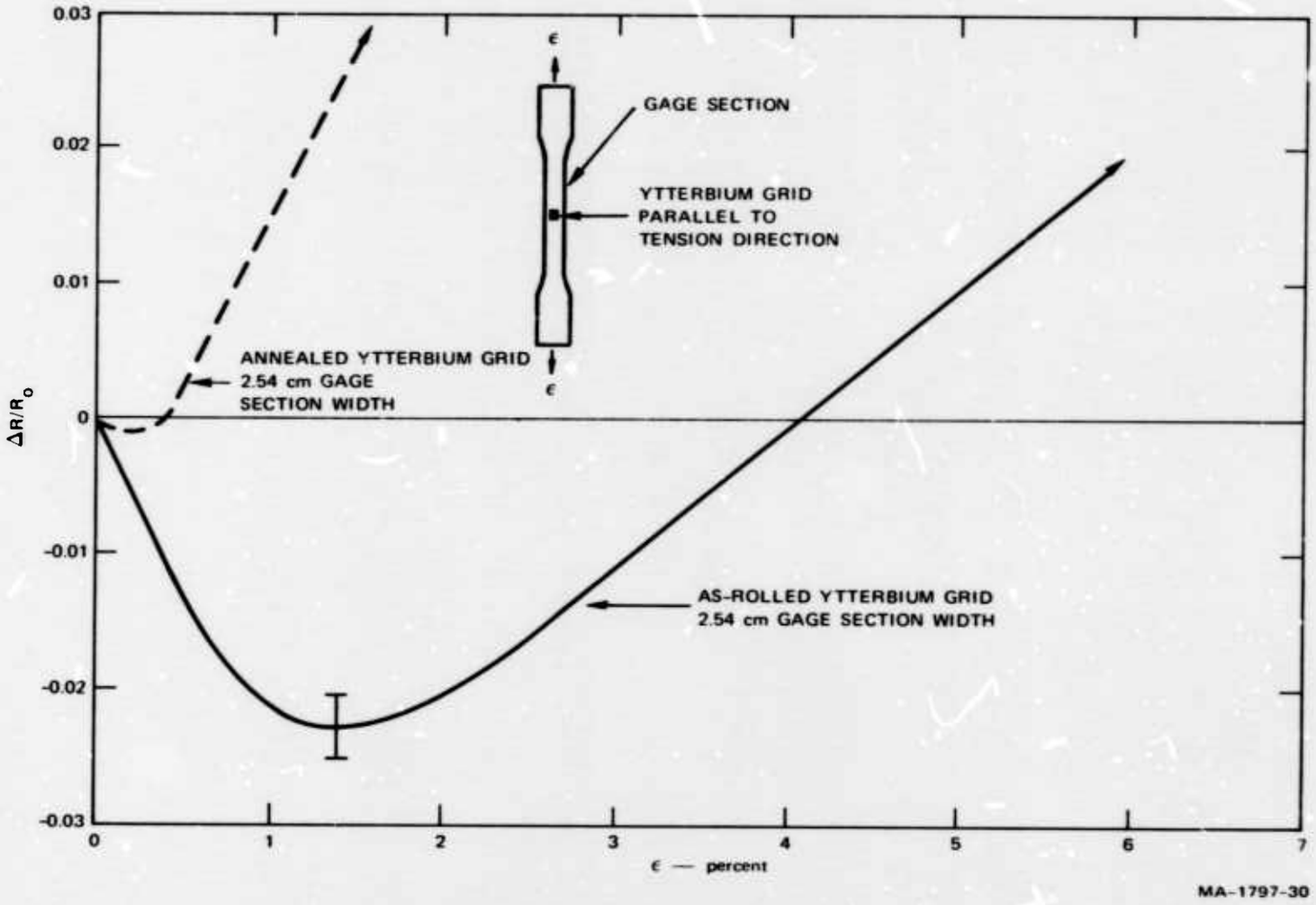

FIGURE 49 FRACTIONAL CHANGE IN RESISTANCE VERSUS TENSILE STRAIN, ANNEALED AND AS-ROLLED YTTERBIUM

Figure 47 shows the results obtained using three different gage section widths and also contains some unloading paths. Figure 49 compares the behavior of annealed and cold-worked (as-rolled) foil, and Figure 48 compares the response of a parallel-mounted grid to a grid bonded with its elements perpendicular to the direction of tensile strain.

4.6.4 Static Compression Piezoresistance Tests--Figure 50 contains the results of the static compression tests done to explore the possibility of the presence of rate effects in the piezoresistant response of ytterbium. Figure 51 contains some results obtained by Smith et al. (1972) for comparison with our data.

4.7 Discussion and Interpretation

In this section the results obtained in this program are analyzed and discussed. First the aspects of the analysis that were common to most of the experiments are considered, such as curve-fitting techniques and estimation of experimental errors. Each of the specific types of experiments performed are treated, and finally some general comments are given about the piezoresistance of ytterbium.

4.7.1 Uncertainties in Experiments and Analysis--Two measured quantities are important to a calibration program. These are the measurement of the ratio of change in resistance to the original resistance of the ytterbium gage, or $\Delta R/R_o$, and the stress levels at which we wish to know $\Delta R/R_o$. The uncertainties in the measured value of $\Delta R/R_o$ can arise from (1) possible systematic or random electronic equipment malfunctions, (2) oscilloscope calibration errors, (3) measurement of circuit parameters in the $\Delta V/V_o$ to $\Delta R/R_o$ correction,* (4) conversion of the oscillograms to digital form, and (5) uncertainty in the estimation of the best value of $\Delta V/V_o$ for a given value of stress from the plotted peak stress and release step DC levels.

---

* See Appendix B.

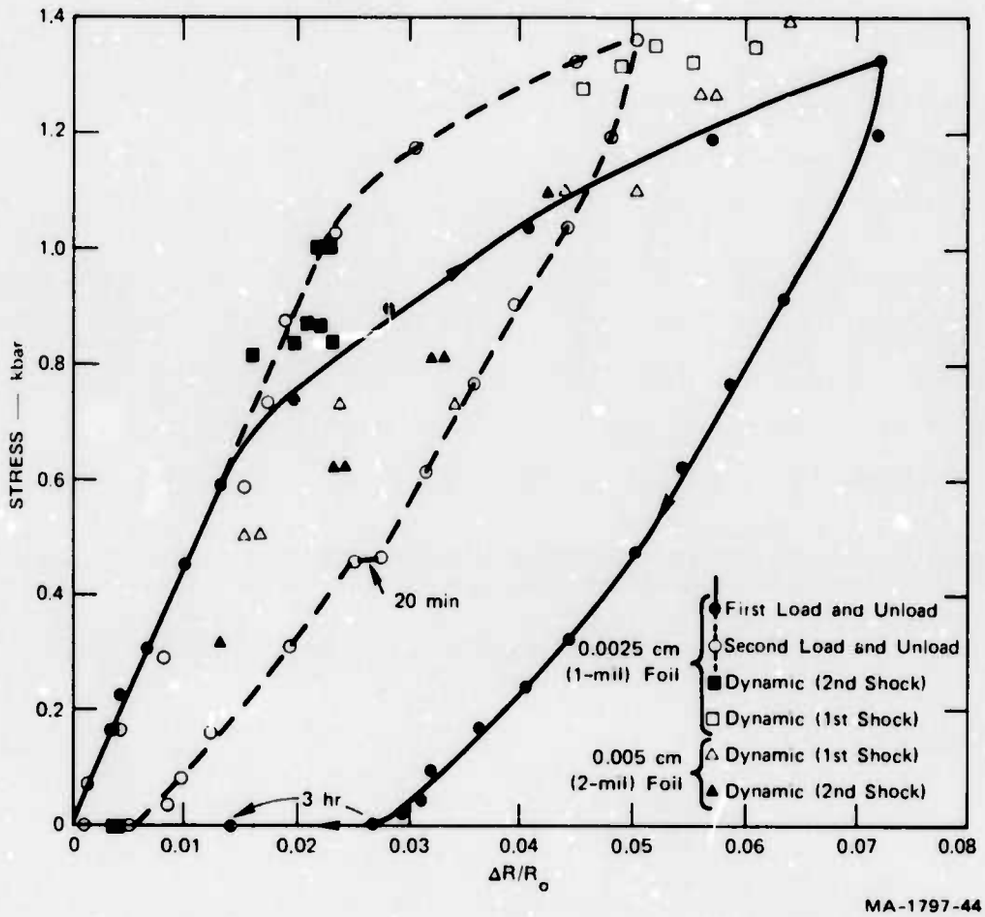

FIGURE 50 STATIC PIEZORESISTANCE DATA COMPARED WITH DYNAMIC DATA

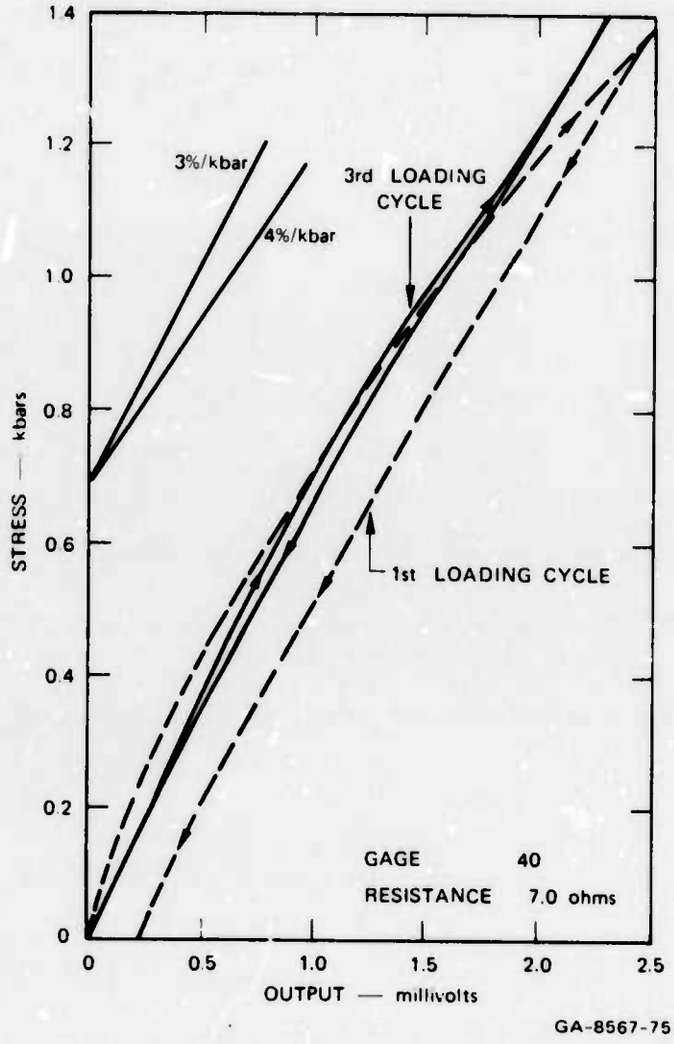

FIGURE 51 STATIC CALIBRATION CYCLES FOR AN YTTERBIUM STRESS GAGE, from Smith, et al. (1972)

We must assume that we can recognize the occurrence of any systematic or random electronic malfunctions that could be large enough to cause major errors. Our systems and experiments had sufficient redundancy and cross-checking capability to eliminate this possibility. Oscilloscope calibration errors can occur if there is some important change in the recording system between the time of the experiment and the time of calibration, and if there are nonlinearities in the system that are not taken into account. We tried to do our calibrations immediately after each shot, and also checked each set of calibrations for nonlinearity from the top to the bottom of the trace. Occasional differences were noticed of up to±2% between readings from the same gage on different oscilloscopes and some changes in calibration from shot to shot on the order of ±1%. Measurement of circuit parameters used in the conversion of $\Delta V/V_o$ values to the actual $\Delta R/R_o$ values was to better than ±1%. Conversion of the raw data to digital form adds practically no error.

We estimate the value of $\Delta V/V_o$ for each level by making a number of readings at different times and averaging the result. The average deviation around the mean $\Delta V/V_o$ for each level was usually less than ±1%.

There is no standard way to add up these uncertainties, so we will claim that the accuracy in any single measured value of $\Delta R/R_o$ at any given experimental stress level was between ±3% and ±5%, with the higher value applicable to the more uncertain cases, such as the last step in a step-release experiment, or a zero-stress residual resistance value.

The identifiable errors in stress in the dynamic compression experiments arise from uncertainties in the measured values of projectile velocity and subsequent conversion to particle velocity and uncertainties in the equations of state used for the target and flyer materials through which the particle velocity is related to stress. We can measure the projectile velocity with an accuracy of about ±2%. Barker and Hollenbach (1970) claim an accuracy of ±2% in their plexiglas and quartz equation of-state data and our glass data are accurate to this level at the low stresses encountered here. We expect, therefore, that an accuracy of

±4% in stress is reasonable for each of the measured stress levels in the calibration experiments.

4.7.2 Curve Fitting--Each of the dynamic calibration experiments was designed to give at least two points on the loading curve, while the majority of the shots were designed to produce unloading data as well. A typical low-stress step-release experiment (glass flyer, Plexiglas target) gave two loading points and eight unloading points. Our ultimate choice of treatment of the data was based on a combination of statistical criteria, convenience of computation, and physical reasonableness. Note that the loading curves are given in the form $\sigma = f(\Delta R/R_o)$ rather than the reverse, whereas $\Delta R/R_o$ is actually a function of stress. This was done to simplify the use of the analytical forms in reading stress gage outputs. If we were to try to look for a physical model to explain the piezoresistance of ytterbium we would refit the curves and put them in the form $\Delta R/R_o = f(\sigma)$.

The unloading curves were fitted to straight lines for peak stresses up to 10 kbar by inspection without using any "best fit" criteria, i.e., we did not try any other functions. It is, however, obvious that the measured paths are linear or are very close to being linear. Fitting the unloading paths originating at peak stress values above 10 kbar was more of a problem; this will be discussed in the next section.

In the discussion that follows, we use the terms experimental value of stress to signify the stress calculated from the known properties of the target and flyer, and the measured projectile velocity. First, the $\Delta R/R_o$ values are converted to stress using one of the calibration equations (equation 1 or 2). Then, the stress derived in this way is compared to the experimental stress. The difference is an indication of the accuracy of each data point.

4.7.3 High-Stress Step-Release Experiments--Shots S1 and S2 were our first lucalox flyer-quartz target step-release experiments. We reached a peak stress of 13.82 kbar during S1 and 29.97 kbar during S2. The data from S1 were not of the expected quality because a substantial amount of shock tilt, coupled with the effects of the relatively thick

(about 0.020 cm) gage package, made the steps less sharp than we would have liked. The peak $\Delta R/R_o$ values for the two gages were 1.492 and 1.485, respectively, the rounded values of which correspond to a peak stress of 13.38 kbar, a deviation of -0.44 kbar from the experimental stress of 13.82 kbar. The release data plotted in Figure 27 also show good reproducibility. We had corrected the tilt problem by the time we fired S2, so the data were more easily read from the oscillograms. The rounded peak values of $\Delta R/R_o$ for the two gages were 4.33 and 4.91, corresponding to deviations of -1.44 and 1.72 kbar, respectively, or 4.6% and 6.1% of the experimental value of 29.97 kbar. The release data obtained during S2 and shown in Figure 31 were somewhat difficult to represent by a polynomial that fit well and did not have too many inflection points. We decided that the unloading curve would be fit reasonably well by the loading curve but with a zero-stress offset, so we added a number of the calculated loading points to the measured population of unloading data, and weighted the zero stress value of $\Delta R/R_o$. The fitted line crosses the loading path twice, but it is a reasonable representation of the unloading behavior from this stress range.

The rest of the series of Lucalox-quartz step release shots were S11 and S12, and S17 through S22 (excluding S20). We obtained acceptable loading and release data from both gages in all shots except S17, in which the peak stress was 33.40 kbar. One of the gages in S17 behaved in the expected manner, but the other showed a rise to a relatively low change in resistance, then a sudden drop to a lower plateau, where it stayed for approximately one μsec until the arrival of the first release step. We rejected this value because we believed that the ytterbium making up this gage had begun to transform into the high pressure (BCC) phase and was showing the behavior noted when the phase change in S20 was studied. It is interesting to note that the other gage did not seem to begin to transform. We inferred that the phase change probably nucleates at local stress concentrations, such as around inclusions, and

quickly grows from these nuclei. It is this phenomenon which leads to our uncertainty in predicting the macroscopic stress at which the transformation will begin, and leads to our recommendation that 30 kbar be the maximum stress at which commercially available ytterbium should be used without a backup system.

The best accuracy was obtained in S21, where the derived peak stress values of the two gages deviated by 2.8% and 2.2% from the experimental value, and in S17 where the deviation was 2.4% for the gage that functioned. The poorest accuracy was exhibited by the data from S22; here the derived value of stress from $\Delta R/R_o$ of the first gage deviated by 11.4% from the experimental value; we did not, however, have any grounds for rejection of these data.

Shots S11 and S12 were done as a pair to check (as well as could be done with one pair of shots) the effect of the fiberglass-epoxy package on the response. The target for S11 contained two bare ytterbium grids; that for S12 two of our regular fiberglass-epoxy encapsulated grids. We tried for 25 kbar in S11 and obtained 24.03, which was then the stress aimed for in S12, where we obtained 23.84 kbar. Given our ±3% estimate of accuracy in stress, the two can be considered to be the same for purposes of comparison. The $\Delta R/R_o$ values from the two encapsulated gages were both lower than either of the readings from the bare gages, but since the highest reading showed a considerable deviation from the mean and the other three formed a cluster, no difference in behavior could be inferred from this pair of shots.

There is one other interesting aspect of the Lucalox-quartz experiments. On examining the records from S1, we noticed that the recording time (over 8 μsec) was significantly longer than expected, and we also noticed this in subsequent shots of this type. We had expected to be able to obtain a value of $\Delta R/R_o$ corresponding to the peak stress and three release calibration steps while the target and enough of the projectile head were in one-dimensional strain states. This was done in all experiments except S1, where dispersion arising

from tilt obscured the third step. However, a zero-stress residual resistance ($\Delta R_H/R_o$) measurement was not expected on these shots because the targets were not expected to last long enough. Given the long recording time, we did measure a value of $\Delta R/R_o$ at a stress level very close to zero and included it with the other $\Delta R_H/R_o$ data. Two things must be remembered here: the stress was not actually zero (but is always under 1 kbar), and the target and gages were not in one-dimensional strain. However, since the gages showed no obviously suspicious behavior, we decided to include these data with the rest of the zero-stress residual resistance data.

Usually the unloading paths were easily fit by polynomials in $\Delta R/R_o$. In some cases, however, fit was sacrificed for physical reasonableness. High order polynomials often fit the data well,* but, given the relatively small number of points, tend to fit very poorly between the experimental data and not to be physically reasonable because of the large number of inflection points. The only release path that had to be force-fit in any way was that from Shot S2, as explained previously.

The standard deviations in stress associated with the fitted release paths vary from 0.235 kbar in S17 to 0.865 kbar in S12. One way of treating this information would be to convert this value to an indication of the percentage uncertainty at the midpoint stress--16.7 kbar in S17 and 15 kbar in S12. The percentage uncertainties in stress at these midpoint stress levels are then 1.35% and 5.76%, respectively.

In summary, we were successful in using the Lucalox-quartz step release experiments to produce a large amount of loading and release data in the range of ~8 kbar and to over 33 kbar despite the resolution difficulties caused by the presence of the thick gage package and the transient disturbances to the flow that were present during the experiments.

---

* Using a least-square criterion.

4.7.4 Low-Stress Step-Release Experiments--Another step-release configuration (glass flyer-Plexiglas target) was used to obtain all of our release data and a large part of our loading data at stress levels of 6 kbar and below. The first series consisted of Shots S4, S6, S8, S10, S13, S14, and S15. Accuracies ranged from excellent in S14, where the two gage readings deviated by 0.08 kbar (0.17%) and 0.02 kbar (0.04%) from the experimental value of 4.72 kbar and S6 and S4, where the accuracy was of the same order, to poor in one shot - S10. In this case the percentage deviations from the experimental stress were 16.5% and 13.1% for the two gages. We believe (and will discuss this in more detail later) that discrepancies of this type arise from differences in the metallurgical history of the foil used to make the gages. However, because we had no practical and reliable way of testing each gage for some indication of this before each shot, we can only suggest this as a reason for the occasional lack of reproducibility.

The series was concluded with Shots S24 and S25, which were done to check for possible time effects by changing the flyer thickness and thereby the step length, and S26 through S28, which were comparisons between annealed and as-rolled ytterbium foil. The only data that were rejected were those from Gage 2 in S13, where the derived stress value was found to differ from the expected value by much more than two standard deviations, a criterion for rejection.

Our treatment of the unloading data derived from these experiments will be discussed first. Each shot (except S13 and the annealed versus cold-worked shots) produced eight points that comprised the data for one release path originating at the peak stress reached in the experiment. These points were plotted, and straight lines were fit to all of the paths up to and including the Lucalox-quartz Shot S22 (8.22 kbar). Some of the results are shown in Figures 36 and 37. We now had a set of 14 straight lines (including Shot X1 -- see Table 4) of the form

$$\sigma_u = A + B \left(\frac{\Delta R}{R_o}\right)_u \tag{3}$$

where σ_u is the stress along the release path, A and B are constants for each individual path but are functions of the parameter σ_p, the peak stress reached in the experiment, and $(\Delta R/R_o)_u$ is the fractional resistance change along the unloading path. We then plotted B as a function of σ_p (Figure 38) and found the best fitting line to be a straight line to be

$$B = 24.26 - 1.81\ \sigma_p \tag{10}$$

To find the best values of A, we noted that

$$\frac{\Delta R_H}{R_o} = -\frac{A}{B} \tag{11}$$

for any given peak stress σ_p, where $\Delta R_H/R_o$ is the zero-stress residual resistance. Our measured $\Delta R_H/R_o$ values were fit to a number of functions and an acceptable fit was found (see Figure 40) to be

$$\frac{\Delta R_H}{R_o} = -\frac{A}{B} = -6.87 \times 10^{-3} + 5.42 \times 10^{-2} \log_e \sigma_p \tag{12}$$

Unfortunately, the problem is now over-defined. We have a value for the slope and both end points of every line as a function of peak stress, and if we use any pair, the value of third quantity does not fit. The only reasonable answer we can give at this time, pending further analytical work on the data, is to say that it is most important that the unloading paths go through the loading curve at the proper peak stress, and the zero-stress end point or slope values must conform to this.

We have constructed a set of unloading paths by drawing straight lines through the zero-stress end points and the corresponding peak stress values. This family of lines is shown in Figure 39. Hearst (1974) has carefully examined the data contained in this report and constructed a set of algorithms for computerized reduction of gage data in both loading and unloading. He reports that they have been used and are satisfactory.

The release data presented in our previous report (Ginsberg, 1971) which were tentative, should not be used. An error arose from our inability to describe the equation of state of Plexiglas in a zone where there was interaction between compression and release waves,* thereby causing both time and stress level shifts in our code output. The release paths presented here were derived from good experimental data and can be used to obtain stress-time unloading data within the stated limits of accuracy.

The available recording time in this series of shots was much longer than the 4 μsec of one-dimensional strain time in the projectile head. The data obtained from steps as long as 7 μsec from impact were consistent with the data taken at earlier times. It should be pointed out, however, that the gages themselves had approximately 6 μsec of time in one-dimensional strain. Shots S24 and S25 were done at about the same stress, but with two different flyer plate thicknesses, 0.317 (S24) and 0.635 cm (S25). After about 4.5 μsec, the projectile heads were both out of the one-dimensional strain time region, but S24 had undergone four release steps whereas S25 had undergone only two. The rest of the steps in S25 took place under mixed strain conditions in the projectile head. However, no apparent difference was seen in the behavior of the gages in the two shots under these two different conditions.

In our previous report (Ginsberg, 1971) we suggested that the metallurgical history of the foil used in the experiments was likely to be important in that variations in history would probably cause variations in electrical response to stress, thereby compromising both the accuracy of the gages and the precision of the calibration. Such differences have been shown to be a problem with manganin (Keough and Wong, 1970; Rosenberg and Ginsberg, 1972) and are not really surprising nor unexpected. Shots S26, S27, and S28 were designed to examine the magnitude of the difference

* Our analysis was based on going from $\frac{\Delta R}{R_o}(t)$ to $\sigma(t)$ by computer code predictions, using available equation of state data.

in dynamic piezoresistant response between as-rolled foil (which is the usual condition) and foil which had been annealed at approximately 475°C* for 30 minutes at a pressure of 10^{-5} mm Hg.† The results showed that there is a very large difference in the behavior of these foils. Plots of two of the oscillograms are contained in Figures 42 and 43, and an approximate loading curve for annealed foil, along with measured release paths, is shown in Figure 44. We had seen previously that the response of the as rolled AREF foil is close to the same as that of the RC foil,†† so the difference can be taken to be between annealed and cold-worked foil. The magnitude of the difference in response suggests that the electrical resistivity of ytterbium is very sensitive to the concentration of strain-induced lattice defects.

The data from Shot S28 also (Figure 43) are of interest here. Note that although the tops of both outputs are distorted by a spike, that of the rolled foil gage is relatively flat while the other is climbing at a rapid rate. We would like to suggest the possibility that defect multiplication is taking place during the two-μsec intervals when the gages are at the peak stress of 1.40 kbar, and this effect is causing the resistance change. We believe, therefore, that the value of $\Delta R/R_o$ for the annealed gage is not an equilibrium value and, if it were, the difference between it and that of rolled foil gage would be much greater. The ratio of $\Delta R/R_o$ of the annealed to the rolled foil in the three shots is: at 5.36 kbar, 2.45; at 3.21 kbar, 3.58; and at 1.40 kbar, 1.37. We must conclude that variations in the metallurgical history of ytterbium foils can be a major source of error. Some agreement on standardization would be helpful. In no case, however, should any foil but cold-worked (as-rolled or unannealed) be used as gage element material.

---

* The melting point of ytterbium is 824°C.

† Obtained from American Rare Earth and Foil, Inc. (AREF).

†† This agreement is further corroborated by Spataro's (1972) data on 0.0025-cm (1-mil) AREF foil up to 4.7 kbar.

4.7.5 Double-Shock Experiments--Shots S3, S5, S7, S9, S29, and S30 were done to produce peak stress loading data and some information on whether or not the loading calibration depended on the path by which the gage reached peak stress. These were the double-shock experiments described in Section 4.4.4. The first four shots were designed so that the gage was loaded, released to zero stress, and then reloaded to a lower stress. The reproducibility of the $\Delta R/R_o$ values associated with the first stress peak was excellent in all of these shots, as can be seen from the data presented in Table 4. The poorest accuracy was shown by gage 2 in Shot S6, where the deviation from the expected value of stress was 7.9%, but this represented an error of only 0.04 kbar at this stress level.

All of the first-peak data from this series were accepted, but, even though the second-peak data looked reasonable, they were rejected for the main calibration curves for the following reasons. When analyzing the reload data, we checked back on previous work (Ginsberg, 1971)* and

---

* Note: The corrected data from our previous work (Ginsberg, 1971) is shown in the following tabulation.

Shot No.	$\Delta R/R_o$	Uncorrected σ kbar	Corrected σ kbar
S3	0.0196	0.78	0.84
	0.0229	0.78	0.84
S4	0.0160	0.77	0.82
S5	0.0208	0.79	0.87
	0.0218	0.79	0.87
S6	0.0225	0.90	1.03
	0.0218	0.90	1.03

found that an error was made in assigning stress values to the measured $\Delta R/R_o$ data. This arose because of an error in the impedance value used for aluminum, a number needed for the impedance match calculation necessary to find the stress level of the second peak. The analysis was based on an assumption that the aluminum was elastic in the stress range involved (below 3 kbar) and so the longitudinal instead of the bulk impedance should have been used. When our old data were corrected, we found that the calibration curve in the region below 1 kbar was shifted considerably to the left. However, having no shock data in this stress range for comparison, we could not ascertain whether the value of $\Delta R/R_o$ associated with the reloading stress was valid for first loadings. Our data from this project help only insofar as all of the old second shock data show a lower piezoresistance coefficient than any of the first shock values obtained in the present project, but this is not conclusive evidence, because there is probably a small difference in the state of work hardening of the 0.0025-cm (1-mil) foil used previously and the 0.005-cm (2-mil) foil used in this project. Within the present series of shots (S3, S5, S7, and S9), the results are not conclusive either, but only because of a lack of data. There seems to be no indication that second shock $\Delta R/R_o$ values are either greater or less than first shock values for a given stress level. To be safe, however, all second shock data were excluded from the calibration curves.

Shots S29 and S3C are also described in Section 4.4.4. In each shot we attempted to compare directly the response of a pair of gages that reached a given stress through a single loading, and a pair that reached the same peak stress in two steps. The results as shown in Table 4 suggest that there is a small effect, based on the observation

that among the data points accepted,* the $\Delta R/R_o$ level reached through a single shock is slightly greater in each case than the level reached after a step load. However, the effect is not large, and we cannot at this time suggest any corrections.

4.7.6 Phase Transition Experiment--The records and a plot of the data from the phase-transition experiment (S20) are shown in Figures 45 and 46. The ytterbium grids each had 1000-Ω resistors in one of the signal legs and the manganin gage had a 50-Ω resistor in one of the signal legs. This is the major reason for the observation that the voltage signal from the ytterbium gages was only three times greater than that from the manganin gage. Figure 46 plots the output from the ytterbium gages and the output from the manganin gage multiplied by a factor of 50 so that the scales would be comparable. The measured peak stress reached during this experiment was 41.5 kbar assuming linear behavior of the manganin gage. The stress level calculated from the measured impedance of the soda-lime glass used for the projectile head and target was 44.7±0.2 kbar assuming linear elastic behavior of the glass. This result indicated that the glass is no longer behaving as a linear elastic solid in this stress range or that the coefficient of manganin is not strictly linear, or both. Insofar as the exact peak stress is not of critical importance, we will accept the 41.5 kbar value.

The most interesting and important feature of Figures 45 and 46 is the difference in the shape of the manganin gage trace and the two ytterbium gage traces. The manganin gage records the actual shape of the input waveform, showing a rise to about 41 kbar, a flat top lasting nearly 2 μsec, and the release back to zero stress. The ytterbium gages both rise with the manganin gage to an average indicated stress of about

---

* Two points were rejected because excessive dispersion and flow interruption by the gage packages prevented the waves from equilibrating at a constant stress level before the arrival of release or recompression waves.

33 kbar and then drop off steeply to half the maximum value of resistance change. The decrease then becomes more gradual at this time and continues smoothly until the arrival of the release wave between 2 and 2.5 μsec when there is another slope change. This new slope apparently represents a combination of the effect of the continuing phase change (until some stress is reached at which it stops) and the normal decrease in resistance of the untransformed material. The bump occurring at about 3.5 μsec is a fracture signal arising from a wave reflection from new free surfaces caused by spallation of the target behind the gage plane.

The difference between the manganin gage trace and the ytterbium gage traces clearly shows the occurrence of the FCC → BCC transition observed under hydrostatic loading at approximately 39 kbar. Rough extrapolation of the portion of the ytterbium traces before the arrival of the release wave to $\Delta R/R_o = 0$* suggests that the transition would be complete in less than 10 μsec, considerably faster than one would expect from the experience of the investigators who used hydrostatic pressure and found that the transformation required hours to complete. It would seem that either the nucleation rate or the growth rate of the BCC phase is dependent on the state of strain or on the generation and concentration of lattice defects.

At one time it was believed that the FCC → BCC transformation involved a change in the energy band structure of ytterbium with an attendant shrinkage of each atom, allowing the transition from a close-packed (FCC) to a more open (BCC) structure. It was subsequently shown, however (McWhan and Jayaraman, 1963) that the required decrease in volume could be accomplished in this manner by a change in the effective coordination number of the BCC phase from 8 to 12 and by recalculating the atomic

---

*The actual resistance ratio of the BCC phase to the FCC phase is 0.8, but this exercise is done simply to estimate the speed of the reaction.

radii based on the new coordination number. The kinetics of the transformation* also suggest that no electronic rearrangement takes place because the change in resistance is too slow, even at the microsecond level. The main (and obvious) conclusion is that ytterbium cannot be used as the active element in any dynamic stress transducer above the stress at which the phase transformation takes place because the metastable FCC phase cannot be retained above the equilibrium transition point.

4.7.7 Static Compression Experiments--Some representative results from our static compression piezoresistance experiments were shown in Figure 50. Figure 51 contains some measurements done by Smith et al. (1972). It shows essentially the same general features-a change in response with stress cycling and a static coefficient in reasonable agreement with the measured dynamic coefficient. In Figure 50, the system was held at stress for 1 min at each point except for once during each loading cycle, when it was held at approximately 1 kbar for 20 min. No change in resistance with time was noted. During the release cycles, we also held once for 20 min and obtained a change from $\Delta R/R_o = 0.0313$ to $\Delta R/R_o = 0.0251$ or a change of less than 10^{-4}%/msec, far less than is of interest to us. The same phenomenon was noted on return to zero stress 3 hrs later. The rate of change of resistance was of the same order as that calculated above.

---

* Note: We briefly attempted to analyze the kinetics of the transition by, for example, fitting the $\Delta R/R_o(t)$ data to the Johnson-Mehl equation (Burke, 1965) which is

$$y = 1 - \exp[-kt^n]$$

where y is the fraction transformed, k and n are constants and t is time. $\Delta R/R_o$ was assumed directly proportional to the fraction transformed. We did not, however, find good agreement, probably because of this assumption and the observed very fast initial transformation rate, which is at variance with the Johnson-Mehl analysis. Since it was not critical to the main part of the program, this effort was abandoned.

Deformation during the stress cycling results in the creation of lattice defects. We believe that the resistance change is probably a result of thermally induced reduction of the number of these defects. This room temperature annealing is a slow process, but the effects are definitely measurable and can be seen in other metals with melting points around that of ytterbium, even in cases where deformation-induced defects have a much smaller electrical effect than in the case of ytterbium.

4.7.8 Tensile Strain Experiments--The results obtained in the tensile strain experiments help considerably in the attempt to understand the piezoresistance of ytterbium and, in a qualitative way, some of the more difficult-to-interpret features of some stress gage records. However, the results of these experiments cannot be uncritically applied to the interpretation of stress gage records because some important questions are still unanswered. The three major ones are: (1) How much tensile strain is actually coupled into the field gage, and is it truly biaxial? (2) How much bending is present? (3) What are the effects of, for example, Poisson contraction of the gage package?

The shape of the curves (Figures 47, 48, and 49) obtained in these experiments is very interesting. If one assumes a constant resistivity and uses Equation (8) to predict resistance changes during tensile loading, the calculation will show that the resistance change is always positive because the length of the specimen increases and the cross-sectional area decreases. If one then goes on to assume perfect plasticity and constancy of volume during deformation (with no resistivity change), the prediction will be both positive and constant (Keough, 1970). The initially negative slope shown in the present data on ytterbium* can be accounted for only if the resistivity change is negative and large enough to overshadow the geometry effects. This is reasonable when we consider that all the initial deformation is elastic and so the major effect of the deformation is a

*Nickel also has a negative elastoresistance coefficient.

change in interatomic distance. We know that the major change in resistance during compression is due to resistivity changes (the magnitude of the effect cannot be accounted for in any other manner) and that in one-dimensional strain the resistivity change reflects a large change in interatomic distance and an accompanying change in band structure. It is not surprising that a tensile strain would reverse this effect and that deformation that affects the band structure in the opposite way from compression should cause negative resistivity changes. Our measured tensile yield strain of 0.005-cm ytterbium foil is approximately 0.27%. At this strain we would expect to see a change in the slope of the ε-$\Delta R/R_o$ plot because the deformation is no longer purely elastic and slip by dislocation movement is taking place. If the material work-hardens, we should expect some additional elastic deformation with accompanying negative resistivity change, and competition between the two processes. Inspection of Figure 47 suggests that a slope change at about 0.27% strain is not unreasonable, given the uncertainty in our data. The minimum value of $\Delta R/R_o$ at somewhat less than 1.50% strain is reached when the positive resistance change arising from geometry effects and from lattice defect generation balances out any further negative resistivity changes, and the subsequent positive slope continued to reflect the predominance of defect and geometry induced changes. Unloading the specimen at any point on the curve caused the resistance to drop back toward zero on a line of slope equal to the initial slope--probably a consequence of recovery of elastic strain.

Without more information we can only say that (1) stretch and bending phenomena are probably the cause of any small negative voltage excursions on field gage records and (2) no matter what the answers to the question raised above, stretch and bending effects are probably negligible at stresses at or above about 3 kbar. A detailed discussion of the role of our tensile data in checking for self-consistency between shock and hydrostratic data and determination of the state of gage strain is presented in Appendix A.

4.7.9 General Comments--Our characterization experiments consisted of resistivity, temperature coefficient, and static mechanical property measurements, as well as X-ray crystal structure determination and an attempt at hardness measurements.

The measured resistivity of ytterbium was found to differ by as much as a factor of three from some previously reported values for heavily cold-worked material (Williams, 1970) and from the annealed material studied as part of this program. In general, materials with lower ambient pressure resistivity tended to have a greater sensitivity to stress than materials of higher ambient pressure resistivity. This suggests that the response of ytterbium is very dependent on lattice defect concentration, and especially on the number of defects actually produced during the dynamic loading process.

When the temperature coefficient of resistance of our foils was measured, we found that the annealed AREF foil had a temperature coefficient of 2.65×10^{-3} Ω/Ω - ^{o}C, the value of the RC foil was 1.35×10^{-3} Ω/Ω-^{o}C, and the as-rolled AREF foil had the lowest coefficient, 0.51×10^{-3} Ω/Ω-^{o}C. Our experience with the difference in chemical composition of random samples of RC foil taken from the same lot suggests that an assumption of compositional invariance for the AREF foil might not be wise, so the difference in coefficients among the RC and AREF foil and between the two samples of AREF foil might be due to either chemistry or metallurgical history effects. In our previous work a coefficient of about 0.6×10^{-3} Ω/Ω-^{o}C was measured for samples of RC 0.0025 cm (1-mil) foil, comparable to the AREF as-rolled 0.005 cm (2-mil) foil, so it seems obvious that this property cannot be predicted from chemical analysis or knowledge of the metallurgical history of the foil. The importance of this measurement derives from the possibility of errors in stress measurement arising from temperature effects in the gage material--the most desirable gage

material would show the least effect of temperature on piezoresistance coefficient, and would probably have a low temperature coefficient of resistance, although this is not strictly necessary.

Lilley and Stephens (1971) studied the effect of temperature on piezoresistance under hydrostatic pressure and found that raising the temperature decreased the sensitivity under those conditions. In our experiments the stress pulse reached the gage after current had pulsed through it for about 10-15 μsec. The field gages are pulsed for considerably longer times, but often with lower currents. Our experience has been that the maximum measured temperature rise in a 6-Ω encapsulated field gage made from 0.005-cm (2-mil) foil is less than 20°C, using a coefficient of 0.6×10^{-3} Ω/Ω-°C. This rise occurred at 10 msec with a voltage of 300 volts across the bridge of which the gage was a part. At 200 and 100 volts, the temperature rise was about 10°C and 2°C, respectively. These changes in temperature should have a very small effect on the response to stress, and we also believe that there should be no temperature problem in transferring our laboratory calibration data to the interpretation of field records.

The mechanical property measurements were done because we have attributed some of the behavior seen in ytterbium to yield point effects, especially the knee in the σ versus $\Delta R/R_o$ curve between 1 and 1.5 kbar, and the lack of zero stress residual resistance at these low stresses. Moreover, we expected that the tensile results would facilitate understanding of the electrical behavior under tension. The results of static compression tests (Table 3) showed ytterbium ingot to have a static compressive yield strength of about 0.3 kbar. Cold-worked foil would have a higher static yield stress, and 1 to 1.5 kbar seems to be a reasonable estimate of the dynamic compressive yield of our as-rolled material.

5. RECOMMENDATIONS FOR FUTURE WORK

Although a considerable amount of work was done during this program, three major areas remain in need of further investigation. These are:

- Quality control improvement
- Understanding the effects of complex strain states, such as those encountered in the field and reloading, on gage response
- Data treatment and development of a standard method of converting gage records to stress-time histories

Improvement in quality control methods for gages and gage material would lead to increased reproducibility and reliability. Some relatively simple test that could be used to identify potentially unsuitable material would be the goal of such a program.

A better understanding of the effects of complex strain states such as those present in divergent flow fields and reloading would help in the analysis and interpretation of stress-time histories obtained with ytterbium gages.

The data generated during this program is extensive. It should be examined and analyzed in more detail, and a best way of using the data for the interpretation of gage records should be designed. This should then become the standard method of converting gage records to stress-time histories.

REFERENCES

L. M. Barker and R. E. Hollenbach, 1970, Journal of Applied Physics, Vol. 41, p. 10.

E. Barsis, E. Williams, and C. Skoog, 1971, Journal of Applied Physics, Vol. 41, p. 5155.

S. R. Brown, 1970, "Development of Piezoresistive Stress History Gages," Lawrence Radiation Laboratory, Livermore, California, Memo DET 70-48.

E. Bucher, P. H. Schmidt, A. Jayaraman, K. Andres, J. P. Maita, K. Nassau, and P. D. Dernier, 1970, Physical Review B, Vol. 2, No. 10, pp. 3911-3917.

J. Burke, 1965, The Kinetics of Phase Transformations in Metals, Pergamon Press, Oxford, p. 45.

A. H. Daane, 1961, in The Rare Earths, F. H. Spedding and A. H. Daane, eds., John Wiley & Sons, Inc., New York, p. 177.

G. E. Dieter, Jr., 1961, Mechanical Metallurgy, McGraw-Hill Book Company, New York, p. 480.

D. C. Erlich, D. C. Wooten, and R. C. Crewdson, 1971, Journal of Applied Physics, Vol. 42, No. 13, p. 5495.

M. J. Ginsberg, 1971, "Calibration and Characterization of Ytterbium Stress Transducers," Final Report, Contract DASA01-69-C-0014, Stanford Research Institute, Menlo Park, California.

D. E. Grady, et al., 1973, "In Situ Constitutive Relation of Rocks," Draft Final Report, Contract DNA001-72-C-0056, Stanford Research Institute, Menlo Park, California (January 1973).

H. T. Hall, J. D. Barnett, and L. Merrill, 1963, Science, Vol. 139, p. 111.

H. T. Hall and L. Merrill, 1963, Inorganic Chemistry, Vol. 2, p. 618.

J. R. Hearst, 1974, Algorithms for Reducing Ytterbium Stress Gage Data, Lawrence Livermore Laboratory UCID-16491.

C. M. Hurd and J. E. A. Alderson, 1973, Solid State Communications, Vol. 12, pp. 375-377.

F. X. Kayser, 1970, Physical Review Letters, Vol. 25, No. 10, pp. 662-664.

F. X. Kayser and S. D. Soderquist, 1969, Scripta Metallurgica, Vol. 3, p. 259.

D. D. Keough, 1967, "Piezoresistive Stress-Time Transducer Development and Granite Adiabat Measurements for Project Pile Driver," Final Report, Contract DA-49-146-XZ-28, Stanford Research Institute, Menlo Park, California (February 1967).

D. D. Keough, 1968, "Procedure for Fabrication and Operation of Manganin Shock Pressure Gages," Final Report, Contract AF29(601)-68-C-0038, Technical Report No. AFWL-TR-68-57, Stanford Research Institute, Menlo Park, California (August 1968).

D. D. Keough, 1970, "Development of a High-Sensitivity Piezoresistive Shock Transducer for the Low Kilobar Range," Final Report, Contract DASA01-69-C-0014, Stanford Research Institute, Menlo Park, California (March 1970).

D. D. Keough, C. W. Smith, and M. Cowperthwaite, 1971, "Constitutive Relations from In Situ Lagrangian Measurements of Stress and Particle Velocity," Interim Report, Phase I, Contract DASA-01-70-C-0098, Stanford Research Institute, Menlo Park, California (January 27, 1971).

D. D. Keough, R. F. Williams, and R. A. Pasternak, 1968, "Piezoresistive Shock Transducer Study Using Lithium," Final Report, Contract 18-5816 for Sandia Corporation, Stanford Research Institute, Menlo Park, California (August 12, 1968).

D. D. Keough and J. Y. Wong, 1970, Journal of Applied Physics, Vol. 41, p. 8.

R. W. Keyes, 1960, "The Effects of Elastic Deformation on the Electrical Conductivity of Semiconductors," in Solid State Physics, Vol. 11, Academic Press, New York, pp. 149-221.

E. M. Lilley and D. R. Stephens, 1971, TID-4500 (UC-4), "Electrical Resistance of Ytterbium as a Function of Temperature and Pressure," Lawrence Radiation Laboratory, Livermore, California.

D. B. MacDonald, 1973, "Piezoresistance Effects in Calcium and Ytterbium," Ph.D. Thesis, Syracuse University, New York, 1971; University Microfilms, Ann Arbor, Michigan, 1973.

D. G. McWhan and A. Jayaraman, 1963, Applied Physics Letters, Vol. 3, p. 129.

C. F. Petersen and D. C. Erlich, 1972, "Dynamic Properties of Rock Required for Prediction Calculation, Draft Final Report, Contract DASA01-71-C-0094, Stanford Research Institute, Menlo Park, California (October 1972).

J. T. Rosenberg and M. J. Ginsberg, 1972, Bulletin of the American Physical Society, Series II, Vol. 17, No. 11, p. 1099.

L. Seaman, et al., 1969, "Classification of Materials by Shock Properties," Final Report, Contract F29601-67-C-0087, Technical Report No. AFWL-TR-69-96, Stanford Research Institute, Menlo Park, California (November 1969).

C. S. Smith, 1958, "Macroscopic Symmetry and Properties of Crystals," in Solid State Physics, Vol. 6, Academic Press, New York, p. 175.

C. W. Smith, 1972, "Stress Wave Measurements on the Mine Dust Explosive Test," Final Report, Contract DNA001-72-C-0235, Stanford Research Institute, Menlo Park, California (August 1972).

C. W. Smith, D. E. Grady, L. Seaman, and C. F. Petersen, 1972, "Constitutive Relations from In Situ Lagrangian Measurements of Stress and Particle Velocity," Final Report, Contract DASA01-70-C-0098, Stanford Research Institute, Menlo Park, California (January 1972).

P. C. Souers and G. Jura, 1963, Science, Vol. 140, p. 481.

S. J. Spataro, 1972, "Shock Studies of Ytterbium Stress Transducers," UOPKK 72-27, Lawrence Livermore Laboratory, Livermore, California.

R. A. Stager and H. G. Drickamer, 1963, Science, Vol. 139, p. 1284.

D. R. Stephens, 1964, Journal of the Physics and Chemistry of Solids, Vol. 25, p. 423.

H. D. Stromberg and D. R. Stephens, 1964, Journal of the Physics and Chemistry of Solids, Vol. 25, p. 1015.

A. Tanuma, W. R. Datars, H. Doi, and A. Dunsworth, 1970, Solid State Communications, Vol. 8, p. 1107.

R. F. Williams, 1970, "Examination of Possible Modifications to the Ytterbium Shock Wave Transducer," N66001-70-C-0572, Department of the Navy, Naval Undersea R&D Center (May 15, 1972).

Appendix A

THE PIEZORESISTANCE TENSOR COEFFICIENTS OF YTTERBIUM

Introduction

Previous attempts to correlate stress-resistance data obtained with piezoresistant transducers in shock wave experiments with hydrostatic data have not been entirely successful. With the exception of a paper by Barsis et al. (1971), explanations have centered on the differing changes in geometry suffered under uniaxial shock wave conditions and hydrostatic conditions and differences in defect production. An often ignored factor in these explanations is the tensor nature of piezoresistance. It is usually assumed that the piezoresistance tensor is spherical and hence representable by a scalar quantity. Barsis et al. (1971) considered the tensor property in a paper on manganin, and MacDonald (1973) has treated the tensor aspects of piezoresistance in some detail.

This tensor nature is important in ytterbium and can assist in explaining the different behavior of dynamic and hydrostatic data. For an isotropic elastic material, the fourth-rank piezoresistive tensor contains two independent terms π_{11} and π_{12}. This is analogous to the elastic stiffness tensor for an isotropic material. The terms π_{11} and π_{12} can be determined from two independent static experiments, and is done in the following analysis with our one-dimensional tension data and with hydrostatic data of Lilley and Stephens (1971). With knowledge of π_{11} and π_{12}, the one-dimensional strain coefficient realized in shock wave experiments can be calculated in the elastic region of the ytterbium. In the plastic region of the material, the resistance change can be

separated into a stress-induced reversible part and a damage-induced irreversible part. The coefficient for the reversible part can be calculated from π_{11} and π_{12} by assuming that material response above the elastic limit is perfectly plastic. We have compared the predicted stress-resistance curve for a reasonable HEL in ytterbium with the stress-induced part of our shock wave data and with Lilley and Stephen's hydrostatic data in Figure A-1. The tensor coefficients π_{11} and π_{12} are consistent with and explain the one-dimensional strain coefficient of approximately 0.04 Ω/Ω/kbar and the hydrostatic coefficient of approximately 0.06 Ω/Ω/kbar (Lilley and Stephens, 1971). The following analysis presents the tensor theory necessary to generate the model.

The piezoresistive tensor has the same representation and satisfies the same symmetry conditions as the piezooptical tensor (Smith, 1958). For cubic symmetry or isotropic materials the resistivity can be written

$$\rho_{ij} = \rho_o \delta_{ij} + \rho_o \pi_{ijk\ell} \sigma_{k\ell} \quad , \qquad \text{(A-1)}$$

where ρ_o is the strain-free resistivity, δ_{ij} is the Kronecker delta, $\pi_{ijk\ell}$ the piezoresistive tensor, and $\sigma_{k\ell}$ the stress tensor. We are interested in the stress-induced change in resistance and we can write Equation (A-1) in the form

$$\frac{\Delta\rho_{ij}}{\rho_o} = \pi_{ijk\ell} \sigma_{k\ell} \quad . \qquad \text{(A-2)}$$

It is convenient to go to the simplified matrix or Brugger notation

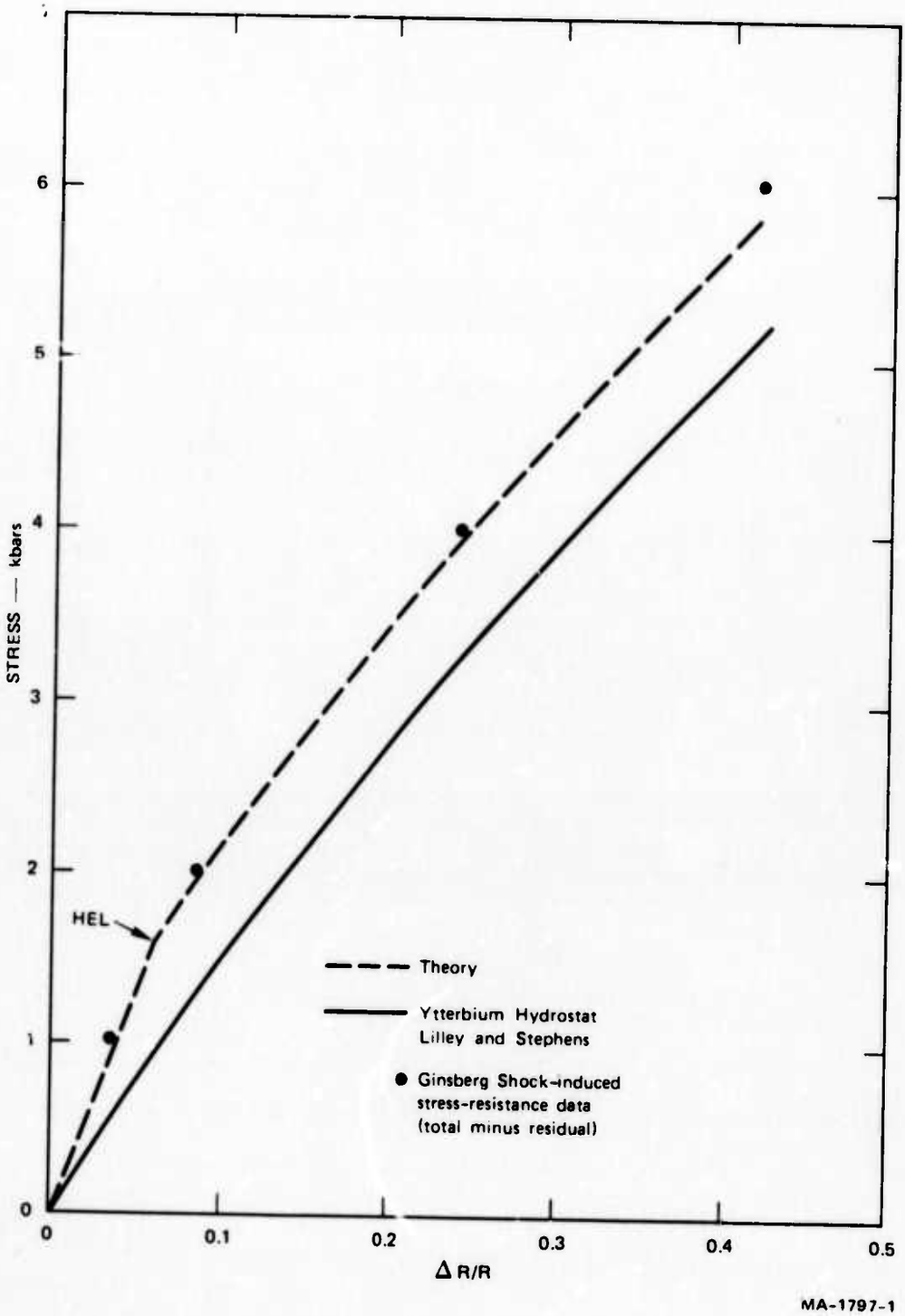

FIGURE A-1 PREDICTED PIEZORESISTANCE OF YTTERBIUM AND HYDROSTATIC DATA

$$\frac{\Delta\rho_i}{\rho_o} = \pi_{ij}\,\sigma_j \qquad (i,j = 1,6) \qquad \text{(A-3)}$$

For an isotropic material (such as polycrystalline ytterbium) this takes the form

$$\begin{pmatrix} \Delta\rho_1/\rho_o \\ \Delta\rho_2/\rho_o \\ \Delta\rho_3/\rho_o \\ \Delta\rho_4/\rho_o \\ \Delta\rho_5/\rho_o \\ \Delta\rho_6/\rho_o \end{pmatrix} = \begin{pmatrix} \pi_{11} & \pi_{12} & \pi_{12} & 0 & 0 & 0 \\ \pi_{12} & \pi_{11} & \pi_{12} & 0 & 0 & 0 \\ \pi_{12} & \pi_{12} & \pi_{11} & 0 & 0 & 0 \\ 0 & 0 & 0 & \pi_{44} & 0 & 0 \\ 0 & 0 & 0 & 0 & \pi_{44} & 0 \\ 0 & 0 & 0 & 0 & 0 & \pi_{44} \end{pmatrix} \begin{pmatrix} \sigma_1 \\ \sigma_2 \\ \sigma_3 \\ \sigma_4 \\ \sigma_5 \\ \sigma_6 \end{pmatrix} \qquad \text{(A-4)}$$

where the piezoresistive coefficients satisfy the isotropy condition

$$\pi_{11} - \pi_{12} = \pi_{44} \quad .$$

The fourth, fifth, and sixth terms on the left-hand side of Equation (A-4) correspond to a current in one direction due to an applied electric field in another because of the shear stresses in the material. These are not of interest in the present analysis and we will consider only the upper submatrix in the piezoresistive coefficient.

$$\begin{pmatrix} \Delta\rho_x/\rho_o \\ \Delta\rho_y/\rho_o \\ \Delta\rho_z/\rho_o \end{pmatrix} = \begin{pmatrix} \pi_{11} & \pi_{12} & \pi_{12} \\ \pi_{12} & \pi_{11} & \pi_{12} \\ \pi_{12} & \pi_{12} & \pi_{11} \end{pmatrix} \begin{pmatrix} \sigma_x \\ \sigma_y \\ \sigma_z \end{pmatrix} \qquad \text{(A-5)}$$

An element of the transducer is shown in Figure A-2 exhibiting the present coordinate system. Note that the resistivity in the z direction is of ultimate interest.

Since we wish to relate the resistance and not the resistivity to the stress, the change in element geometry (area and length) must be accounted for. This can be done simply by generating an additional matrix to account for the geometry change. The change in resistance is related to the change in resistivity and geometry by

$$\frac{\Delta R_i}{R_o} = \frac{\Delta\rho_1}{\rho_o} + \frac{\Delta\ell_1}{\ell_o} - \frac{\Delta A_i}{A_o} \qquad \text{(A-6)}$$

where i corresponds to the x, y, or z direction. The geometry changes can be related to the strain. For instance

$$\frac{\Delta\ell_x}{\ell_o} = e_x \quad \text{and} \quad \frac{\Delta A_x}{A_o} = e_y + e_z .$$

The strain can be related to the stress through

$$e_{ij} = \frac{1+\upsilon}{E}\sigma_{ij} - \frac{\upsilon}{E}\sigma_{kk}\delta_{ij}$$

where υ is Poisson's ratio and E is Young's modulus. The final result is

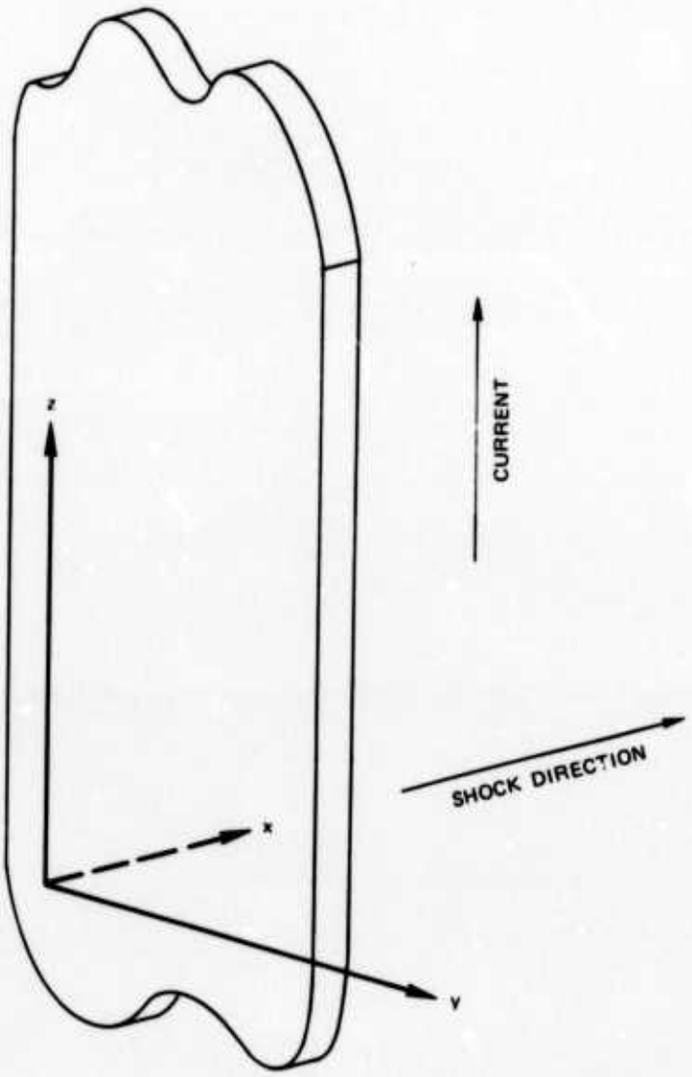

FIGURE A-2 COORDINATE SYSTEM FOR GAGE ELEMENT

$$\frac{\Delta R_i}{R_o} = \pi_{ij}\sigma_j + G_{ij}\sigma_j \qquad \text{(A-7)}$$

where

$$G_{ij} = \begin{pmatrix} \frac{1+2\upsilon}{E} & -\frac{1}{E} & -\frac{1}{E} \\ -\frac{1}{E} & \frac{1+2\upsilon}{E} & -\frac{1}{E} \\ -\frac{1}{E} & -\frac{1}{E} & \frac{1+2\upsilon}{E} \end{pmatrix} \qquad \text{(A-8)}$$

Elastoresistance Tensor

The elastoresistance tensor relates the change in resistivity to the strain tensor rather than the stress tensor and thus provides considerable simplification when the elastic state of the material is more easily represented by the strain field such as a uniaxial strain experiment. In tensor notation, the elastoresistance tensor provides the modulus relating the resistivity and strain field.

$$\frac{\Delta\rho_{ij}}{\rho_o} = M_{ijk\ell}\, e_{k\ell}$$

It can be related to the piezoresistance tensor by using

$$\frac{\Delta\rho_{ij}}{\rho_o} = \pi_{ijk\ell}\,\sigma_{k\ell}$$

and the stress-strain relation

$$\sigma_{k\ell} = C_{k\ell mn}\, e_{mn}$$

to obtain

$$\frac{\Delta\rho_{ij}}{\rho_o} = \pi_{ijk\ell} C_{k\ell mn} e_{mn} .$$

Therefore

$$M_{ijk\ell} = \pi_{ijmn} C_{mnk\ell} .$$

For isotropic material the following relations result

$$M_{11} = (\lambda + 2\mu)\, \pi_{11} + 2\lambda\, \pi_{12} \qquad \text{(A-9)}$$

$$M_{12} = \lambda\pi_{11} + 2(\lambda + \mu)\pi_{12} \qquad \text{(A-10)}$$

$$M_{44} = 2\mu\pi_{44} \qquad \text{(A-11)}$$

The coefficients λ and μ are the Lame' constants.

A geometry matrix relating the resistance change to the strain is obtained with the product of G_{ij} in Equation (A-8) and the elastic stiffness matrix. The result is the geometry matrix

$$G_{ij} = \begin{pmatrix} 1 & -1 & -1 \\ -1 & 1 & -1 \\ -1 & -1 & 1 \end{pmatrix} \qquad \text{(A-12)}$$

The desired result is the change in resistance related to the strain

$$\frac{\Delta R_i}{R_o} = M_{ij} e_j + G_{ij} e_j \qquad \text{(A-13)}$$

where

$$M_{ij} = \begin{pmatrix} M_{11} & M_{12} & M_{12} \\ M_{12} & M_{11} & M_{12} \\ M_{12} & M_{12} & M_{11} \end{pmatrix} \qquad \text{(A-14)}$$

is provided by Equations (A-9) and (A-10).

We can now calculate the coefficients of piezoresistance or elasto-resistance tensor from appropriate static data and with this predict the dynamic coefficient or at least establish consistency between present static and dynamic data. The first step is accomplished with our present uniaxial tension-resistance data and the hydrostatic pressure-resistance data of Lilley and Stephens (1971). The second step follows by assuming that the ytterbium transducer material mechanically deforms in an elastic-perfectly plastic manner.

The one-dimensional tension data used in the calculation of π_{11} and π_{12} are shown in Figure A-3. Ytterbium gages were bonded to aluminum dog-bone specimens which were strained in one-dimensional tension. Notice that the tension coefficient is initially negative. The elastic piezoresistance coefficient (the broken line in the figure) can be estimated by drawing a line through the data. For one-dimensional tension $\sigma_z \neq 0$ and $\sigma_x = \sigma_y = 0$. From Equation (A-7) this gives

$$\frac{\Delta R_z}{R_o} = (\pi_{11} + \frac{1 + 2\upsilon}{E}) \sigma_z \quad . \qquad \text{(A-15)}$$

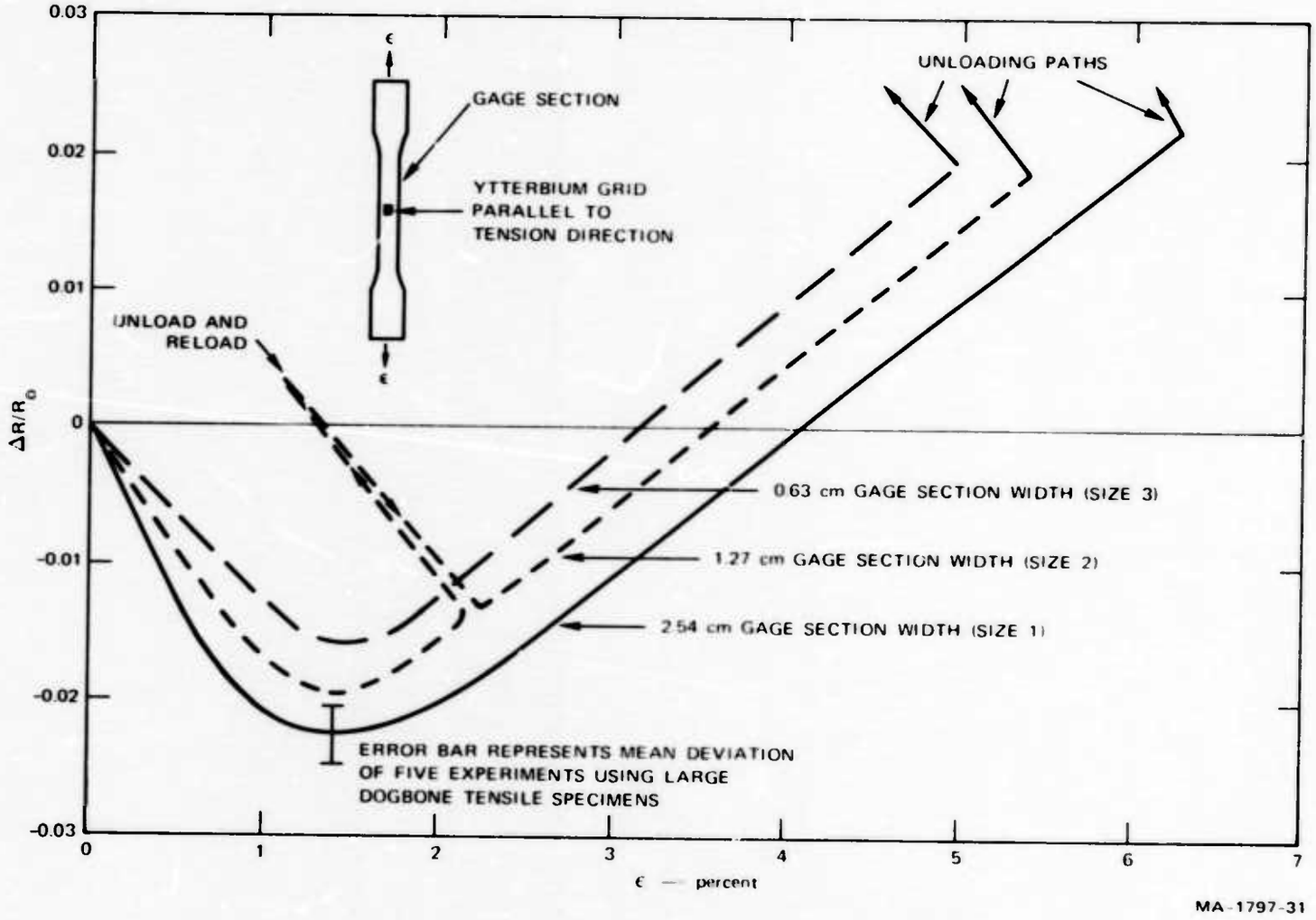

FIGURE A-3 FRACTIONAL CHANGE IN RESISTANCE VERSUS TENSILE STRAIN

Thus, from the tension data

$$\pi_{11} + \frac{1 + 2\upsilon}{E} = -0.012 \quad .$$

Given the following data on ytterbium,

Longitudinal sound velocity	$C_\ell = 1.88$ mm/μsec
Shear sound velocity	$C_s = 1.02$ mm/μsec
Bulk sound velocity	$C_o = 1.46$ mm/μsec
Density	$\rho_o = 6.97$ g/cm^3
Bulk modulus	$B = 148$ kbar
Young's modulus	$E = 187$ kbar
Shear modulus	$\mu = 72.5$ kbar
First Lamé constant	$\lambda = 100$ kbar
Poisson's ratio	$\upsilon = 0.290$

we can obtain the first piezoresistive coefficient of Yb, which is

$$\pi_{11} = -0.020 \quad .$$

Under hydrostatic stress $\sigma_x = \sigma_y = \sigma_z = -P$ and Equation (A-7) gives the expression

$$\frac{\Delta R_z}{R_o} = -(\pi_{11} + 2\pi_{12} - \frac{1}{3B})P \qquad \text{(A-16)}$$

Lilley and Stephens have measured the initial hydrostatic coefficient of resistance of ytterbium. Their result gives

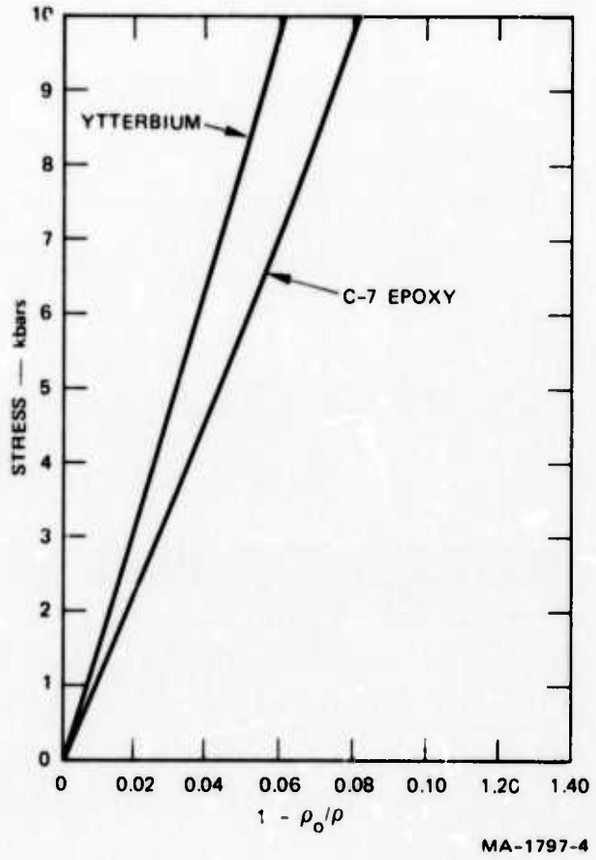

FIGURE A-4 COMPRESSIBILITY OF YTTERBIUM AND C-7 EPOXY

$$\pi_{11} + 2\pi_{12} - \frac{1}{3B} = -0.062 \quad .$$

With the known bulk modulus and the previously calculated value for π_{11} the second piezoresistive coefficient is obtained

$$\pi_{12} = -0.019 \quad .$$

To obtain the dynamic coefficient it is assumed that the elastic strain in the ytterbium is one-dimensional. This assumption is not evident, since the element is usually mounted in an epoxy resin and since lateral spreading of the ytterbium might be expected in the softer epoxy. However, the assumption can be justified by noting the comparable compressibilities of ytterbium and epoxy. In Figure A-4 the P-V curve for ytterbium is compared with that for C-7 epoxy. Homalite epoxy, which we used when obtaining our shock data, is about 10% denser than C-7 epoxy. This would further improve the comparison.

Assuming one-dimensional strain during the elastic shock loading, Equation (A-13) gives

$$\frac{\Delta R_z}{R_o} = (M_{12} - 1)e_x$$

or

$$\frac{\Delta R_z}{R_o} = \frac{M_{12} - 1}{\lambda + 2\mu} \sigma_x \quad .$$

Using the calculated values of π_{11} and π_{12} the elastic shock coefficient provides the relation

$$\frac{\Delta R_z}{R_o} = -0.039\ \sigma_x \quad .$$

If elastic-perfectly plastic behavior is assumed above the elastic limit, there is no further deformation of the unit cell and the coefficient is the hydrostatic coefficient at that pressure obtained by Lilley and Stephens. In this region the dynamic curve has the same slope as the hydrostatic curve but is offset at a constant value above the hydrostatic curve.

The calculated coefficient is compared with the experimental data in the following manner. Shock-induced resistance change has been shown to consist of two parts; one part is due to the stress state, the second is due to the introduction of damage during the shock process. The latter part remains as residual resistance after the material has been reduced to zero stress. This residual resistance was measured by Ginsberg (1971) and, in Figure A-1, the residual resistance was subtracted from the total resistance to obtain a plot of the stress-induced resistance change. Also shown in Figure A-1 is the hydrostatic curve obtained by Lilley and Stephens on an ytterbium gage obtained from SRI. The predicted shock curve determined from static data is also shown. The value used for the HEL was estimated from the tension data in Figure A-3.

The agreement is reasonably good. This simple theory using the lowest order piezoresistive tensor coupled with the assumption of elastic-plastic material response appears to explain the fundamental difference between dynamic shock and hydrostatic piezoresistance data. The theory also serves as a caution when ytterbium stress transducers are used in different configurations in the low stress region. The coefficient can differ by almost a factor of two depending on the state of strain achieved in the gage element.

Appendix B

CALCULATING $\Delta R/R$ GIVEN $\Delta V/V$ FOR FOUR-LEAD STRESS GAGES

The constant current circuit configuration for obtaining the resistance changes of the active element of a four-lead gage is shown in Figure B-1. The problem is to relate the measured voltage changes across R_{10} to the actual resistance changes of R_1, the active element of the gage. The solution presented here is a DC analysis which accounts for both the nonconstant current in the main circuit and the small finite current in the monitoring circuit and is based on the treatment by Wilkinson (in Keough, 1968).

In Figure B-1, R_1 through R_5 represent those gage resistances which vary during the loading cycle. R_1 is the resistance of the active element; R_2 and R_3 are the resistances of the piezoresistant portions of the current leads actually in the applied stress field. (The rest of the current-lead resistance, if any, is constant either because it is nonpiezoresistant or because it is outside the area being loaded and it is lumped into R_7 and R_8.) Similarly R_4 and R_5 are changing portions of the signal-lead resistances, and R_9 contains the constant portions.

R_6 to R_{10} are constant resistances. R_6 is the ballast resistance in the power supply. R_7 and R_8 are the external ballast resistors plus the portions of the current lead resistances which are constant. R_9 is the coaxial signal cable termination resistance at the gage plus the constant portions of the signal lead resistances. R_{10} is the resistance across which the voltage is being monitored, usually either the internal resistance of the oscilloscope or the scope resistance in parallel with a 51-ohm cable termination resistor (in which case the scope resistance can be neglected).

For this circuit the voltage V across R_{10} is given by

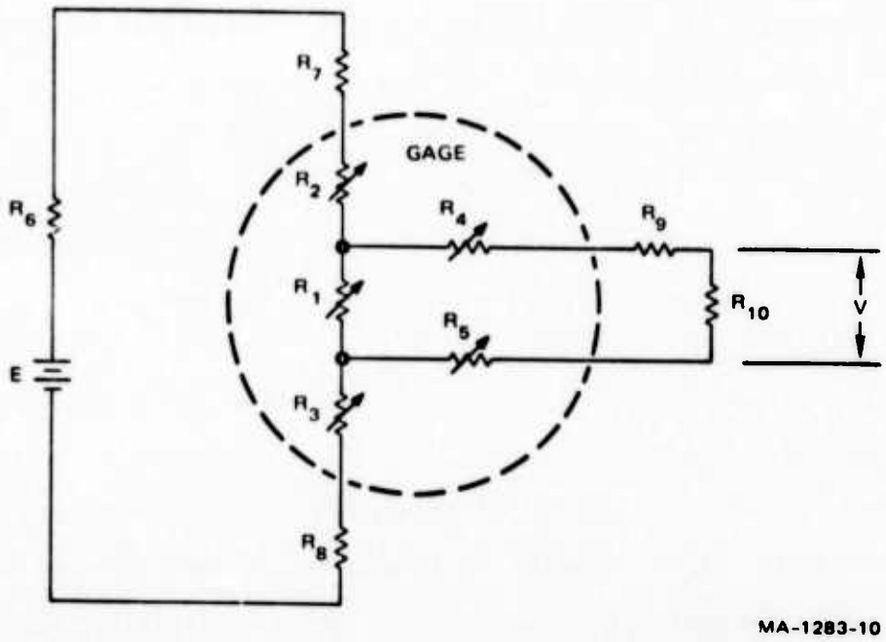

FIGURE B-1 CONSTANT CURRENT CIRCUIT TO OBTAIN RESISTANCE CHANGES ACROSS ACTIVE ELEMENT, R_1, OF 4-LEAD GAGE

$$V = \frac{R_1 R_{10} E}{(R_1 + R_2 + R_3 + R_6 + R_7 + R_8)(R_1 + R_4 + R_5 + R_9 + R_{10}) - R_1^2} \qquad \text{(B-1)}$$

The problem is to calculate $\Delta R/R_o$ as a function of $\Delta V/V_o$ given the initial values of R_1 to R_{10} with R_1 to R_5 varying together such that

$$(\Delta R_i/R_{i,o}) = (\Delta R_j/R_{j,o}) \qquad i = 1, \ldots, 5 \text{ and } j = 1, \ldots, 5.$$

The subscript o is being used to denote initial value before loading, and the subscript on the relative resistance change being calculated has been dropped since all the relative resistance changes are assumed equal (but it is understood that the resistance of interest is R_1, the active element). Note that since only relative voltage and resistance changes are being calculated, E in Equation (B-1) will cancel out and may be dropped.

This equation may be solved numerically using the RESIST program reproduced in BASIC at the end of this appendix. The input data to RESIST consist of the initial values of the 10 resistances plus the largest R_1 to be calculated, and the size of the increments by which R_1 is to be increased. The printout gives the input plus $\Delta R/R_o$, $\Delta V/V_o$, and $(\Delta R/R_o)/(\Delta V/V_o)$.

The term $(\Delta R/R_o)/(\Delta V/V_o)$ is the correction factor by which an experimentally observed $\Delta V/V_o$ should be multiplied to obtain the true $\Delta R/R_o$ of the gage element. It is an increasing function of the observed signal $\Delta V/V_o$. Note that for data reduction purposes, a plot of the correction factor vs $\Delta V/V_o$ is a considerably more sensitive method for obtaining $\Delta R/R_o$ than the more direct approach of plotting $\Delta R/R_o$ vs $\Delta V/V_o$ directly.

The corrections employed in the calibration data presented here ranged from about 1% to 8%. When very large changes in resistance were anticipated, the value of R_9 was increased to lower the correction factor. This also lowers the signal, but it was more than sufficient for our purposes. It must be remembered that each gage user should analyze his situation with respect to power and recording and see if this correction scheme applies to his system before using it. In particular, this analysis does not apply to bridge-type power and recording circuitry.

```
PRJGRAM RESIST

20      REM   "RESIST" CALCULATES THE RATIJ JF THE CHANGE IN VJLTAGE
21      REM   TJ THE INITIAL VJLTAGE AS A FUNCTIJN JF THE CHANGE IN
22      REM   RESISTANCE JF R1 JVER THE INITIAL VALUE JF R1 FJR
23      REM   MANGANIN RECJRDING CIRCUITS.
24      REM   INPUT -
25      REM     A,B,C - THE INITIAL, FINAL AND INCREMENT JF THE
26      REM             RESISTANCE R1
27      REM     RESISTANCES R2,R3,R4,R5,R6,R7,R8,R9,AND S1(=R10)
28      REM   JUTPUT -
29      REM     DELTA R/RO AND DELTA V/VO JF R1, RATIJ JF
30      REM       DELTA R/RO/DELTA V/VO
31      REM
50      READ A,B,C
60      READ R2,R3,R4,R5
70      READ R6,R7,R8,R9,S1
80      PRINT "R1 =",A
90      PRINT "R2,R3,R4,R5 =",R2,R3,R4,R5
92      PRINT "R6,R7,R8,R9,R10 =",R6,R7,R8,R9,S1
94      PRINT
96      PRINT "DELTA R/RO","DELTA V/VO","DELTA R/RO/DELTAV/VO"
100     FJR R1=A TJ B STEP C
110     LET S2=R2*R1/A
120     LET S3=R3*R1/A
130     LET S4=R4*R1/A
140     LET S5=R5*R1/A
150     LET L=R1*S1
160     M=R1+S2+S3+R6+R7+R8
170     N=R1+S4+S5+R9+S1
180     P=R1*R1
190     V=L/((M*N)-P)
200     IF R1=A THEN 500
205     IF V=VO THEN 220
207     Z=(R1-A)/A/((V-VO)/VO)
208     GJ TJ 210
210     PRINT (R1-A)/A,(V-VO)/VO,Z
220     NEXT R1
230     GJ TJ 999
500     VO=V
510     GJ TJ 205
999     END
READY.
```